Spring 2015

Mechanical stimulation of cartilage induces mitochondrial reactive oxygen species production mediating metabolic responses

Marc James Brouillette
University of Iowa

MECHANICAL STIMULATION OF CARTILAGE INDUCES MITOCHONDRIAL REACTIVE OXYGEN SPECIES PRODUCTION MEDIATING METABOLIC RESPONSES

By

Marc James Brouillette

A thesis submitted in partial fulfillment
of the requirements for the
Doctor of Philosophy degree in Biomedical Engineering
in the Graduate College of
The University of Iowa

May 2015

Thesis Supervisor: Associate Professor James A. Martin

Graduate College

The University of Iowa

Iowa City, Iowa

CERTIFICATE OF APPROVAL

_____

PH.D. THESIS

_____

This is to certify that the Ph.D. thesis of

Marc James Brouillette

has been approved by the Examining Committee
for the thesis requirement for the Doctor of Philosophy
degree in Biomedical Engineering at the May 2015 graduation.

Thesis Committee: _____
James Martin, Thesis Supervisor

_____
Nicole Grosland

_____
Tae-Hong Lim

_____
Edward Sander

_____
Michael Mackey

Dedicated to Rachel Bottjen Brouillette

ACKNOWLEDGMENTS

I would first like to thank Dr. James Martin. Employing any new graduate student is a risk, and the opportunity he has given me has both directed and changed my life. Again, thank you.

Also I would like to thank Dr. Prem Ramakrishnan who mentored me for the majority of my research. He would stop anything he was doing if I needed help. After Dr. Ramakrishnan left the University, that mentoring role largely fell to Dr. Mitchell Coleman. I would like to thank him as well, as without his knowledge, willingness to discuss anything frankly, and reminders to hurry up and write, this dissertation would not have been finished.

I would also like to especially thank Abigail Smith. She is largely responsible for my competency in laboratory activities. She was always willing to teach me any endpoint measurement or assay. Her patience and thoroughness in explanations had helped me tremendously.

There are far too many other names to list for everyone that has helped me in this academic journey; advisors, committee members, labmates, classmates, and collaborators are the easiest way to list them. Thank you everyone.

Lastly I would like to thank my wife, Rachel Brouillette. She has been with me every step of the way and has supported me more than can be repaid by a simple mention here. Her scientific writing and editing expertise has been invaluable. Thank you, Rachel; you made this possible.

ABSTRACT

This dissertation project is unique in that it seeks to link two historically independent concepts: mechanical loading of cartilage (1) induces reactive oxygen species (ROS) release from specific mitochondrial complexes, and (2) results in observable metabolic alterations. It is well known that ROS are released from certain loading conditions. It has also been shown that chondrocytes respond favorably to cyclic loading at moderate stresses, as determined metabolically by proteoglycan and collagen production. However, this study aims to demonstrate that these phenomena are interdependent, and in doing so, locates both the source(s) of load-induced ROS and the resultant molecule(s) responsible for metabolic stimulation.

To further this investigation, an osteochondral explant mechanical loading platform was built that allowed the imposition of physiological stresses on cartilage explants to further characterize cartilage metabolism. National Instruments hardware and LabVIEW controls a stepper motor driven platen, which when coupled with a load cell, allows for dynamic and static compression stimulation of articular cartilage.

Firstly, static stress (0.05 – 1.0 MPa for one hour) induces ROS release, which is mitochondrial in origin, relies on an intact cytoskeletal network, and tracks linearly with bulk tissue strain ($r = 0.87$). Dissolution of the cytoskeleton with cytochalasin B, blocking complex I of the mitochondria with rotenone, or addition of the cell-permeable SOD mimetic, manganese(III) tetrakis(1-methyl-4-pyridyl)porphyrin (MnTMPyP) reduces this ROS release at 0.25 MPa.

Next, under dynamic stress (0.25 MPa/0.5 Hz for one hour), this mitochondrial ROS release was shown to be necessary for stimulating glycolytic energy production 24

hours after stress application. The ROS release from mechanical stimulation was blocked by the addition of rotenone or Mitoquinone (MitoQ10). These treatments also both blocked the increase in intracellular adenosine triphosphate (ATP) content, and therefore show that the ROS from the mitochondria are required for stimulating ATP production.

Probing the mitochondria directly with targeted inhibitors in unloaded conditions shows that forcing superoxide generation at ubiquinol: cytochrome c-oxidoreductase (complex III), and efficiently turning this superoxide into hydrogen peroxide, resulted in a dose-dependent increase in ATP content that resembles the response to loading. Here, ATP content increased with increasing doses of antimycin A, which, when accompanied with the SOD mimetic, Galera (m40401), is always higher than antimycin A alone.

Finally, if overloading proceeds for too long (three hours at 1.0 MPa or 0.25 MPa at 0.5 Hz for 7 days), ROS-related damage ensues, resulting in significantly impaired mitochondrial function and reduced intracellular ATP content. The damage and deleterious effects are negated by administration of the antioxidant, N-acetylcysteine (NAC).

Together, these results show that mechanical stimulation of cartilage produces mitochondrial ROS and resultant products, whose role in articular cartilage is complex. In short term mechanical stimulations, these ROS act to stimulate metabolism. At higher stresses, and over longer durations, ROS cause damage which results in mitochondrial dysfunction and suppressed ATP production. These findings have important implications for the progression of osteoarthritis, which has already been linked to mitochondrial dysfunction.

PUBLIC ABSTRACT

This dissertation project seeks to explain how cartilage produces energy. Cartilage is the tissue that covers joints and allows them to move freely, and a source of energy is required for maintenance of healthy tissue. Energy production in cartilage is known to require the forces that the body imparts on it during motion, such as impacts that occur on the hip, knee, and ankle cartilage during walking. Energy production pathways are most classically characterized in oxygenated tissues, in which oxygen is used directly in a process called oxidative phosphorylation. These tissues receive oxygen from the circulating blood; however, cartilage does not have access to blood and is thus adapted to produce most of its energy through glycolysis, which is a process considered independent of oxygen consumption. Interestingly, though, oxygen is still indirectly required for glycolysis in cartilage, in that complete removal of oxygen inhibits such energy production. This dissertation demonstrates that the forces from walking cause a reaction where oxygen is converted into peroxide. This peroxide then stimulates glycolytic energy production in cartilage. Therefore, in cartilage this oxygen is not directly used to produce energy, but instead is required to produce peroxide, which ultimately acts to stimulate glycolysis to produce energy

TABLE OF CONTENTS

LIST OF FIGURES

LIST OF EQUATIONS

LIST OF ABBREVIATIONS

ADP. adenosine diphosphate

ANT A. antimycin A

ATP. adenosine triphosphate

BW. body weight

Cyto B. cytochalasin B

DAQ. data aquisition

DHE. dihydroethidium

ECAR. extracellular acidification rate

ECM. extracellular matrix

FAD+. oxidized flavin adenine dinucleotide

FADH2. reduced flavin adenine dinucleotide

FBS. fetal bovine serum

FMN. flavin mononuceotide

GAG. glycosaminoglycan

Galera. m40401

GTP. guanosine triphosphate

HIF1. hypoxia inducible factor 1

HPLC. high performance liquid chromatography

Hz. hertz

LDH. lactate dehydrogenase

L-NAME. N-Nitro-L-arginine methyl ester

MitoQ10. mitoquinone

MMP. matrix metalloprotease

MnSOD. manganese superoxide dismutase

MnTMPyP. manganese(III) tetrakis(1-methyl-4-pyridyl)porphyrin

MPa. megapascal

N. netwon

NAC. n-acetylcysteine

NAD+. oxidized nicotinamide dinucleotide

NADH. reduced nicotinamide dinucleotide

O2•-. superoxide

OA. osteoarthritis

OCR. oxygen consumption rate

PCM. pericellular matrix

PG. proteoglycan

PPR. proton production rate

Q. ubiquinone

QCIP. quantitative cell image processing

QH•. ubisemiquinone

QH2. ubiquinol

RA. rhuematoid arthritis

ROS. reactive oxygen species

ROT. rotenone

tBHP. tert-butyl hydroperoxide

TCA. tricarboxylic acid

TGF-β. transforming growth factor β

TPP. triphenylphosphonium

CHAPTER 1:

BACKGROUND AND SIGNIFICANCE

Introduction

This dissertation project aims to more completely characterize a mechano-response phenomenon in articular cartilage, whereby the resident cells (chondrocytes) respond to tissue-level mechanical stimuli by increasing reactive oxygen species (ROS) production, which in turn regulates energy production. Recently, Martin et al. showed that both impact and overloading increase ROS levels and cell death, which can be prevented by antioxidants [1, 2] , mitochondrial complex I inhibitor, rotenone, or dissolution the cytoskeletal network [3]. They also found that rotenone, under unloaded conditions, inhibits a pathway necessary for glycolytic energy production, irrespective of complex I's customary function as a member of the electron transport chain [4]. This dissertation work builds on these initial findings.

Cartilage biosynthetic activity is enhanced by moderate stress loading, but there appears to be a threshold above which cartilage biosynthetic activity is decreased by loading [5-8]. This overloading is also associated with the most prevalent disease of cartilage, osteoarthritis (OA) [9]. OA is a debilitating disease that causes pain in the joints due to cartilage degradation. In 2007 it accounted for 149 billion dollars in health care costs [10]. The incidence of arthritis was 47.8 million people in 2005 and is projected to increase to 65 million by 2030 [11], representing a growing burden on the quality of life of those affected as well as on the health care system taking care of them. Understanding that ROS release is a critical biochemical response to injury within

cartilage, and that these molecules can lead to cell death, we seek to better understand the role(s) of ROS in cartilage metabolism in order to develop therapeutic strategies that may prevent the early onset of OA without interfering with normal metabolic function.

Articular Cartilage

Articular cartilage covers diarthrodial joints and is responsible for providing a near frictionless transmission of force across the joint. It is a unique tissue in that it is isolated from the rest of the body. It has no access to nutrients via the blood and lacks any nerve ingrowth. This isolation creates a harsh environment for cartilage and poses unique challenges in how it maintains itself.

Structurally, cartilage is primarily water, collagens, and proteoglycans [12]. These proteoglycans create an anionic environment conducive to water binding, which is partially restricted by the dense collagen network. This restriction and tightly bound water provides cartilage with its impressive ability to cushion mechanical loads [13, 14]. Cells comprise only about one percent of the total tissue volume, but are responsible for maintaining the surrounding extracellular matrix (ECM) [15]. These cells are locally surrounded by a pericellular matrix (PCM), which is distinct from the bulk of the ECM in that it incorporates type VI collagen [16-21]. The ECM stiffness increases with depth [22, 23], but the PCM stiffness remains constant [23]. This results in cellular strains that are amplified in the deeper zones of cartilage when compared to the local tissue strains [24]. In OA, this PCM is known to weaken [25], which would theoretically result in higher cellular strains.

The cells are attached to this PCM via ECM receptors, a subset of which, integrins, are known to be constitutively expressed by chondrocytes in various isoforms

[26, 27]. These integrins span the cellular membrane and are largely known to attach intracellularly to the cytoskeleton via actin microfilaments [28]. The external forces can therefore be converted into intracellular signals, a process generally referred to as mechanotransduction. These integrins are known to play a critical role in chondrocytes, where blocking α5β1 integrin or actin polymerization inhibits isolated chondrocyte hyperpolarization after mechanical stimulation [29]. Loss of α1 integrins also accelerates the development of OA in knockout mice [30], and the integrin pattern also changes in the most damaged OA tissue [31]. Cytochalasin B and D can prevent the formation of actin filaments and therefore dissolve the actin network to which these integrins bind, which has been shown to decrease the mechanical properties of chondrocytes [32]. A review of the differences among the tissue zones, ECM and PCM compositions, as well as cellular attachment factors have been more thoroughly described previously [33].

Because cartilage exists in a very unique physiological environment, culturing the tissue requires significant deviation from standard culture. The extracellular and pericellular matrices play critical roles in shaping the tissue's response to external stimuli [34, 35]. When cells are extracted from this environment, they lose their chondrogenic phenotype rapidly, shifting production away from key matrix molecules, such as collagen II [36, 37]. The oxygen concentration in which they normally exist is also much lower than standard culture, roughly 6% at the superficial zone and synovial fluid, decreasing to 2% in the deep zone [38-43]. When cartilage is not kept in an environment that mimics this oxygen tension, cellular behavior changes. Proteoglycan synthesis is inhibited at both higher and lower oxygen concentrations [44-46], while glucose concentration seems

inversely related to oxygen concentration [47], indicating optimal oxygen tension is between 5-10%.

The loading environment must also be maintained, as under-loading leads to reduced aggrecan and hyaluronan content, resulting in cartilage softening and thinning, respectively [48-50]. These alterations can never fully recover, even after remobilization [48, 51, 52]. Overloading also has negative effects, reducing biosynthetic activity [53], causing cell death [1], and increasing risk of developing OA [54, 55].

It was previously believed that only a single cell type exists within this tissue: the chondrocyte, however recent studies have shown a progenitor cell population that is capable of higher degrees of repair and replication [56-61].

Glycolytic Energy Production

Biological systems are not in equilibrium; they require a constant influx of metabolites to produce enough energy to maintain all of the functions required to survive. Biological systems instead exist in a 'steady state', meaning they operate at the maximum efficiency their environment allows. Energy production in mammalian cells occurs primarily through two processes: glycolysis and oxidative phosphorylation. These two processes are distinct in where they occur intracellularly; glycolysis occurs in the cytosol, whereas oxidative phosphorylation occurs in the mitochondria.

The main output of both energy production methods is adenosine triphosphate (ATP), which consists of an adenosine molecule attached to a chain of three phosphates (α, ß, γ, proximal to distal, respectively). The phosphates are connected to one another via phosphoanhydride bonds, while the α-phosphate is connected to adenosine via a phosphoester bond. The extent to which either mechanism is used to produce ATP

depends on the oxygen concentration available to the tissue at a given time. In tissues where oxygen is readily available, oxidative phosphorylation usually provides most of the ATP. However, when ATP depletion is too rapid, glycolysis usually takes over, as it can produce ATP at a rate 100 times faster than oxidative phosphorylation.

The principal energy molecule available to cartilage is glucose, which is transferred to the cytosol by specialized transporters. But since cartilage is avascular and alymphatic, nutrients are mainly acquired through the inefficient process of passive diffusion, reducing the availability of both oxygen and glucose compared to other tissues. Because higher concentrations of oxygen are required for oxidative phosphorylation, glycolysis is the predominant driver of energy production, despite low glucose availability. Glycolysis converts glucose, oxidized nicotinamide dinucleotide (NAD^+), and adenosine diphosphate (ADP) to pyruvate, reduced nicotinamide dinucleotide (NADH), and ATP, respectively. The reaction can be seen in Equation 1.

Equation 1. Generalized Balanced Glycolysis Equation

$$Glucose + 2\,NAD^+ + 2\,ADP + 2\,P_i \rightarrow 2\,Pyruvate + 2\,NADH + 2\,ATP + 2\,H_2O + 4\,H^+$$

NAD+, the oxidizing molecule in glycolysis, needs to be recycled for the cyclic pathway to continue. Under anaerobic conditions, this recycling can be accomplished by lactate dehydrogenase (LDH), which regenerates two NAD^+ by using NADH and hydrogen to convert pyruvate into lactate (Equation 2). Importantly, the LDH mechanism of NAD^+ recycling only consumes only two of the four hydrogen atoms made available

by glycolysis, therefore netting a gain of two hydrogen atoms each cycle. This accumulation of hydrogen atoms leads to acidification of the surrounding media and this change in pH is measured as an output in some of the experiments detailed later in this dissertation.

Equation 2. Lactate Dehydrogenase Reaction

$$2\ Pyruvate + 2\ NADH + 2\ H^{+} \xrightarrow{LDH} 2\ Lactate + 2\ NAD^{+}$$

Chondrocytes are unique in that they do not rely on mitochondria for energy production; instead, substrate-level glycolysis fulfills almost all the cell's energy requirements [46]. This explains why mitochondria occupy a significantly lower percentage of intracellular volume than mitochondria in oxygenated tissues (1-2% vs 15-20%) [62, 63]. However, chondrocytes still require oxygen to maintain ATP/lactate production [46, 63], albeit at a rate 26-fold lower than in promonocytes [64].

Mitochondrial Electron Transport

In most tissues, mitochondria provide the bulk of energy production via oxidative phosphorylation. Every glucose molecule that is completely oxidized to CO_2 through this pathway provides a maximum of 26 of the 30 total ATP molecules that are formed [65]. Mitochondria are intracellular organelles that have both inner and outer membranes that create two distinct spaces: the space inside the inner membrane, or matrix, and the space between the membranes, or the intermembrane space. Mitochondria also have their own

DNA separate from the nuclear DNA, even though several mitochondrial proteins are encoded by nuclear DNA [65].

Mitochondria are sometimes called the "powerhouses of the cell" because, in eukaryotes with sufficient oxygen, their primary function lies is energy production. Oxidative phosphorylation takes place within mitochondria and involves taking fuel sources through a step by step chain of redox reactions for maximal energy extraction. First, passive diffusion of pyruvate across the outer membrane, which is then transported along with a hydrogen atom into the mitochondrial matrix by the symporter, pyruvate translocase. Once inside the matrix the pyruvate dehydrogenase complex decarboxylates pyruvate into acetyl CoA, reducing NAD^+ to NADH. The acetyl CoA then enters the citric acid cycle, also known as the tricarboxylic acid (TCA) cycle or Kreb's cycle. Here the acetyl CoA is oxidized to produce three NADH, one reduced flavin adenine dinucleotide ($FADH_2$), and one guanosine triphosphate (GTP) molecule per acetyl CoA [65].

These high energy molecules then transfer their electrons through a series of proteins that span the inner membrane to create a proton gradient which is later used to create ATP. The membrane proteins are generally called the electron transport chain and consist of NADH: ubiquinone oxidoreductase (complex I), succinate-ubiquinone oxireductase (complex II), ubiquinol: cytochrome c-oxidoreductase (complex III), and cytochrome c oxidase (complex IV). These complexes create a proton gradient between the intermembrane space and the matrix, which, when coupled with F_1F_0-ATPase (ATP synthase, also referred to as Complex V), form ATP from ADP. When all of these

electron transport steps are combined, this process of ATP generation is called oxidative phosphorylation, or respiration.

Complex I is the start of the chain and uses NADH as an electron donor. It is also the largest and most complex protein in the electron transport chain. Two electrons from NADH are first transferred to a flavin mononuceotide (FMN), then down a series of iron-sulphur (Fe-S) clusters, and finally, each sequentially to ubiquinone (Q), first forming ubisemiquinone ($QH^{\cdot}$) with the addition of a proton from the matrix, then ubiquinol (QH_2) with the subsequent addition of another proton [65, 66]. The entire process also transports four protons across the matrix to the intermembrane space. Complex II is the site of entry for $FADH_2$ into the electron transport chain. It is similar to complex I in that it uses Fe-S clusters to transfer electrons to ubiquinone sequentially, though in the process, no protons are pumped into the intermembrane space [67, 68].

Complex III is the common acceptor of ubiquinol from both complex I and complex II. In its simplest form it exists as a dimer of cytochrome bc_1 molecules [69]. The three active subunits of the cytochrome bc_1 monomer are cytochrome b, cytochrome c1, and the Rieske iron-sulfur protein [70]. Cytochrome b also contains two heme groups which accept incoming electrons and enable transfer to further subgroups [69, 70]. The two ubiquinol/ubiquinone reaction centers are located on opposite ends of the inner mitochondrial membrane and are designated center P (also called site Q_o) for the site of ubiquinol oxidation which lies closer to the intermembrane space and further from the matrix. The other reaction center is designated center N (also called site Q_i) for the site of ubiquinone reduction, which lies closer to the matrix [69, 71, 72]. The designation of

Q_i or Q_o is in regards to proton input or output, respectively, while center P or center N refers to whether it is closer to the positive or negative side of the inner membrane [73].

The mechanism of electron flow into complex III starts with QH_2 binding to center P and transferring one electron to the Rieske iron-sulfur protein. This electron is eventually transferred to cytochrome c, which will be used later in the electron transport chain. The other electron is transferred to one of the heme groups of cytochrome b, this then goes on to reduce a separate Q at center N. This process releases the two protons from QH_2 at center P into the intermembrane space. However, the full reduction of the separate Q at center N requires two QH_2 molecules to be processed. Thus the second electron from the heme group further reduces this Q at center N, which is associated with the addition of two protons from the matrix to form QH_2 at center N. The full processing results in 4 protons being pumped across into the intermembrane space while sequestering two others from the matrix.

The exact mechanisms of proton and electron transfer in complex III are still being investigated (see reviews [69, 72, 74], with some data indicating simultaneous bindings of two QH_2 molecules to center P [75, 76]. The exact mechanism of electron transfer at center P is also still researched, with data indicating simultaneous reduction of QH_2, avoiding a ubisemiquinone species altogether [77].

Complex IV binds four reduced molecules of cytochrome c produced by complex III to again pump protons into the intermembrane space. Complex IV consists of two heme groups (designated a and a_3) and two copper centers, one made from two copper ions with a cysteine bridge (Cu_A) and the other containing one copper ion oriented by three histidine residues (Cu_B) [65]. Four reduced cytochrome C molecules bind

simultaneously to complex IV, then two of these cytochrome c molecules are oxidized sequentially then released. The first electrons passes from Cu_A to heme a, then to heme a_3, and finally to Cu_B. The second electron follows the same path but ends at heme a_3 since Cu_B is already reduced. Oxygen (O_2) then accepts the two electrons from heme a_3 and Cu_B and creates a peroxide bridge between the two. Two other cytochrome C molecules then bind to Complex IV and are oxidized in the same manner. Passing these electrons onto the peroxide bridge along with two protons breaks the peroxide bridge, creating hydroxyl groups on the heme a_3 and Cu_B. Then the addition of two other protons allows the formation of H_2O from both hydroxyl groups. In this process 4 additional protons are pumped into the intermembrane space though the mechanism of this release is still under investigation.

Complex V takes advantage of the electrochemical gradient created by all of the hydrogen atoms that have been pumped into the intermembrane space to make ATP. ATP synthase consists of two general functional units, designated by F_0 and F_1. The F_0 subunit is a hydrophobic transmembrane protein, while the F_1 is water soluble and is attached to the F_0 subunit in the matrix. F_1 is further categorizd as containing 5 subunits, consistiting of 3α , 3β, 1γ, 1δ, and 1ε. The α and β subunits form a hexamer, in which the β subunit binds ADP + P_i. The F_0 subunit which consists of a membrane embedded ring proton channel consisting of 10-14 **c** subunits, with one **a** subunit, two **b** subunits, and one δ subunit. A simplified explanation of ATP formation, is that a proton enters the **a** subunit of F_0, protonates an amino acid residue, which allows a partial rotation of the **c** subunit. This also rotates the γ subunit which causes conformational changes in the β

subunit. Three sequential conformational changes from the rotation allow for binding ADP + P_i, ATP synthesis, and finally ATP release. [65]

Mitochondrial ROS Production

Ideally, the complexes of the electron transport chain work in concert to ultimately pass electrons onto the terminal electron acceptor, oxygen, at complex IV. However, during normal metabolite processing, a low basal rate of electron transfer onto oxygen occurs at preceding complexes to form superoxide ($O_2^{\cdot -}$). It has been estimated that, *in vitro*, 0.12-2% of molecular oxygen is incompletely reduced to superoxide [78], with *in vivo* estimates being much lower. The detailed explanation of electron flow preceding this section is necessary to understand how these events can occur and where metabolic inhibitors interact with these complexes to ablate electron flow. Mitochondrial ROS were first discovered by indirect detection of peroxide from isolated mitochondria [79-81]. Not long after this, a protein that converts superoxide to peroxide was identified to reside within mitochondria [82, 83]. From here it became understood that superoxide was in fact the ROS produced in mitochondria, but it was secondarily converted into the peroxide that was detected initially [84, 85].

Since the discovery of mitochondria-produced superoxide, the investigation into the mechanisms of its formation have been ongoing. The main sites of superoxide production have historically thought to be from complex I and III; however, the details that entail exactly how the complexes are producing ROS has remained elusive.

The conditions in which ROS would be produced from complex I are largely understood. Generally, there are three conditional states that are now considered to produce mitochondrial ROS from complex I [78]. The first state (mode 1) occurs when

ATP production in mitochondria is low and the pool of NADH is heavily reduced. In this state, NADH is readily oxidized by complex I and forms superoxide in relation to the increased ratio of $NADH/NAD^+$ and oxygen tension [86]. This mode 1 is considered forward electron transport (FET) since complex I is oxidizing NADH as it would in normal electron transport. When complex I was isolated from the cell and other mitochondrial proteins, and supplied with pure NADH, its production of superoxide was unaffected by its inhibitor, rotenone [86]. However, when intact mitochondria were used and complex III activity was completely suppressed, treatment with rotenone actually increased the levels of ROS [87]. In doing so, the overall mitochondrial activity toward mode 1 state, as the overall NADH concentration increased due to forced interaction with O_2 instead of Q.

The second state (mode 2) of mitochondrial ROS production occurs under reverse electron transport (RET). This mode also occurs when ATP production is low; however, here the driving force is a highly reduced Q pool (QH_2) and is usually driven by supplementation of succinate [87, 88]. This state is, however, much more sensitive to polarization of the mitochondria, requiring a much higher polarization to maintain ROS production, and having a strong reaction to even slight changes in the proton gradient [89]. The third state (mode 3) of mitochondrial ROS production occurs during normal ATP production in the mitochondria. Here the $NADH/NAD^+$ ratio is low, and this state produces very little ROS when compared to the other two modes of ROS production [87].

Complex III was previously thought to be a major source of ROS; however, recently it has been shown that the conditions in which complex III produces ROS are artificial, and most previously, assumptions of complex III ROS could be attributed to

complex I [78, 90]. Complex III can form superoxide, though only when in the presence of antimycin A, a Q_i site inhibitor. Antimycin A causes an unstable semiquinone species that passes its electron to oxygen, causing superoxide to form [91-95].

A diagram of sites for superoxide production and inhibitors for mitochondrial complexes can be seen in Figure 1. Rotenone increases ROS produced from complex I in forward electron flow, but blocks ROS in reverse flow. Antimycin A increases ROS under all conditions. Myxothiazol mainly blocks complex III Q_o site inhibitor with would reduce Antimycin A induced ROS at complex III, but alone has been shown to have variable effects alone, possibly due to its ability to also inhibit complex I or also form an unstable intermediate at complex III [88, 96].

This mitochondrial ROS has been shown to serve many purposes and is not simply faulty metabolic machinery, or if it is, it has been adapted to serve a role. P53 has been shown to accumulate to the mitochondria and bind MnSOD, which in turn causes p53 accumulation to the nucleus [97].

As superoxide is very reactive and can cause cellular damage, mammals have three versions of superoxide dismutase (SOD) to convert highly reactive superoxide to less reactive peroxide. The three forms are found in specific cellular regions, cytoplasmic, mitochondrial, and extracellular (SOD1, SOD2, and SOD3, respectively), and function to detoxify excess superoxide in their respective areas. When mitochondrial SOD is knocked out, T cell maturation is significantly reduced due to significant apoptosis; however, superoxide scavengers rescue this [98].

As the importance of reducing mitochondrial ROS has grown, so has research into cell-permeable mitochondrial antioxidants. Of particular focus in this dissertation is

manganese (III) tetrakis (1-methyl-4-pyridyl) porphyrin (MnTMPyP), M40401 (Galera), and Mitoquinone ($MitoQ_{10}$). Mn (III) porphines such as MnTMPyP are commonly used SOD mimetics, and do not produce fenton chemistry if the manganese is dislodged from the compound, unlike similar iron containing compounds [99]. MnTMPyP works as an ion superoxide oxireductase, meaning it is first reduced by NADPH and GSH and then reduces superoxide to hydrogen peroxide [100, 101]. Long exposures to MnTMPyP results in an oxidized glutathione pool and $NADP^+$ build-up, which would reduce a cell's ability to detoxify peroxide and thus cause increased ROS levels [101, 102]. $MitoQ_{10}$ has been shown to localize to the mitochondria, as the cationic triphenylphosphonium (TPP) cationic group causes rapid accumulation in the mitochondria due to the charge difference from the cytoplasm [103]. $MitoQ_{10}$ also readily reacts with superoxide, forming MitoQH, which disproportionates to mitoQ and $mitoQH_2$ [104]. Galera is a small molecule SOD mimetic, which catalyzes the reaction of superoxide to peroxide at a rate near the native SOD enzyme, thus being able to achieve significant reductions in superoxide levels [105].

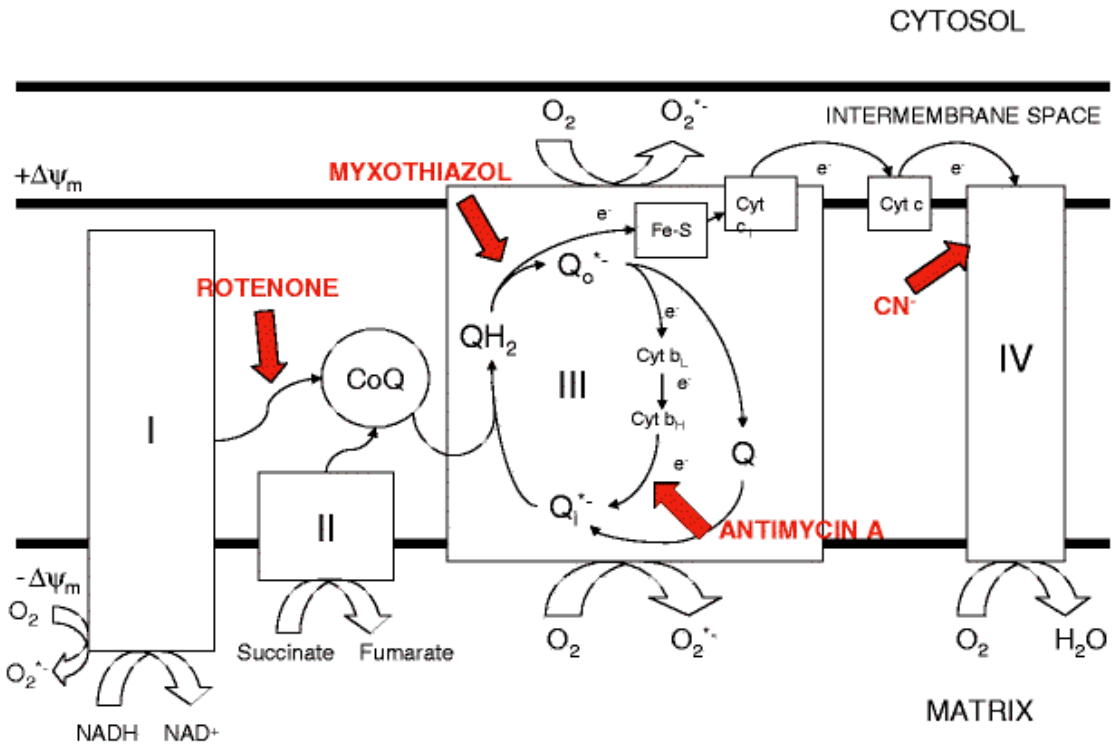

Figure 1. Sites of mitochondrial superoxide, with inhibitors listed in red [106]

Articular Cartilage and Mechanical Load

Understanding normal *in vivo* stress conditions provides valuable insights into the forces that chondrocytes encounter. The articular joints of the ankle, knee, and hip all experience loads from movement based on body weight and motion, involving a variety of stresses onto the tissue, namely compressive, hydrostatic, and shear [107]. Since articular cartilage is responsible for absorbing these loads, the levels of these loads and their effects on cartilage, especially chondrocytes, needs to be understood.

The estimates of what loads these movements impart on the joint vary. Using ground reaction forces, early estimates of tibofemoral average contact stress during walking to be 3.9 times body weight (BW) and increasing to 8 times BW if walking

downhill, translating to approximately 2.4-5 MPa, respectively (70 kg BW, 1100 mm^2 contact area) [108]. More recent estimates using biomechanics and gait analysis have the peak contact load in the knee only reaching 3 times BW [109]. When using these BW load estimates, the contact stresses for simulated gait and deep flexion were much higher: 15-20 MPa, depending on knee position as measured by K-Scan pressure sensors attached to cadaveric knee joints [110]. However, the cadaveric specimens were from a geriatric population from which the authors noted reduced contact area in deep flexion. An even more recent study using a similar pressure sensitive film (Tekscan) reported much lower peak contact stresses from 6 MPa and increasing to 9 MPa with a partial meniscectomy [111]. These more recent studies place the average contact pressure applied by normal walking articulation below 2 MPa [111-114]. However, higher peak stresses can be seen in the hip, with stresses reaching 20 MPa in prosthesis during stair climbing [115].

The strains associated with normal movements *in vivo* are quite low, reaching only 12% after standing on one leg for 5 minutes [116]. Even with additional weight, a lunge still only manages to achieve 30% strain in the knee [117]. It is also important to note that strains are not uniform throughout the tissue. If the cartilage is divided into three zones (superficial, middle, and deep), the largest strain is seen in the superficial zone and this strain decreases with increased depth [118-120]. This increased strain in the superficial zone is associated with decreased mechanical properties through the depth [119], however, similar reductions in cell height and volume are seen regardless of which zone the cells are in when bulk cartilage tissue strains are held at 15% [120].

The effect that mechanical loading has on cartilage/chondrocytes is complicated. There is a significant amount of evidence to show that moderate physiological loading is necessary for tissue maintenance whereas either overloading or underloading leads to cartilage degradation [121]. Obesity and body mass index is strongly correlated with developing OA [122]. An MRI-based reconstruction of patient-specific contact stresses also found that increased contact stress was a statistically significant predictor of OA development [9]. ACL transections, which are thought to alter loading patterns in a joint to cause overloading, causes decreased collagen content, increased water content, and decreased hyaluronan; these are all signs of cartilage degradation [123]. When cartilage is unloaded, the same result of cartilage degradation ensues. Immobilizing canine joints for eleven weeks reduces aggrecan and hyaluronan content, which is associated with a reduction in equilibrium modulus [48, 51]. Similar degradation and cell death was also seen in a sixteen-week rat contracture model [50]. These degradative changes are not recovered after remobilization of the joints [48, 51]. Therefore within a moderate physiological range, loading promotes tissue maintenance. In canines, this moderate loading increased proteoglycan (PG) content [124]. This has also been shown in cultured explants [125]. The tissue loading has been shown to transmit through the cytoskeleton and cause nuclear deformation [126, 127], which is inhibited by dissolving the actin network with cytochalasin D [127].

The loading of isolated chondrocytes is also a growing field, trying to understand intracellular responses of the cells without having the dense extracellular matrix to work around. One such method involves aspirating the cells with a pipette that has an inner diameter that is smaller than the cell diameter. By lowering the pressure within the

pipette as it is in contact with a cell, it is drawn into the pipette slightly, thus deforming it. When a pressure of 10 cm of water is applied over 6 minutes (2 cm/min) to isolated chondrocytes, nuclear and mitochondrial reticulum distortion occurs that is associated with an intracellular calcium increase at one minute in 80% of the cells [128]. The mitochondrial and nuclear distortion is significantly reduced with cytochalasin D or nocodazole treatment when normalized to aspiration length, indicating that the intact cytoskeleton was necessary to transmit these distortions.

Articular Cartilage and ROS

The production of ROS, as its name implies, requires oxygen to be present. Oxygen concentrations in articular cartilage, however, are extremely low at roughly 4-5% at the superficial zone and decreasing to 2-3% in the deep zone [38-43]. In cartilage, this low oxygen concentration is required for glycolytic energy production, as when cartilage is completely deprived of oxygen, glycolytic energy production is severely inhibited [46]. It is not oxygen directly, though, that needs to be present to support glycolysis, as chemical oxidants can rescue glycolysis in an anoxic environment [63].

Therefore it would seem that oxygen-dependent ROS production is required for glycolysis, despite the traditional view on glycolysis, which regards it as an oxygen-independent process. A main source of ROS in oxygenated tissue is the mitochondria, from which *in vitro* studies reveal that 0.12-2% of molecular oxygen is reduced to superoxide, with *in vivo* estimates expected to be lower [78]. Based on the understanding that mitochondria are not used for energy production and are in very low supply in cartilage, it would seem that mitochondria would not be a likely source of ROS. However, in cartilage explants, mitochondrial ROS act to stimulate glycolysis, as when

complex I of the mitochondria is blocked, ROS decreases along with ATP content [4]. Corroborating evidence is seen with the role that mitochondrial ROS has in regulating intracellular pH in chondrocytes, which would vary with glycolytic fluctuations. Here when complex I is blocked, both ROS production and proton efflux are reduced, which can be recovered by external oxidant supplementation in the inhibitors presence [129].

ROS production is also known to be stress related in cartilage, with higher cyclic stresses resulting in higher ROS production, though its origins were not investigated directly [130]. At high stresses, this ROS inhibited PG formation, and the antioxidant ebselen was able to recover this PG synthesis in a dose-dependent manner [130]. Impact injuries on cartilage explants also produce ROS at high enough levels to cause significant cell death [2, 131, 132]. The cell death can be significantly reduced by supplying an antioxidant [2], or blocking complex I of the mitochondria [131] immediately after injury. Dissolving the actin cytoskeleton before the impact also significantly reduces ROS production and cell death associated with impact in the same model [3]. This, coupled with the fact that mitochondrial distortion is known to occur during mechanical stress in cartilage, suggests a link between mechanical stress and mitochondrial ROS production.

OA and RA are also associated with overloading and redox imbalance and mitochondrial dysfunction [133-138]. A more comprehensive understanding of loading effects, especially with ROS release, would enhance not only our understanding of normal cartilage function, but also how it can be perturbed, as it is in arthritis. Currently we know that both traumatic joint injury [139] and overloading can significantly increase risk of developing OA [54, 55], and once arthritis develops, excess ROS are detected by

increased lipid peroxidation [140], nitric oxide and nitrotyrosine [141, 142], oxidized immunoglobulin G [143], and oxidized DNA damage [144]. Mitochondrial DNA also accumulates damage in OA [145], which is thought to be caused by mitochondrial ROS [146]. This is likely a result of weakened antioxidant defenses observed during OA, including decreased concentrations of MnSOD [147-149] and glutathione peroxidase [148]; however a causal relationship has yet to be established. Combining these concepts with the fact that ROS is needed for matrix metalloprotease (MMP) activation [150, 151] provides a dangerous scenario for amplifying the matrix degradation seen in OA [152-154]. The proinflammaotry cytokine, IL-1β, is also known to increase NO synthesis, which decreases matrix synthesis, although inhibition of nitric oxide synthase can reverse this path [155].

Dissertation Aim and Tissue Model

This dissertation project aims to provide a link between a mechanically-activated ROS production pathway and energy production in cartilage. A more complete understanding of this process could provide insights into the mitochondrial abnormalities that have been discovered in OA [156], and provide ideas for intervention in overloading scenarios, or even proactive measures for preventing disuse atrophy associated with prolonged unloading.

To study various biological responses of cartilage in a controlled environment, bovine stifle joints were obtained from a local butcher shop (Bud's Custom Meats, Riverside, IA). The joints were dissected under sterile conditions, and small square explants (~15 mm width) were carved from the lateral tibial plateau. The pieces were

taken so as to minimize meniscus-covered and non-weight bearing regions (Figure 2), and the subchondral bone was left attached to allow fixation in loading devices.

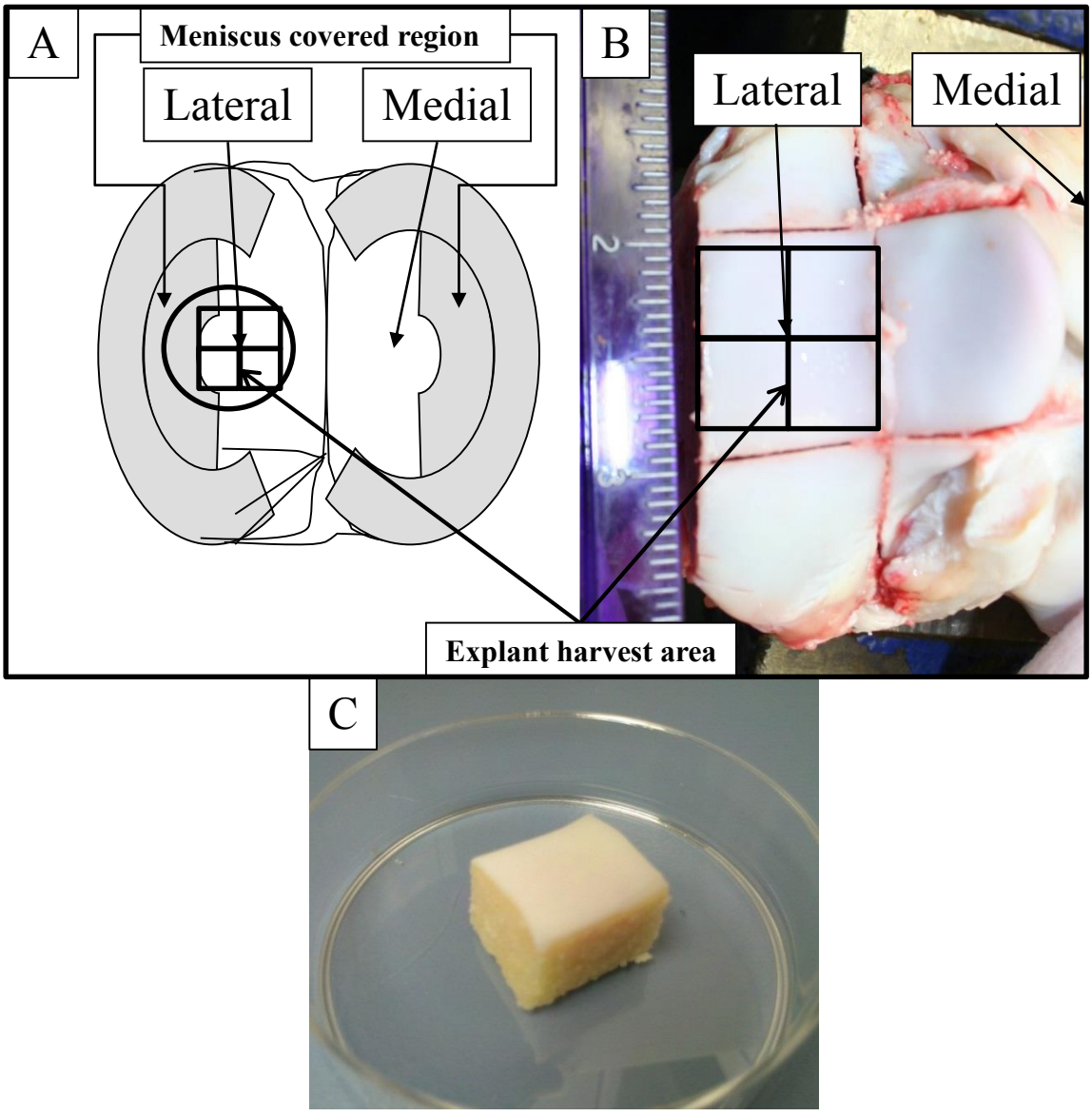

Figure 2. (A) Diagram of the knee surface, showing the region where explants are harvested. (B) Actual bovine tibial plateau with harvest site marked. (C) Typical explant when cut into quarters from the harvest site

CHAPTER 2:

DEVELOPMENT OF A MODULAR MECHANICAL STIMULATION SYSTEM FOR ARTICULAR CARTILAGE

Introduction

Cartilage explants are uniquely difficult to study *ex vivo*. Because the biosynthetic activity and phenotypic characteristics of cartilage are heavily dependent on its structural and physiological environment, the challenge lies in effectively mimicking these conditions in a culture setting. This chapter focuses on the process by which the current mechanical stimulation machine was designed. The techniques to stimulate cartilage for biochemical response studies have been evolving for the last 30 years. Early stimulation methods ranged from electric or mechanical stretching [157], to resting weights on an indenter [158]. Most impressive was the development of a cyclic compression machine, which was computer-controlled and had oscilloscope and pen register data recording capabilities [159]. More modern techniques employ calibrated pneumatic [130, 160] or hydraulic pressure [161], or use stepper motors to apply loads [162].

The mechanical stimulation machine was designed according to a simple set of criteria: it needed to be easy to operate and clean as well as be able to fit inside an incubator. Also, ideal materials would be autoclavable and inert to biological tissues. In the final design, National Instruments components and LabVIEW were used to drive and control stepper motors with affixed cylindrical platens, while continuously monitoring load feedback with an inline load cell. Also, a custom built miniature stand and media

chamber allowed for rigid fixation, media immersion, and usage in a low oxygen incubator.

The final loading platform was the result of many iterations, first building an inexpensive device, obtaining promising results, and then developing the device further. The initial machine was a hand-driven chamber containing a micrometer (Figure 3). The cartilage thickness was approximated as the average of four edge thickness measurements. The micrometer was then turned at a set rate (0.001 in/s) until the desired tissue strain was achieved. The micrometer was fixed in place, and then set inside a low oxygen incubator for one hour.

Figure 3. Initial strain application method involved manually spinning a micrometer to apply specific strains by compressing cartilage against a polyethylene block. The strain was held constant for one hour.

This design proved to have too many uncontrollable factors. The ideal displacement application was 0.001 in/s; however, at cartilage tissue strains greater than 20%, the force required to twist the micrometer led to inconsistent movement speeds and force applications. To address this, we designed a computer-controlled mechanical loading platform.

Design Parameters and Materials

The computer-controlled platform was designed with consideration of the same basic criteria as the hand-driven platform and was built to perform displacement/load-controlled cyclic compression. The maximum stress expected was 2 MPa, with the

largest loading area being an 8 mm cylindrical indenter (50.2655 mm^2) necessitating force generation of 100.5 newtons (22.6 lbf). Cartilage was not expected to exceed a thickness of 3.5 mm, and the highest frequency of loading expected was 1 Hz. Assuming complete compression was achieved (overestimation), a travel speed slightly higher than 7 mm/s would be required due to the time needed to change direction.

Considering these parameters, the Ultramotion Nema17 Digit linear actuator was chosen to apply the force; it is capable of traveling at 5 in/s (101.6 mm/s) and applying 100 lbf (444.8 N). A computer fitted with a National Instruments motion control PCI board (NI PCI-7334), in conjunction with a National Instruments motor drive (NI MID-7604), both controlled and powered this unit. An attached optical encoder, which accurately measures rotational changes in the stepper motor shaft position (2000 counts/rotation), monitored the displacement position. When coupled with the linear actuator's lead screw thread pitch (0.025 in/rev), this can accurately determine linear displacement.

To measure the force application, a National Instruments data acquisition (DAQ) board (NI PCI 6014) was also installed into the computer with an NI BNC-2110 connecter block used to interface between the signal and the DAQ board. A tension/compression load cell with a 50 lb limit was chosen (Honeywell type 34), as they were already available, and it would be able to handle more than double the maximum force that our tests should apply. The load cell was excited by a signal transducer amplifier (Honeywell UV-10), which provides a 10 volt power supply to the load cell, and converts the resultant millivolt signal, which is based on the applied load back to volts. This output signal is then passed to the BNC-2110 for measurement by the

computer. National Instruments LabVIEW will be used for programming device control and data recording as it supports all National Instruments components and provides the best support for custom control programs where automation and rapid data monitoring is required.

For materials that will come into contact with media, biocompatibility is a high priority. Polysulfone is biocompatible [163, 164] and was used to fabricate the culture chambers and explant fixators. It is also autoclavable, thus making sterilization easy. Due to the corrosive environment in which the cylindrical indenter will reside during loading, we used 316 stainless steel.

Results

The design frame was comprised primarily of custom cut stock material. Aluminum composed the majority of the frame, with a 2" cylindrical rod creating the vertical post to hold everything up. High-density polyethylene was used as the base to shield the attached load cell from the stepper motor, which was in contact with the aluminum to reduce electrical noise. The base was affixed by a single set screw. The stepper motor was affixed to the rod by a tension-driven one inch thick aluminum adjustable rectangular mount (Figure 4). This simple design worked well; however, improvements were needed in the specimen holder and chamber design, as the silicone o-ring developed a tendency to leak (Figure 4). Also, having only one loader limited our testing throughput, so three loading stands were built to accommodate (Figure 5).

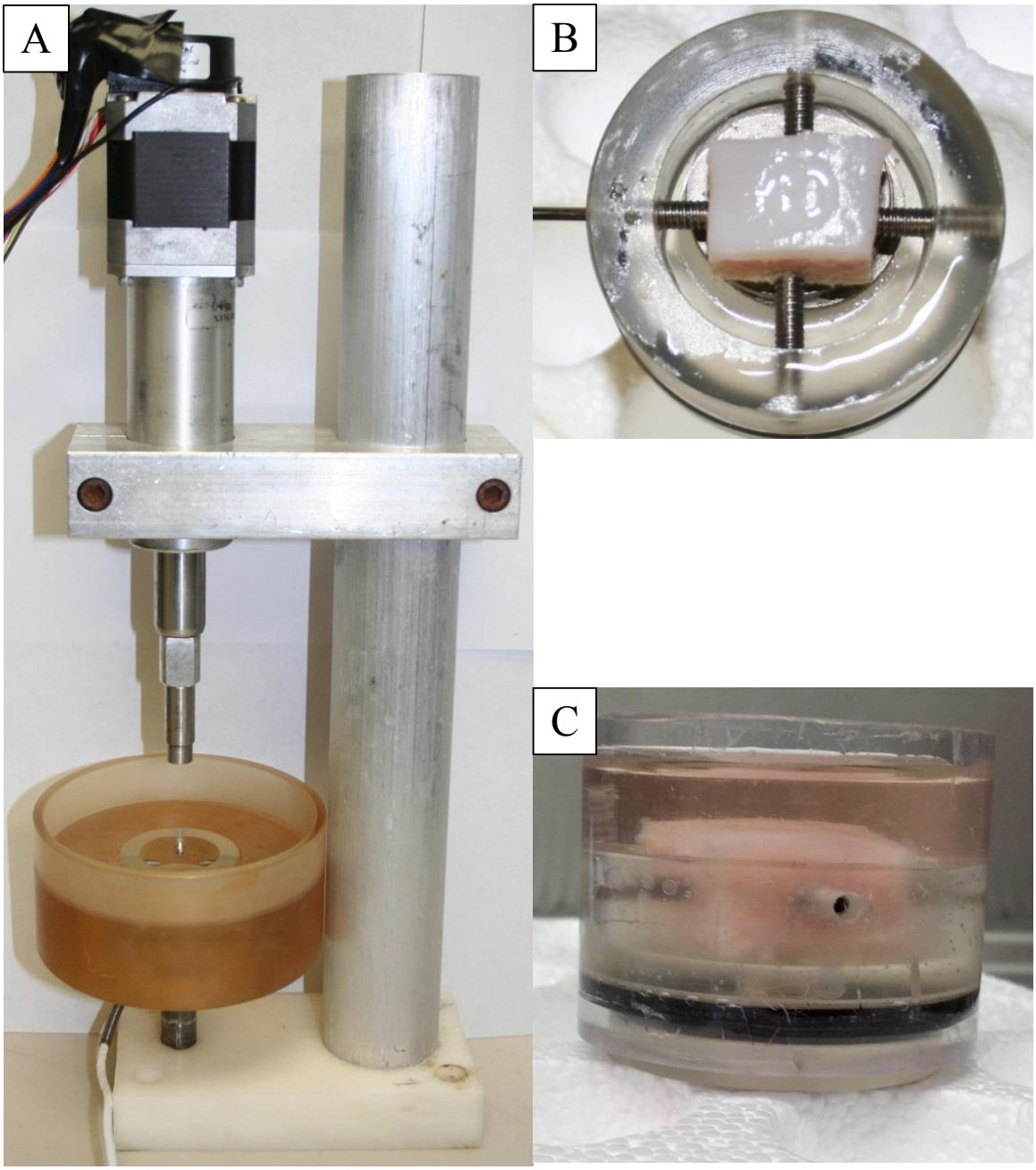

Figure 4. (A) The initial loader fully built. (B) Specimen fixator shown with affixed cartilage. (C) Silicone o-ring (black ring) used to seal the hollow chambers.

One stand base was built for use in our explant model, but also as a platform to allow stimulation of cells in scaffolds grown in a 48-well microplate (See Appendix). Also, the media chamber was redesigned to be completely sealed with the set screw now affixed to the bottom of this piece, thus separating it from the explant fixation. The explant fixator now press fits into the media chamber, which solved the leaking problem and allows for culture of the explant/fixator combo, which was not possible before due to the set screw being attached to the bottom of this piece. Other improvements include the addition of hand screws for all adjustable parts, removing the need for a hex wrench. The current computer system and components can accommodate up to four simultaneous stepper motor/loading sessions, but the current program only runs two concurrent stepper motors. Expanding to four stepper motors would only require copying the motion control portion of the program to accommodate the additional motors. The front panel of the LabVIEW program is shown in Figure 6, which includes generalized instructions on how to operate the machines.

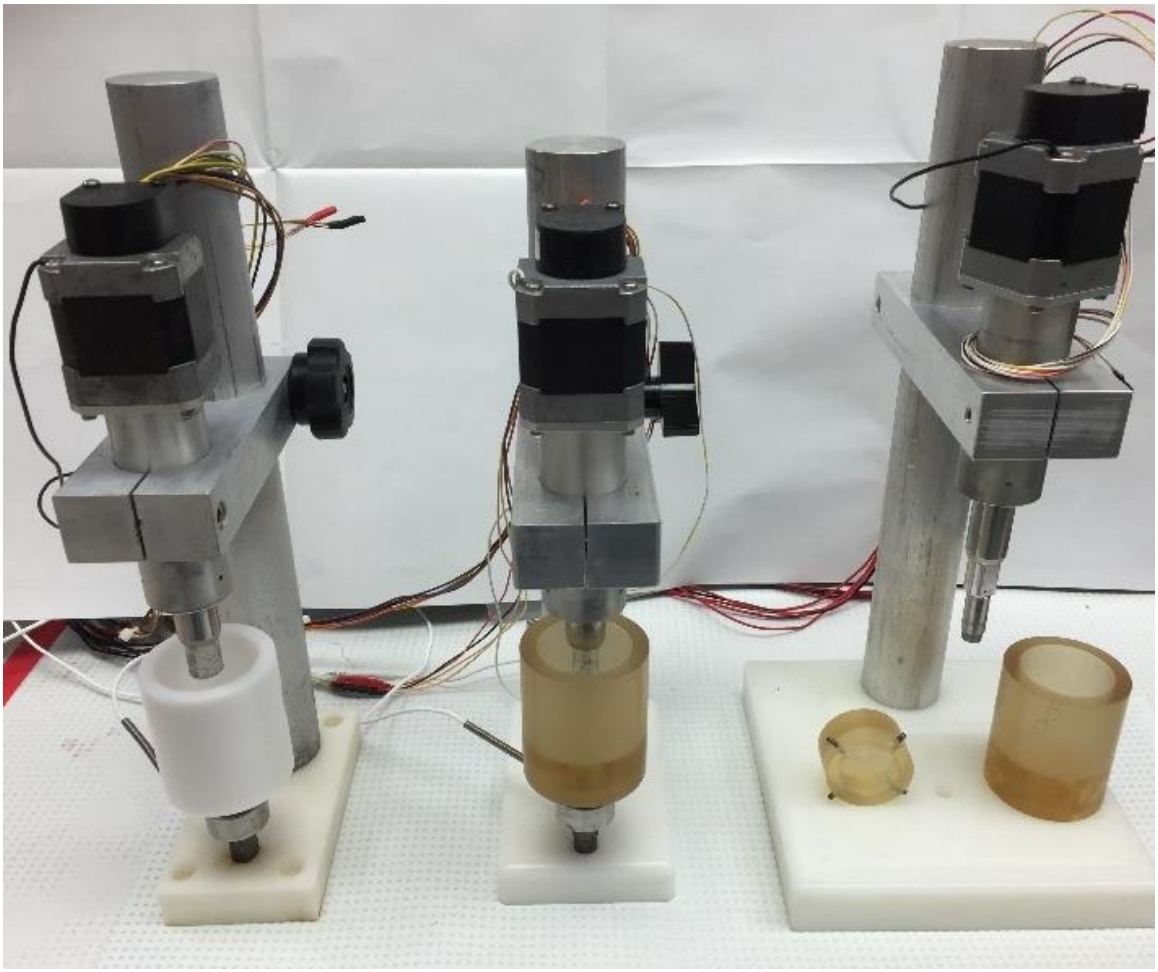

Figure 5. Current loading machines, showing the fully sealed media chamber and removable fixator that can be cultured with the cartilage explant for multiple day loading sessions.

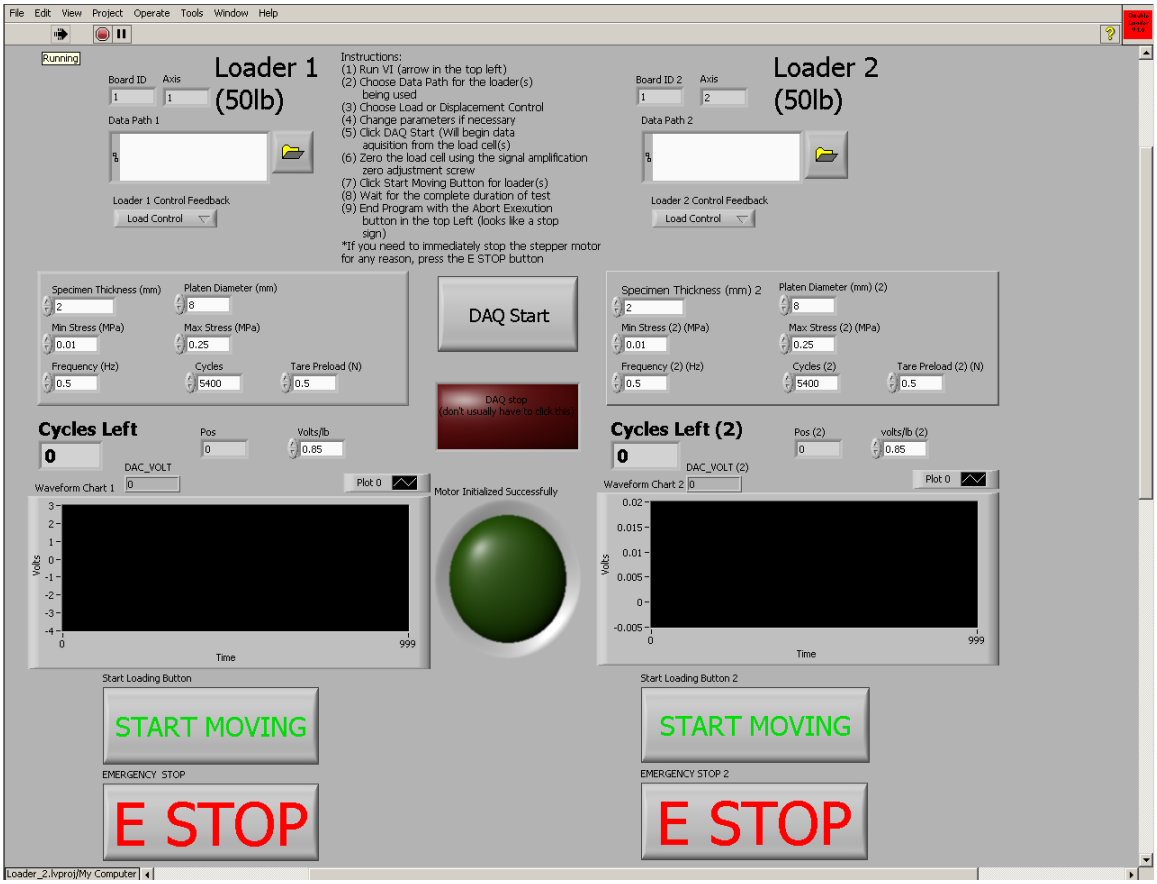

Figure 6. Front panel for the latest LabVIEW program, which controls and records mechanical stimulation parameters

The LabVIEW program is designed around the paradigm of the LabVIEW state machine. The program will transition between states based on either user input, sensor data, or detected errors. In following the instructions, the user would first run the program. This starts the initialization of all the components, and will alert the user upon successful initialization. A diagram of these initialization checks can be seen in Figure 7. Next the user would define the selectable variables to start the state machine. These variables include input of the file path and name, specimen thickness (if applicable), control mechanism (load or displacement), the associated constraints of stress/load or

displacement/strain, and the number of cycles and frequency at which the test will be run. The data acquisition from the load cells is then started by pressing the DAQ start button. This button initializes the data acquisition board and starts a timed loop, which reads the value of any attached load cells every five milliseconds, stores that information in a local variable, and plots the load cell value on a graph. Any errors that occur during initialization will elicit a dialog box notifying the user where the error occurred and stop the program (Figure 7). After successful initialization, the user would manually adjust the zero point on the load cell using the signal amplifier to account for the weight of the specimen and holding container.

Figure 7. Logic state chart for initialization steps with indications where erros would occur and signal

Next, the user would press the "Start Moving" button, which would transition the program into the motion state in which the stepper motor will start moving to initialize contact with the cartilage surface. In stress/load feedback control, the speed at which the motion contact is set to 1% of the cartilage thickness (as entered by the user). This is usually between 0.01 mm/s to 0.03 mm/s. Once contact with the surface of the cartilage is established by the load cell reporting a load > 0.1-0.5 Newtons (user adjustable), the

velocity is increased by a data derived function (Equation 3). This velocity is then used for the first cycle to depress the piston until the desired force is measured by the load cell.

Equation 3. Equation to determine the initial stepper motor velocity after contact has been established.

$$(Stress\ (MPa) * 0.5((Strain\ \%)/MPa))/(1/2 * Period\ (s)\ ) * Thickness\ (mm) = Velocity\ (mm/s)$$

Once the compressive force reaches its target, the stepper motor reverses the velocity until the stepper motor reaches zero load or passes the initial contact point displacement. It then checks to see if the number of cycles has reached the set value. If it has reached the set cycle number, the stepper motor will return to its starting position and wait for further user input. If it did not reached the set cycle number, it will compare the time it took to complete the last cycle to the desired cycle period based on the frequency set. If it is too slow or fast by >10%, it will increase or decrease the velocity by 5% to correct in the appropriate direction. If the period is off by <10%, but >2%, it will increase the velocity by 2%. These two checks ensure that the total test duration is within 5% of the predicted duration based on both cycles and frequency.

The data recording is set to be handled in one of two ways: (1) continuous recording at the pace of the timed measurement loop (every 5 ms) or (2) only recording after a movement constraint has been reached. Each recording style has its respective pros and cons, which is why both options are available. Recording continuously provides

intra cycle information, but produces excessively large data files that can be cumbersome in spreadsheet applications. Recording only when a constraint has been reached produces a much smaller data set, but with the loss of intra cycle information. The dynamic stress experiments reported below used the constraint-based recording method; however, the continuous recording was used to develop a program to measure the friction of articular cartilage (See Appendix). A flow chart to illustrate the program logic and flow with constraint-based recording can be seen in Figure 8.

The current version of the dynamic loading program is an invaluable tool that has allowed for expedited research into cartilage mechanobiology. The design of this program is intentionally modular, and it has provided the framework to develop multiple other programs for a variety of devices that are controlled by stepper motors (See Appendix).

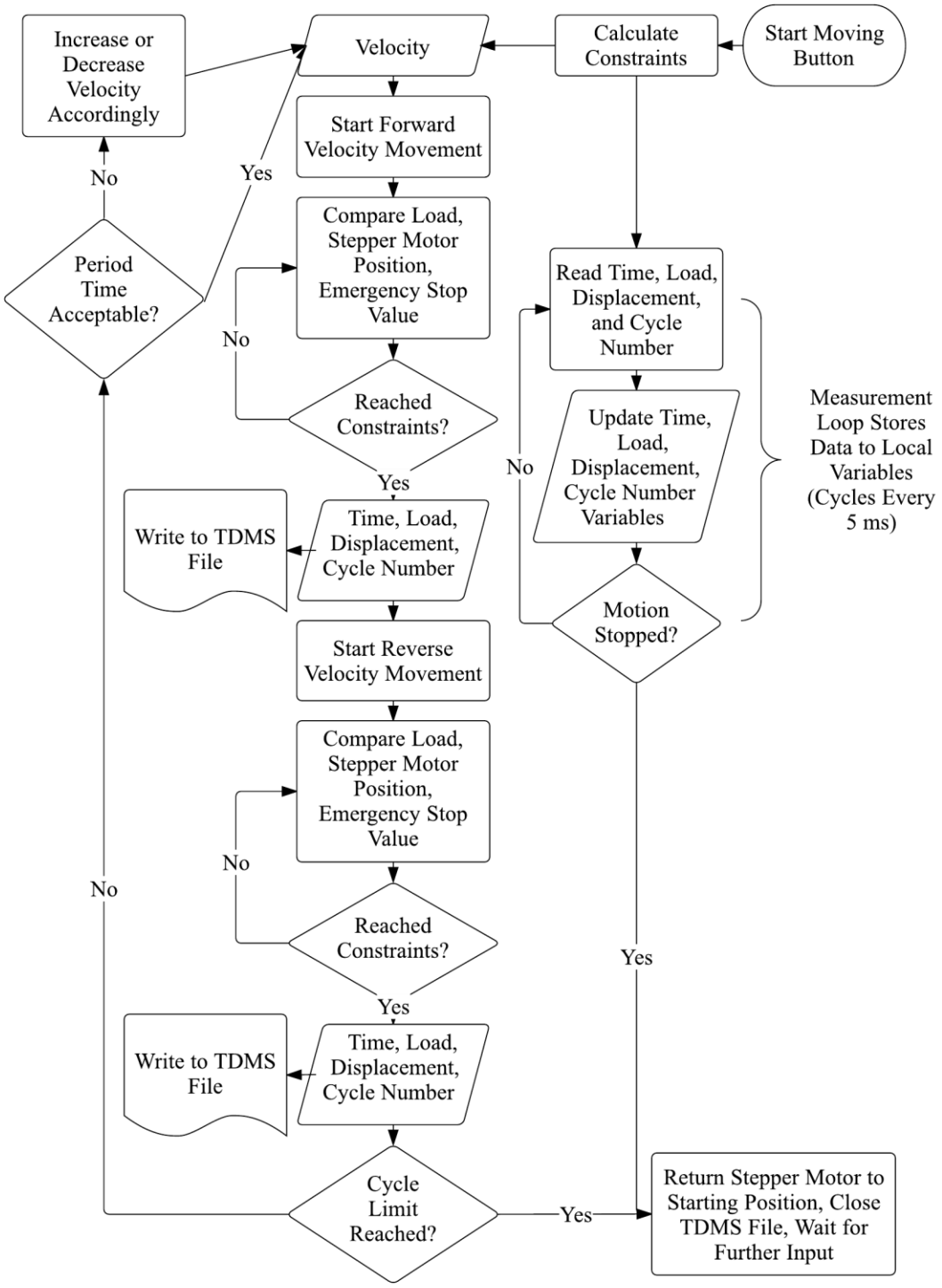

Figure 8. Flow chart showing the motion control and data recording logic used in the dynamic loading program.

CHAPTER 3:

STATIC MECHANICAL STRESS INCREASES MITOCHONDRIAL ROS PRODUCTION IN ARTICULAR CARTILAGE

Introduction

We and others have previously shown that ROS are deleterious in overloading conditions, in that one hour of excessive cyclic loading (5 MPa) causes significant cell death. This effect could, however, be attenuated with various antioxidants, such as N-acetylcysteine (NAC), vitamin E, the SOD mimetic (MnTBAP), or even the nitric oxide synthase inhibitor, N-Nitro-L-arginine methyl ester (L-NAME) [1]. While these experiments did not demonstrate that ROS was released in response to cyclic loading, they did indicate that blocking ROS post-injury was beneficial.

Single blunt impact injury was also linked to ROS release. First we observed that NAC spared chondrocytes from death 48 hours after 7 J/cm^2 impact, and that delaying treatment by several hours was still beneficial [2]. This led us to believe that there was an increased oxidative environment after impact, and that the cells were not immediately killed from mechanical forces. This theory was confirmed with increased dihydroethidium (DHE; ROS probe) staining over time as a result of a blunt impact [131]. DHE is an oxidation sensitive probe that can react with various ROS, though the superoxide-specific product has a much higher fluorescence intensity, making it somewhat more sensitive to this species [165-167]. Here, rotenone was used to block complex I of the mitochondria on these impacted explants, which significantly reduced the ROS levels, with pre-administration showing the most reduction in ROS and longer

delays showing less effect [131]. This treatment also prevented most of the cell death associated with the impact, again even with up to a two-hour delay in treatment.

These early studies provided the basis that mitochondrial-derived ROS are produced in response to injurious loading and impacts. Therefore, the next step was to assess if the ROS observed in impact injuries could be modulated by varying the stress applied to cartilage over a one-hour testing period. We hypothesized that ROS production would be proportional to tissue strain and remain sub-lethal within normal strain range. To test this, we measured tissue strain, ROS production, and chondrocyte viability in osteochondral specimens exposed to increasing static compressive (0.05- 1.0 MPa) and hydrostatic (0.5-1.0 MPa) stresses. Chemical treatments of rotenone, cytochalasin B (Cyto B), and manganese (III) tetrakis (1-methyl-4-pyridyl) porphyrin (MnTMPyP) were also tested to assess the location, mechanotransduction pathway, and species of ROS produced by static stress. Rotenone blocks the ubiquinone binding site in complex I inhibits reverse electon flow associated superoxide production. Cytochalasin B prevents actin from polymerizing and thus disrupts the cytoskeletal network. MnTMPyP is a superoxide dismutase mimetic that would catalyze the conversion of superoxide to peroxide. These chemicals helped to determine whether the ROS originated in mitochondria, were cytoskeleton-dependent, and were primarily superoxide.

Methods

After harvest, osteochondral explants were equilibrated in phenol red-free media containing 10% FBS for 48 hours in low oxygen conditions (5% O_2, 5% CO_2, 90% N_2) at 37°C. This 'equilibration' allows the metabolic activities of cultured cartilage to adjust to the new medium and allows time for any damage ensued from harvesting to subside.

At the time of these experiments, only one loader was available (Figure 4), as the development of the multiple station dynamic loading system was not yet complete. Instead, a previously designed LabVIEW creep test program [162] was modified to be used with a single inline load cell.

First, cartilage thickness was measured with an ultrasound device calibrated to measure the distance between the cartilage surface and the subchondral bone (Olympus NDT, See Appendix for validation). The explant was then fixed in the holder using set screws to secure to the subchondral bone and submerged in fresh media. Using the mechanical loading device (Figure 4) and an 8 mm stainless steel flat cylindrical indenter, various static compressive stresses were applied to explants for one hour in low oxygen conditions. The stepper motor slowly depressed until it made contact with the cartilage, denoted by the 0.1 N force registered by the load cell. It then proceeded at a constant strain rate of 0.1 /s, as based on the cartilage thickness, until it reached the chosen stress level. This stress was then held for one hour, as the cartilage depressed. Feedback was recorded by the LabVIEW program.

To apply hydrostatic pressure, individual explants were placed inside heat-sealed bags with 10 mL of low oxygen-equilibrated phenol red-free media and placed inside a custom-built pressure chamber [168, 169] (Figure 9). This chamber was filled with water to use as a pressurizing liquid and sealed. The entire chamber rested in a temperature-controlled water bath set to 37°C. A LabVIEW program controlled a stepper motor (Ultramotion, Nema 23) with a hydraulic piston attached while a pressure transducer (Sensotec FP2000) monitored pressure. The hydraulic piston was depressed at 0.0625 in/s (1.5875 mm/s) until the chosen pressure was reached. Then only small adjustments

were made if the pressure differed from the set by ≥ 2%. This static hydrostatic stress was applied for one hour, after which specimens were removed from the heat-sealed bags and processed.

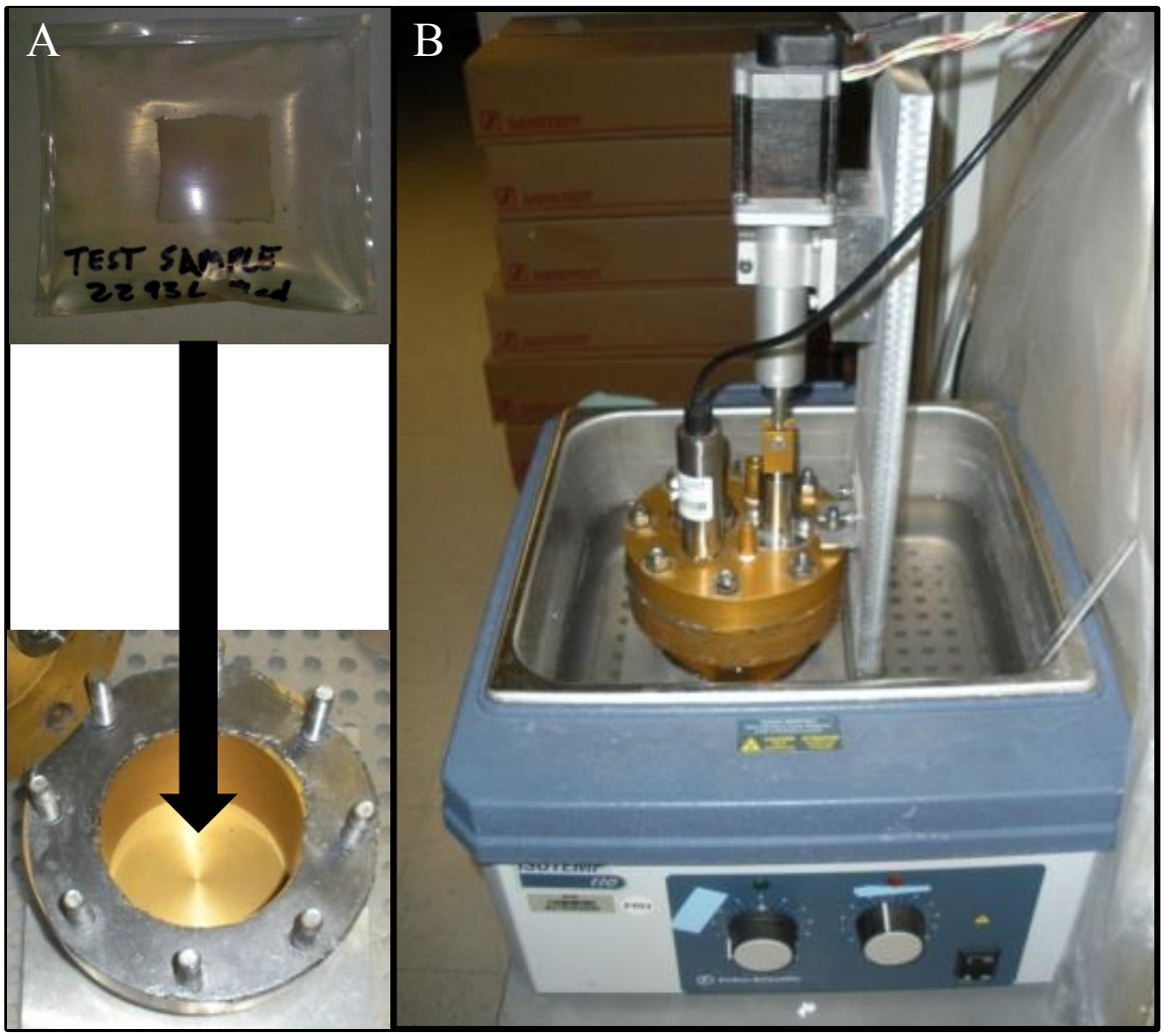

Figure 9. Explant in heat-sealed bag seen in A with arrow pointing to the chamber which it was placed in, which was then filled with water and sealed. B shows the full stepper motor drive hydrostatic pressure chamber sealed and placed inside a water bath to maintain the desired temperature within the chamber.

Immediately following any stress application, the explants were stained with various fluorescent dyes. The explants were incubated in media containing 1 µM Calcein AM (live cell indicator, Invitrogen) and 5 µM dihydroethidium (ROS indicator, Invitrogen) or 1 µM ethidium homodimer (dead cell indicator, Invitrogen) for thirty minutes. After the incubation, the explants were moved into fresh media without fluorescent dyes, and confocal microscopic images were taken to measure the amounts of ROS or cell death after the stress application. Three z-stacked images were taken throughout the central explant region (contact region for static stress) to a depth of roughly 200 µm at 20 µm intervals. An automatic image analysis program, Quantitative Cell Image Processing (QCIP™) was developed and used to count cells in the images [168, 169]. Cell counts for live cells and the associated ROS stained or cell death stained cells are displayed as a percentage of total cells stained with either stain.

To determine if superoxide was the source of DHE staining, we pre-treated the explants with 100 µM MnTMPyP for one hour prior to and during static stress application. MnTMPyP acts as a SOD mimetic converting superoxide to peroxide. Then to determine if these ROS were released from mitochondria, explants were pre-treated for one hour with 2.5 µM rotenone before and during static stress application. Rotenone blocks the ubiquinone binding site in complex I. To assess the role of the cytoskeleton in mechanical stress-induced ROS production, explants were pre-treated with 20 µM cytochalasin B for four hours before stress application. A flow chart depicting the experimental design can be seen in Figure 10.

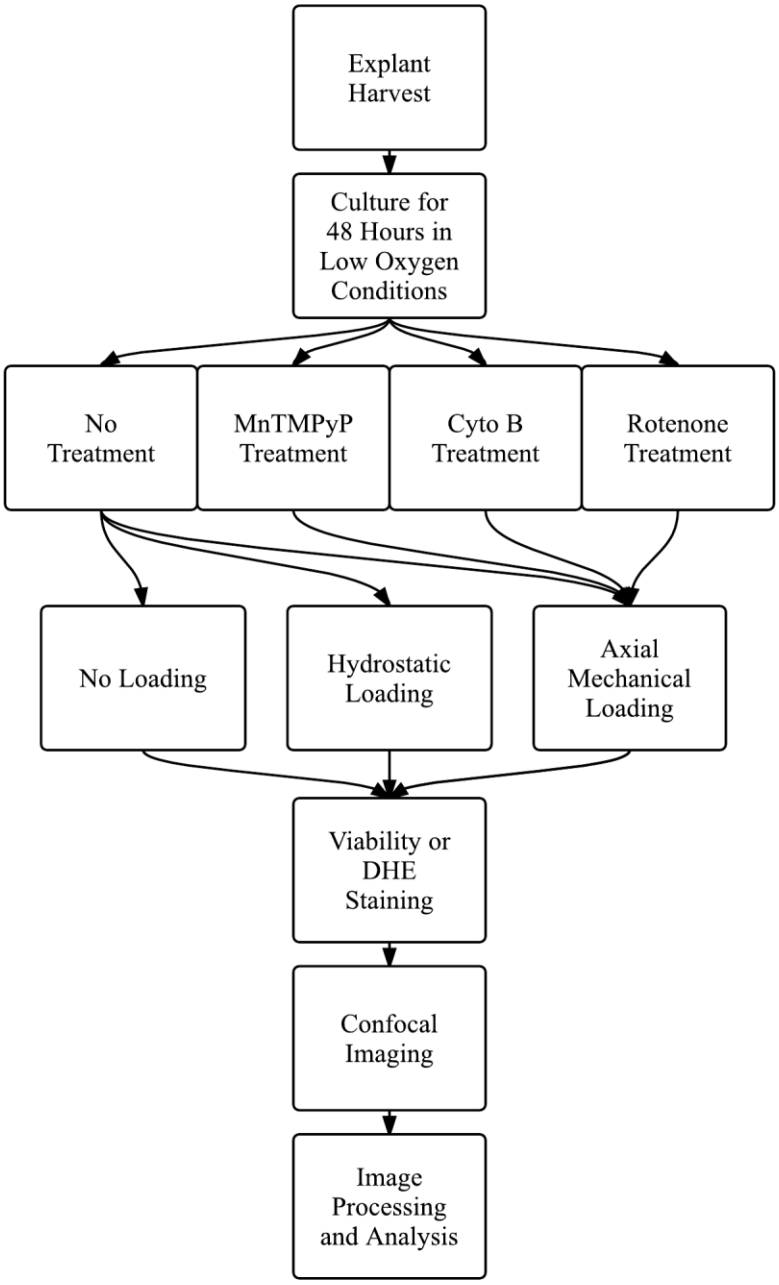

Figure 10. Flow chart showing the experimental design for explants undergoing one hour of static stress application.

Results

The number of explants used for these experiments was at least 5 for every group. Representative strain curves for each stress are displayed in Figure 11. Average maximal strain increased with increasing stress, but because strain never plateaued, the system must not have reached steady state after one hour. The average strain for each group was 13.2 ± 5.8 %, 18.4 ± 2.9 %, 32.3 ± 3 %, 54.2 ± 7.1 %, and 71.1 ± 3.1 % for 0.05, 0.1, 0.25, 0.5, and 1.0 MPa, respectively (Figure 11).

The follow-up staining and confocal microscope images showed that increased stress and strain both correlated with increased ROS (Figure 12, Figure 13, Figure 14) [169]. The average percentage of cells that were above the intensity threshold for DHE increased with each stress. The percentage of stain-positive cells were 2.7 ± 4.3 %, 5.9 ± 6.3 %, 10.3 ± 6.6 %, 35.6 ± 18.3 % , 56.6 ± 12.3 %, and 76.7 ± 8.7 % for 0, 0.05, 0.1, 0.25, 0.5, and 1.0 MPa, respectively (Figure 12, Figure 13). When the maximal strain of each explant was plotted against the average number of positively stained DHE cells for the three confocal images, it formed a positive linear relationship ($r^2 = 0.87$, Figure 14). Cell death, quantified as percent of cells above the threshold that stained positive with ethidium homodimer, was 3.9 ± 3.2 %, 2.6 ± 3.8 %, 7.4 ± 7.1 %, 7.5 ± 8.3 %, 12.7 ± 8.1 %, and 38.3 ± 10.0% for 0 – 1.0 MPa, respectively (Figure 13). An exponential, rather than linear, relationship was observed between cell death and maximal strain for each explant (Figure 14). Cell death only occurred at supraphysiological strains >40% (Figure 14). Lack of physical distortion, namely hydrostatic pressure, did not show the same ROS response as compressive stress (Figure 13).

Treatment with the superoxide dismutase mimetic, MnTMPyP, showed that ROS could be inhibited at both 0.5 MPa (Figure 14) and 1.0MPa (Figure 15, Figure 16). This reduced the percentage of cells stained with DHE to 16.5 ± 13.6 % from 56.6 ± 12.3 % at 0.5 MPa. At 0.25 MPa, the percentage was reduced to 4.8 ± 4.62 % from 35.6 ± 18.3 %. Dissolving the cytoskeleton with cytochalasin B or blocking complex I of the mitochondria with rotenone significantly decreased ROS at 0.25 MPa (13.1 ± 14.4 % and 11.8 ± 10.5 % respectively) but were ineffective at 0.5 MPa (55.5 ± 14.4 % and 41.4 ± 23.2 %, respectively) (Figure 15, Figure 16).

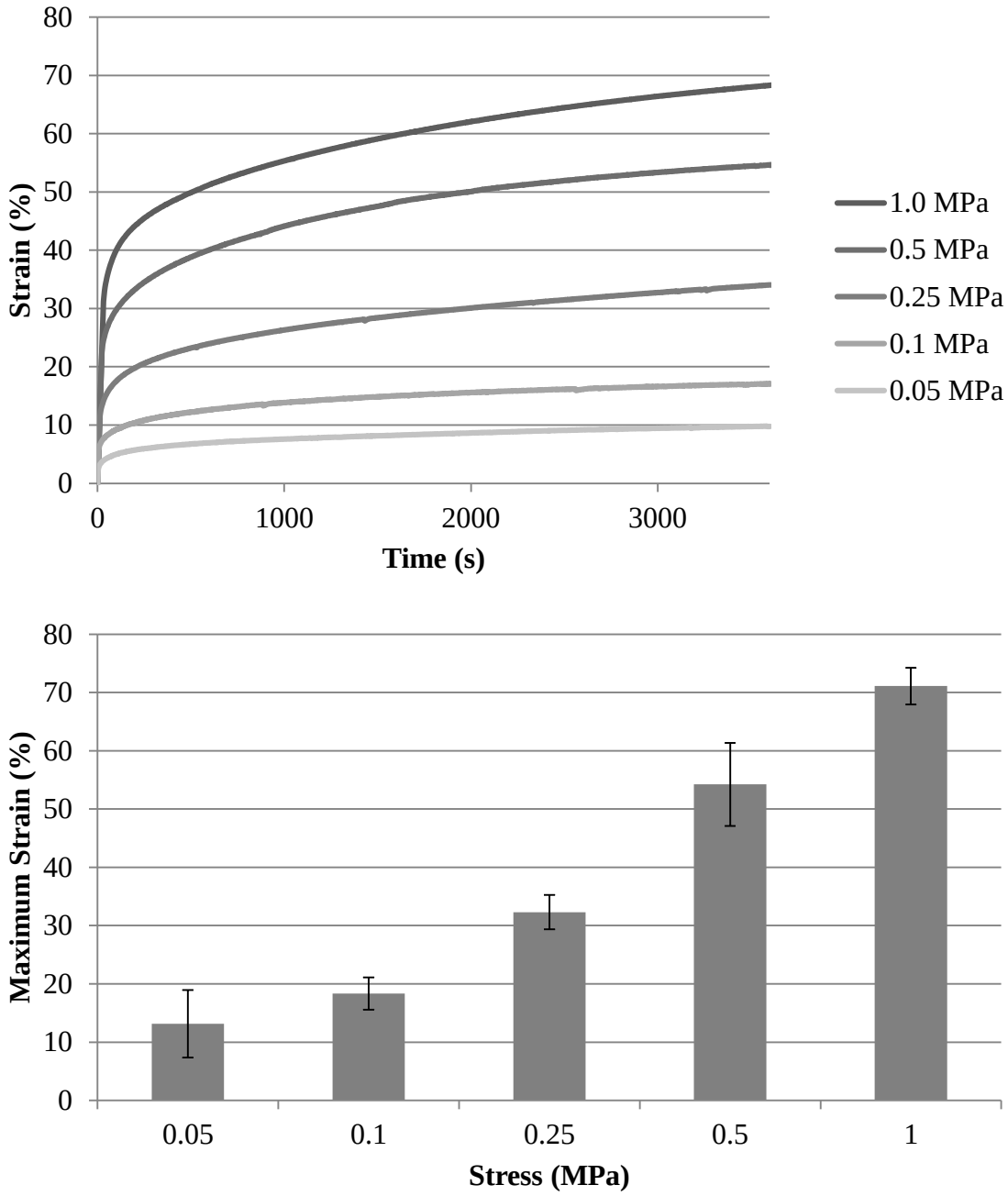

Figure 11. Top graph shows representive strain plots over time for each of the static stress groups. Bottom graph is the average maximum strain achieved for all explants in each stress group, error bars indicate the standard deviations.

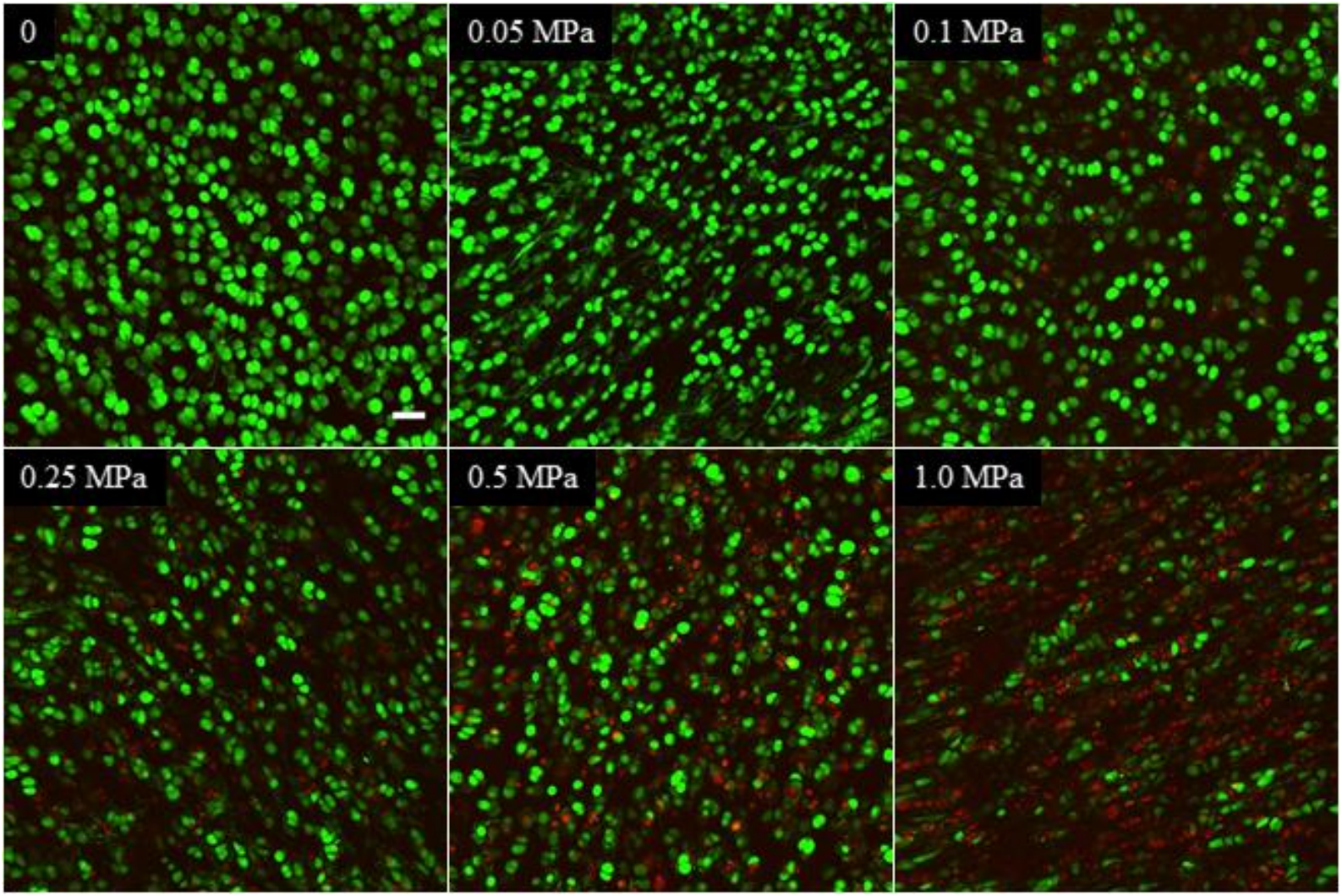

Figure 12. Calcein AM (green, live cells) and DHE (red, ROS) staining seen increasing by stress applied for 1 hour

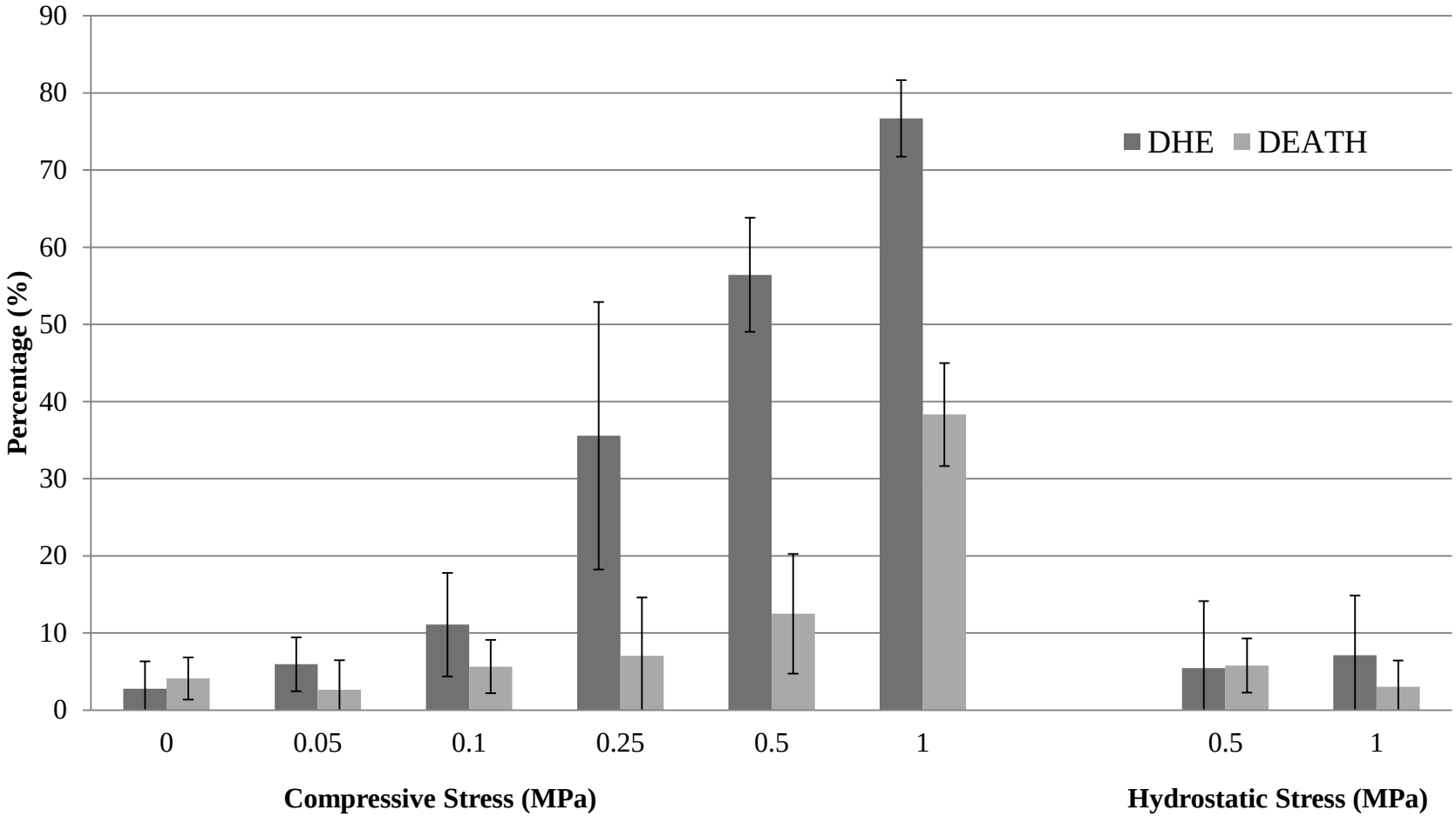

Figure 13. Compilation of image analysis data for specimens under varying compressive or hydrostatic stresses. ROS (DHE) increases steadily for each compressive stress, while cell death only increases significantly at the highest compressive stress.

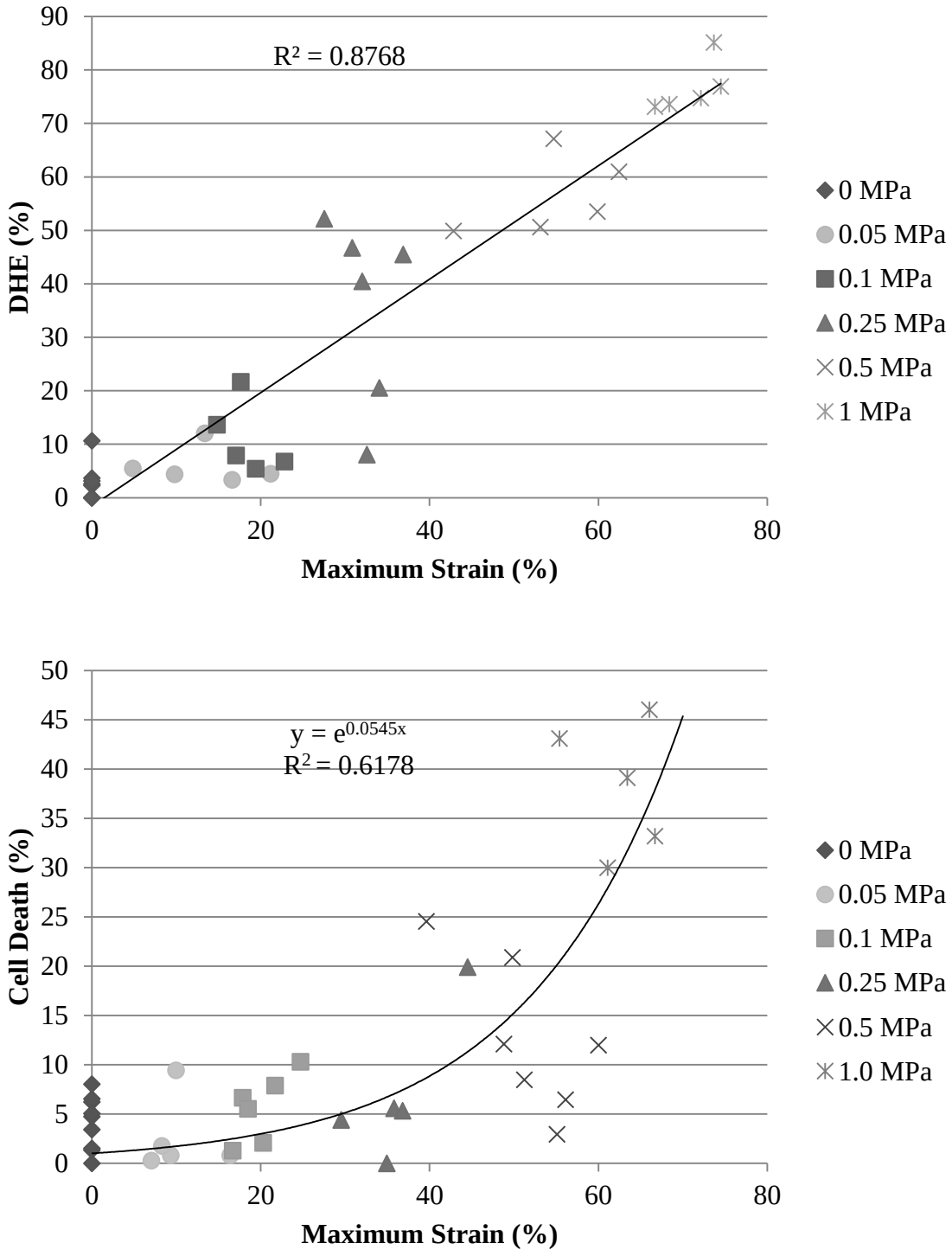

Figure 14. Top Panel: Regression analysis of the percentage of cells stained with DHE compared to the recorded strain at the end of the 1 hour static stress application. Right Panel: Cell death plotted against this same maximum stress

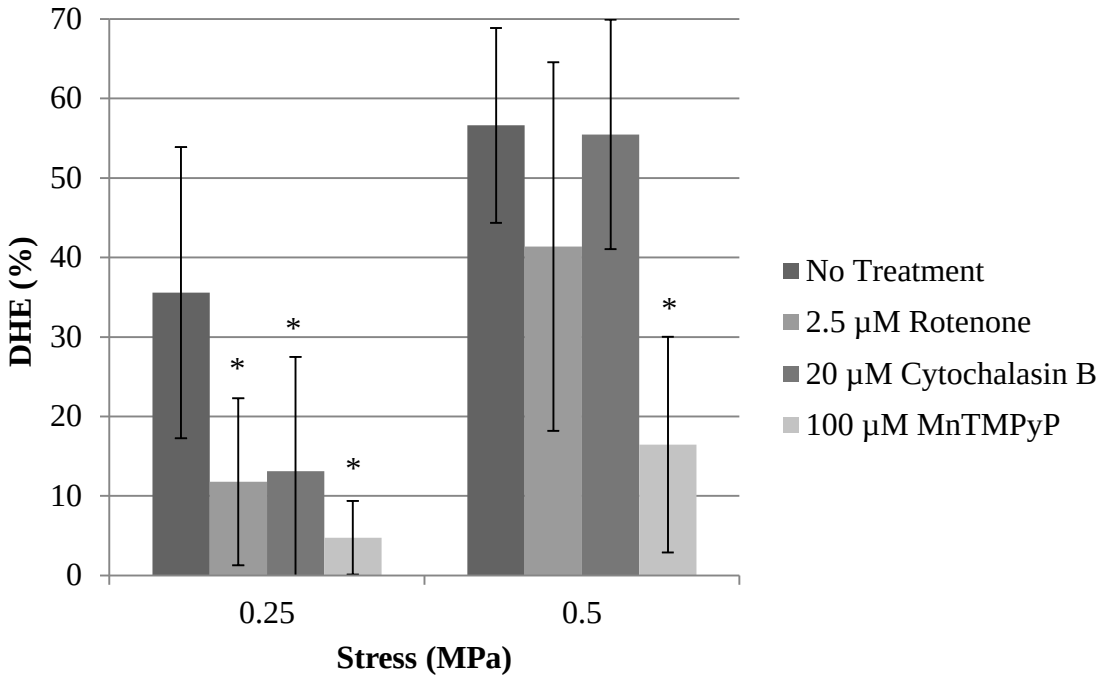

Figure 15. Chemical treatment effects on static stress application at 0.25 and 0.5 MPa. Rotenone, Cytochalasin, and MnTMPyP all reduce ROS at 0.25 MPa, but only MnTMPyP is able to reduce ROS at 0.5 MPa. Significance against untreated control at same stress denoted by asterisk $p < 0.05$.

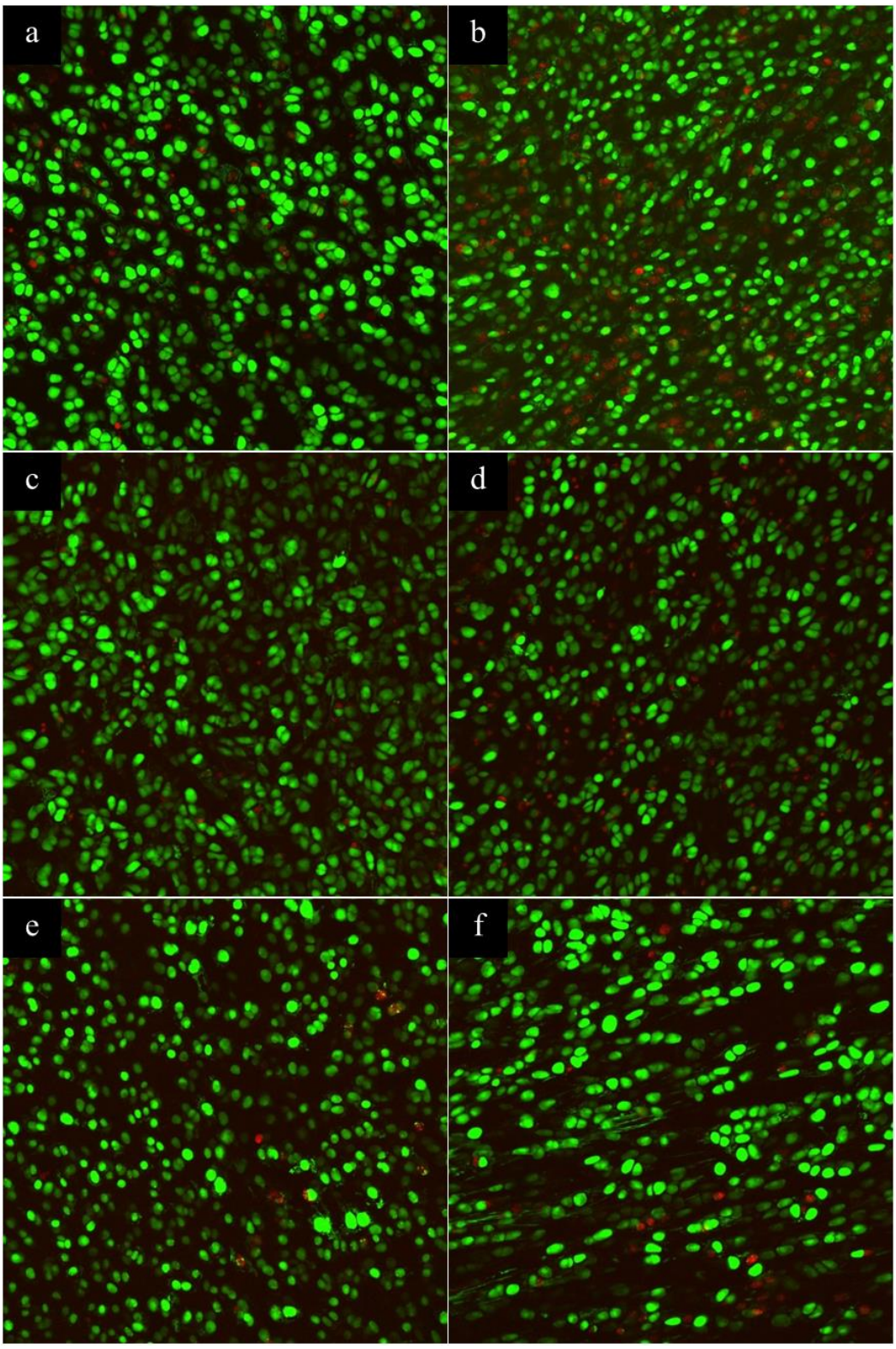

Figure 16. Calcein AM (green, live cells) and DHE (red, ROS) staining from rotenone (a, b), cytochalasin B (c, d), and MnTMPyP (e, f) on with the left image from each set indicating 0.25 MPa and the right indicating 0.5 MPa.

These experiments confirmed that mechanical stimulation outside of impact scenarios could modulate ROS levels, which was in agreement with previous studies [130, 170]. It also provided evidence that the same mechanism that seemed to control injurious impact ROS release [131] also controlled the release of ROS at these lower stress levels. DHE staining increased linearly with both stress and strain, while cell death seemingly followed an exponential function when plotted against strain, but a linear trend when plotted against stress.

To determine if the main species of ROS causing the DHE staining was superoxide, we inhibited the availability of superoxide with MnTMPyP. This chemical is cell-permeable and reduces intracellular superoxide levels. MnTMPyP works as an ion superoxide oxireductase and must be reduced intracellularly by NADPH and GSH before it can itself reduce superoxide to hydrogen peroxide [100, 101]. Therefore the ROS reducing properties are usefule short term, but longer exposures result in oxidized glutathione and $NADP^+$ build up which would result in higher peroxide levels [101, 102]. In this short term experiment, MnTMPyP greatly reduced the DHE staining at both 0.25 and 0.5 MPa, indicating that superoxide was, in fact, the main species of ROS causing DHE staining in lower stress levels. Treatment with rotenone showed that this superoxide was mitochondrial in origin and inhibitable at 0.25 MPa, but not at 0.5 MPa. The reason rotenone did not block DHE staining at 0.5 MPa could possibly be that, at higher stresses/strains, other sources of superoxide also play a role, or that the mechanism of electron flow at this higher stress is different from that at lower stress, as rotenone would only block ROS if reverse electron flow were occurring.

To show what was causing the release of ROS, we subjected cartilage explants to hydrostatic stress and noticed that there was no ROS response, suggesting that the physical distortion was likely mediating the response we saw for compressive stresses. To see if this bulk tissue distortion was being transmitted via the cytoskeleton to signal ROS production, the actin cytoskeleton was degraded in cells by inhibiting polymerization with cytochalasin B. At lower stress (0.25 MPa), dissolution of the cytoskeleton did reduce the DHE staining. A similar result was seen in a blunt impact injury model in which dissolution of the cytoskeletal network prior to impact prevented both ROS release and cell death [3]. However, similar to the rotenone treatment, dissolving the cytoskeleton was ineffective at 0.5 MPa. This again points to a different mechanism or source of ROS at this higher stress level.

The main findings from this study are that, at moderate stresses and strains, superoxide is released from the mitochondria in proportion to the stress/strain encountered. This response is cytoskeleton-mediated and is not immediately lethal. Importantly, these data are only representative of our *ex vivo* explant culture system, and static stress at these magnitudes is not expected to be seen physiologically. However, these aspects of cartilage mechanobiology can only be properly assessed under controlled conditions, so further *in vivo* experimentation would be needed to confirm physiological relevance. Further studies in this dissertation expand on this mechanoresponse using more physiological loading conditions.

CHAPTER 4:

DYNAMIC MECHANICAL STRESS INDUCES MITOCHONDRIAL ROS PRODUCTION THAT IS COUPLED WITH ATP PRODUCTION

Introduction

Considering both the newly realized role of mitochondria in strain-induced ROS release, and the fact that static stress has been shown to down regulate matrix production [171] and decrease solute diffusivity [6], our next goal was then to apply dynamic mechanical stimulation to our previous explant system. The first version of the dynamic loading program was finished at this time and was designed to better mimic the dynamic stresses seen *in vivo*. Because only one loading stand was available for the following experiments, each loading session was performed independently.

It is well known that dynamic loading stimulates cartilage matrix synthesis [125, 130]. It is also known that cartilage produces ROS in response to injury or load [130]. However, no study has attempted to establish a link between these two phenomena. ATP content has been shown to consistently correlate with lactate production, glucose consumption, and radioactive sulfate incorporation in chondrocytes [46, 63, 171] as well as correlate with radioactive proline incorporation (unpublished). We therefore attempted to correlate mitochondrial ROS release with the metabolic output, ATP content. The 0.25 MPa stress level that was chosen was not associated with significant cell death when loaded statically, yet the cells still responded to our treatments to reduce ROS production. The 0.25 MPa stress matched maximal physiological strains observed

in vivo, and was not associated with an increase in cell death, despite having a significant increase in ROS.

The following experiments apply dynamic compression to cartilage with or without the presence of rotenone, a complex I inhibitor, or Mitoquinone ($MitoQ_{10}$), a superoxide-specific antioxidant that accumulates in mitochondria. ROS was measured immediately after loading, while the metabolic response was measured after 24 hours.

Methods

For this study, explant specimens were harvested and equilibrated in the same manner as described for the static load experiments. Explants were separated into six treatment groups: loaded or unloaded and with or without a chemical inhibitor, namely rotenone or $MitoQ_{10}$. Inhibitor-treatment explants were pre-treated with assigned chemical for one hour prior to mechanical loading at 2.5 µM (Rotenone) and 4 µM ($MitoQ_{10}$).

The explants were then dynamically loaded or allowed to freely culture in the explant fixation system. The dynamic loading conditions included 0.25 MPa of pressure at a frequency of 0.5 Hz in low oxygen for one hour. Again, DHE (5 µM) and calcein AM (1 µM) were incubated with the cartilage for 30 minutes immediately after loading. Confocal images were captured and the explants were placed back in low oxygen culture for 24 hours, after which ATP content was assessed (See Appendix for method). Briefly, an 8mm diameter full thickness cartilage plug was removed from the loaded region of the explant and cut in half. One half was cryoembedded in tissue freezing medium, and the other was placed in a phosphatase inhibitor solution and boiled to extract cellular ATP, which was then measured with an ATP luminescence assay (Sigma, FLAA).

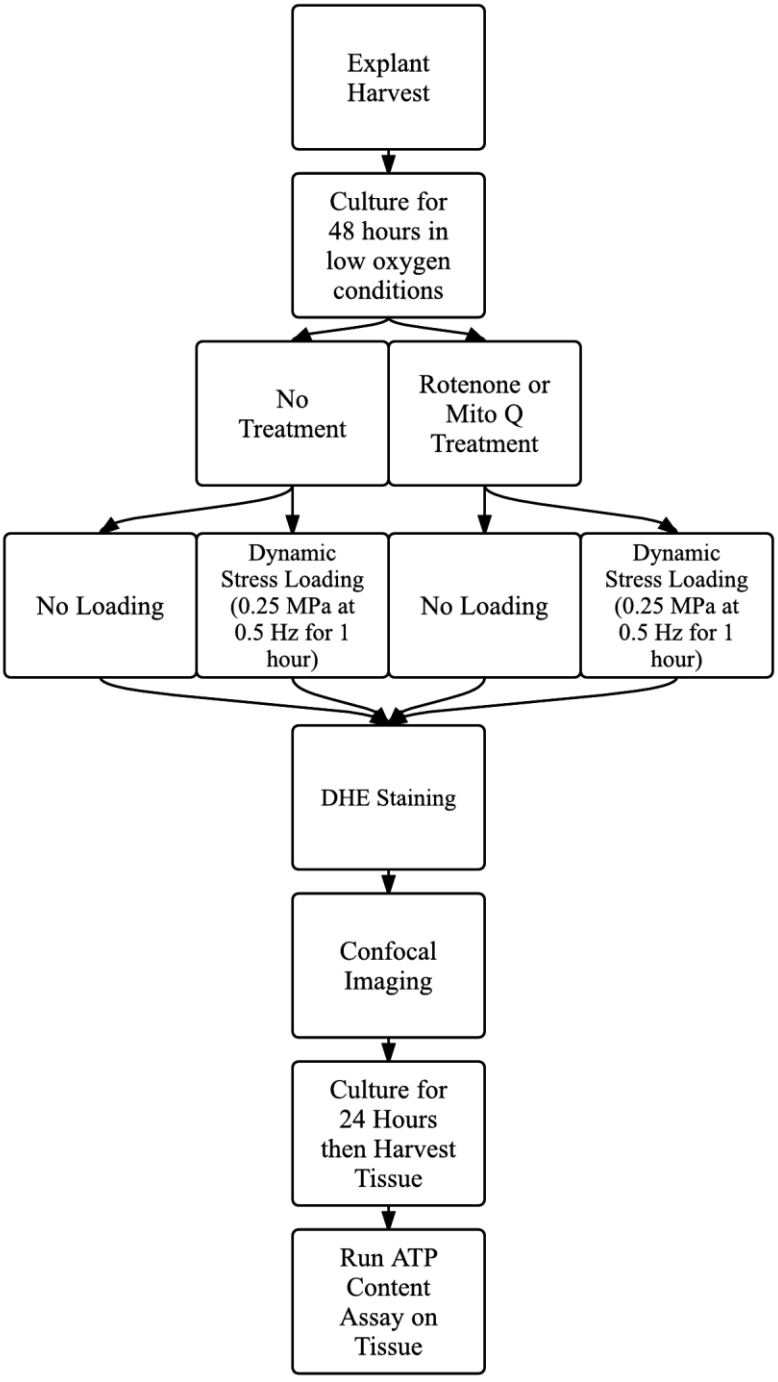

Figure 17. Flowchart describing the experimental protocol for dynamic mechanical stimulation in this chapter.

Results

The explant number was 7 for unloaded specimens, 9 for rotenone treated and unloaded, 3 for mitoquinone treated and unloaded, 7 for 0.25 MPa dynamically loaded, 6 for rotenone treated and 0.25 MPa dynamic loading, and 4 for mitoquinone treated and 0.25 MPa dynamic loading. We observed strong DHE staining in the loaded explants (Figure 18) [172], as with the previous experiments. The percentage of DHE stained cells increased from 1.8 ± 2.3 % in unloaded explants to 43.1 ± 18.8% in explants dynamically loaded at 0.25 MPa. The strong DHE signal co-localized with calcein AM, indicating that the cells were still alive. This ROS production in dynamically loaded explants could be reduced to unloaded levels with the addition of rotenone (6.1 ± 7.8%) or $MitoQ_{10}$ (4.7 ± 4.3 %) (Figure 18, Figure 19). This confirmed that the ROS released from cyclic mechanical stimulation was superoxide and from the same mitochondrial source as we previously observed in impact injuries and static stress.

ATP content trended with DHE staining, with unloaded control explants having an ATP content of 12.3 ± 7.8 pmol/mg tissue and dynamically loaded explants having 45.1 ± 14.8 pmol/mg (Figure 19). Treatments with rotenone and $MitoQ_{10}$ also reduced ATP content to unloaded levels. The maximum cartilage tissue strain was unaffected by any chemical treatment and remained at an average of 21%. This was lower when compared to the 0.25 MPa static stress treatment, which averaged 32%. The percentage of cells that were counted by the automated software as being positively stained with DHE was not statistically different being 35 ± 17% for static stress and 43±19% for dynamic stress. However, a difference was apparent when assessed visually, in that more live cells were staining brightly with DHE in the dynamically loaded explants.

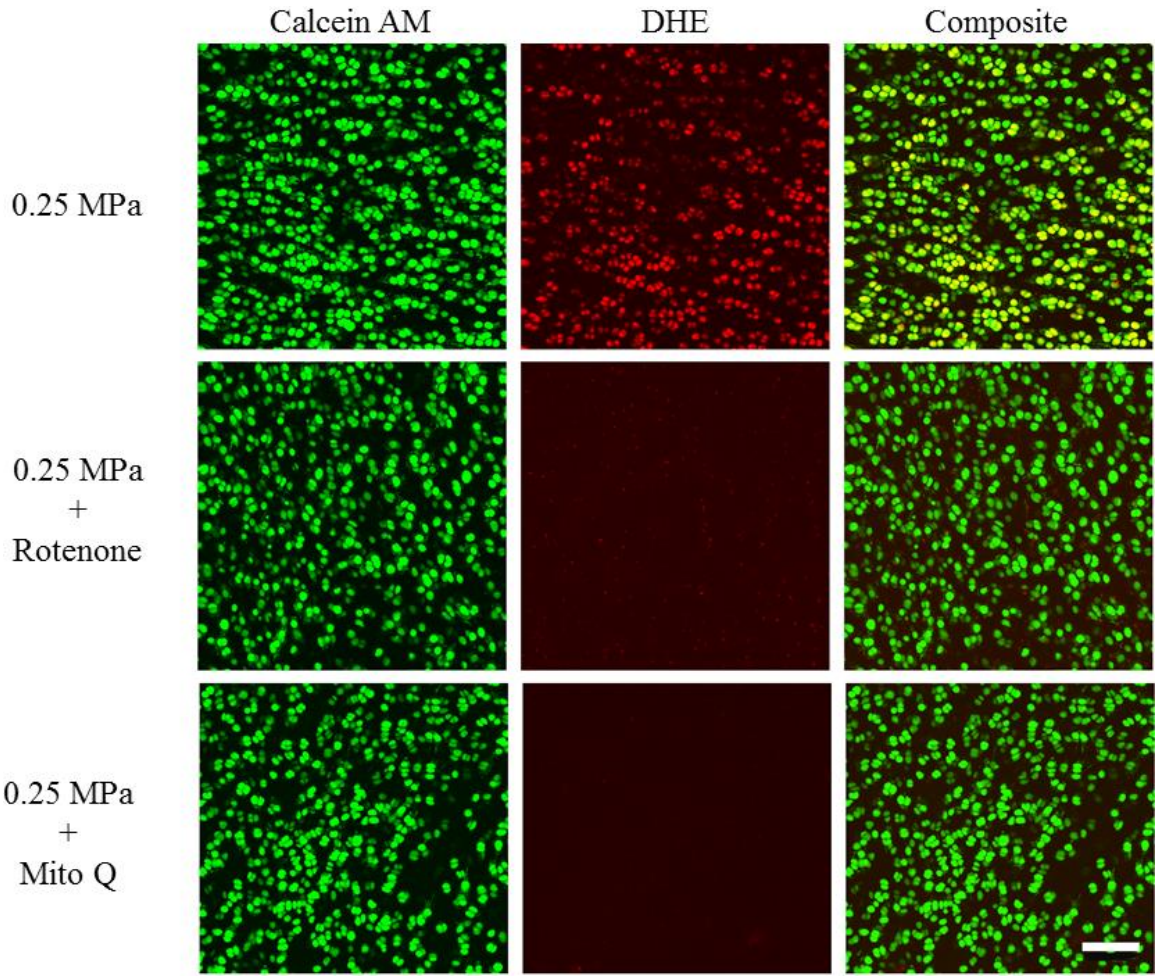

Figure 18. ROS signal is seen strongly in live cells at 0.25 MPa, which can be blocked with the addition of complex I inhibitor rotenone, or mitochondrial specific antioxidant mitoquinone ($MitoQ_{10}$)

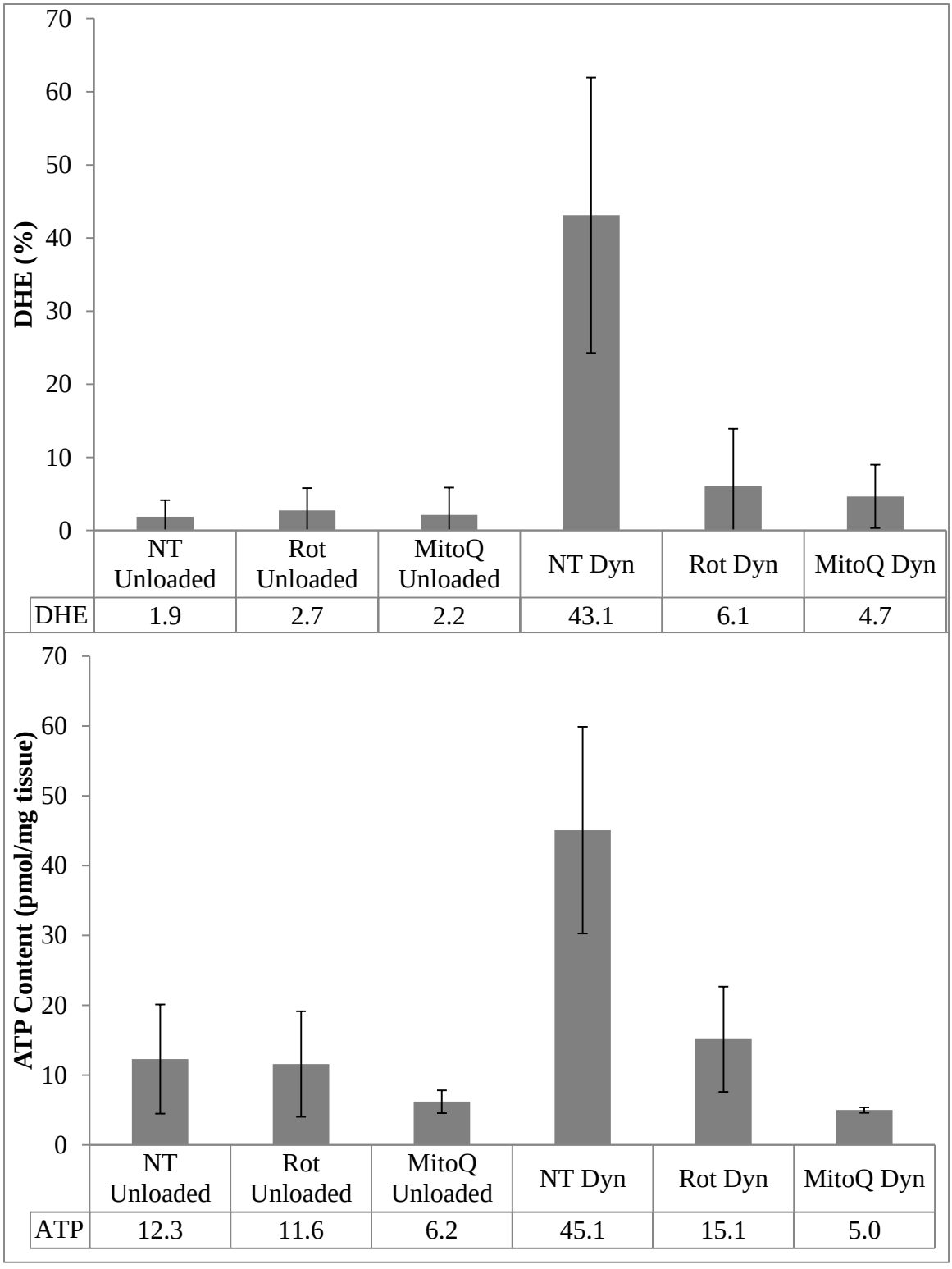

Figure 19. DHE staining was increased with dynamic stress and inhibited with rotenone and Mito. Bottom: ATP content followed the same trend as DHE, however $MitoQ_{10}$ suppression of ATP content was much stronger than rotenone.

This work begins to reveal parts of the complex mechanism by which cartilage responds to load. Cartilage responds to mechanical stimulation by increasing ROS. These ROS originate from the mitochondria, as indicated by the reduction in DHE staining with both rotenone and $MitoQ_{10}$. The ROS are also required for intracellular ATP production, as demonstrated by the reduction in ATP content when ROS release is inhibited. This study confirmed that load-induced mitochondrial ROS are required for increased ATP content. To our knowledge, this work is the first to link these two concepts in cartilage mechanobiology. Dynamic loading was known to increase GAG synthesis [125] and PG content [124], and even upregulate glycolytic enzymes [132], yet, until now, the stimulatory pathway was unknown. This work builds on the idea that cartilage metabolism requires mitochondria to produce a basal level of ROS in order to maintain glycolysis [4]. Exactly why this ROS is required to support glycolysis, though, is still under investigation. Further work in this disseration expand upon the idea that modulating mitochondrial ROS can impact cartilage energy production.

CHAPTER 5:

CHEMICALLY STIMULATING MITOCHONDRIAL ROS PRODUCTION INCREASES ATP

Introduction

In Chapter 3, we demonstrated that blocking the ubiquinone binding site of complex I with rotenone reduces ROS release, which, as demonstrated in Chapter 4, is associated with reduced energy production in the form of ATP. It is important to note, though, that the effect rotenone inflicts on mitochondria varies depending on the state of both electron flow and energy production within the organelle. As such, when operating in reverse electron flow, rotenone treatment is associated with a reduction in superoxide, but during forward electron flow, the effect of rotenone is the opposite and is associated with increased superoxide. Our data imply that rotenone may act to inhibit reverse electron flow, which appears to increase during mechanical loading due to the increasing ROS levels that are inhibitable with rotenone. However, the importance of the site specificity of superoxide and the concentration dependence for metabolic stimulation has not been directly addressed. The species of ROS that is responsible for the metabolic stimulation has also not been concretely identified, as superoxide can react with many chemicals to form distinct ROS species.

This chapter, therefore, addresses the question of whether the source of the mitochondrial superoxide is critical to the ATP increase associated with mechanical loading, and whether it can be modulated with increasing levels of ROS. He were used antimycin A treatment to force superoxide production to occur at complex III of the

electron transport chain. Antimycin A causes an unstable semiquinone species to form because of the site of its binding (Q_i site), which passes its electron to oxygen causing superoxide to form and accumulate in both the matrix and the intermembrane space [94, 95]. Then to determine whether superoxide or peroxide is the main ROS that modulates energy production, we applied varying concentrations of antimycin A to the explants with or without the superoxide dismutase mimetic Galera (M40401), which reacts with superoxide at a very high rate to form peroxide [105]. In this scenario Galera treatments in conjunction with antimycin A would theoretically increase peroxide levels above antimycin A alone, because Galera would react with superoxide more often to form peroxide and thus limit other superoxide reactions.

We also characterized how isolated chondrocytes cells responded to mitochondrial inhibitors to block complex I, complex III Q_i site, complex III Q_o site, and complex V (rotenone, antimycin A, myxothiazol, and oligomycin) with the Seahorse Bioscience XF96 Extracellular Flux Analyzer. This specialized device places a detector probe inside each well of the 96-well plate, which seals the chamber to measure the oxygen consumption rate and pH change in the media of each sealed well over a set time period (usually 3-5 minutes). The well is subsequently unsealed, the media is gently mixed, and another sealed measurement is taken. The oxygen consumption rate is usually tied to the rate of mitochondrial oxidative phosphorylation. The pH change is usually a result of glycolysis producing lactate, and acidifying the media in the process.

These experiments aim to ascertain if artificial stimulation of superoxide at complex III can elicit the same metabolic response as mechanical loading, and determine which of superoxide or peroxide is associated with increased ATP content.

Methods

Initial experiments indicated that three hours of incubation with mitochondrial inhibitors was sufficient to resolve any measureable metabolic change. Explants were thus incubated in low oxygen for three hours with complex-specific inhibitors 2.5 µM rotenone (complex I), 2 or 20 µM myxothiazol (complex III Q_o site), and 5, 10, or 50 µM antimycin A (complex III Q_i site)}. Antimycin A was expected to increase superoxide production, while the others were expected to reduce it [91-93]. Galera was also used to readily and specifically convert superoxide to peroxide, with a rate constant near the native SOD enzyme [105].

Separately, chondrocytes were isolated from cartilage harvested from bovine tibial plateaus, using 0.15% collagenase and pronase in culture media to digest the matrix. After 18 hours of digestion, an equal volume of serum-containing media was added to the digestion mixture, and this solution with the cells and matrix debris was filtered through a 45 µm mesh size filter, pelleted by centrifugation, resuspended in fresh media, and pelleted again to remove any excess matrix proteases. Cells were then plated at a density of 25,000-30,000 cells/well in a Seahorse Bioscience 96-well microplate. These cells were allowed to equilibrate and attach to the microplate for five days. On the fifth day, the microplate was analyzed inside a Seahorse Bioscience XF96 microplate reader to characterize the metabolic effects of the varying mitochondrial inhibitors.

The Seahorse Bioscience XF96 Extracellular Flux Analyzer ran a modified program to assess the response of chondrocytes to the mitochondrial inhibitors rotenone, antimycin A, myxothiazol, and oligomycin (complex V, ATP synthase). This machine usually runs a standard protocol to assess mitochondrial health. This standard run uses

predefined set and order of mitochondrial inhibitor injections, however, here, we only want to determine the effect of individual mitochondrial inhibitors on oxygen consumption and media acidification as an estimate of glycolysis and oxidative phosphorylation.

The first step in the modified Seahorse run was to change the media in the wells of the microplate to media with a known buffer capacity, which allowed for more accurate measurements of pH change. The plate was then inserted into the XF96, and the machine mixed the media in each well, created an airtight seal in each well, and then measured the decrease in oxygen concentration, called the oxygen consumption rate (OCR), and pH change, called extracellular acidification rate (ECAR), with probes that were submerged in the media over three minutes. Then, the seal lifted and the media was mixed to allow oxygen tension and pH to re-equilibrate. The probe seal and measurement process was then repeated. These initial OCR and ECAR measurements establish a metabolic baseline against which inhibitor treatments can be compared. After three baseline measurements, each of the various drugs were injected during a mixing phase. Eight more OCR and ECAR measurements are taken after the injection of inhibitor for comparison against the established baseline. Each inhibitor group included at least six wells per run in two independent runs. After each run, the cells were removed from the plate surface with trypsin and counted with a hemocytometer to normalize to cell count.

Results

Three-hour application of rotenone, myxothiazol, and antimycin A had varying results. Rotenone and myxothiazol showed no effect on ATP content. Antimycin A,

however, showed a strong increase in ATP content, increasing to 105.9 ± 70 pmol/mg tissue from 43.2 ± 12.7 pmol/mg tissue. The large variance within the antimycin A treatment group was due to low sample size (only three explants), however the lowest ATP content value for the 50 µM antimycin A treatment was 61 pmol/mg. Therefore, this treatment group was still statistically different from all other groups. This increase of ATP was also associated with an increase in ROS, which was visualized by a strong DHE signal (Figure 21). The number of explants was 9, 4, 5, and 3 for control, rotenone, myxothiazol, and antimycin A treatment groups respectively.

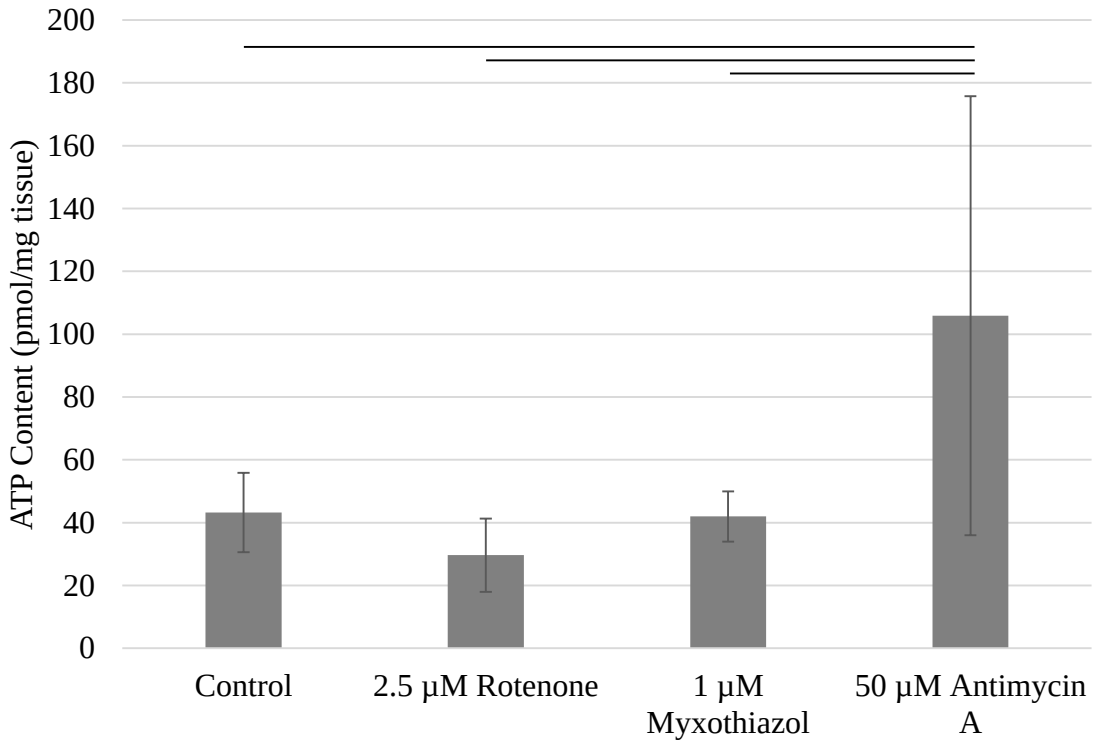

Figure 20. Cartilage explants treated with rotenone, myxothiazol, or antimycin A for three hours. Statistical significance is indicated by the bars between groups ($p < 0.05$).

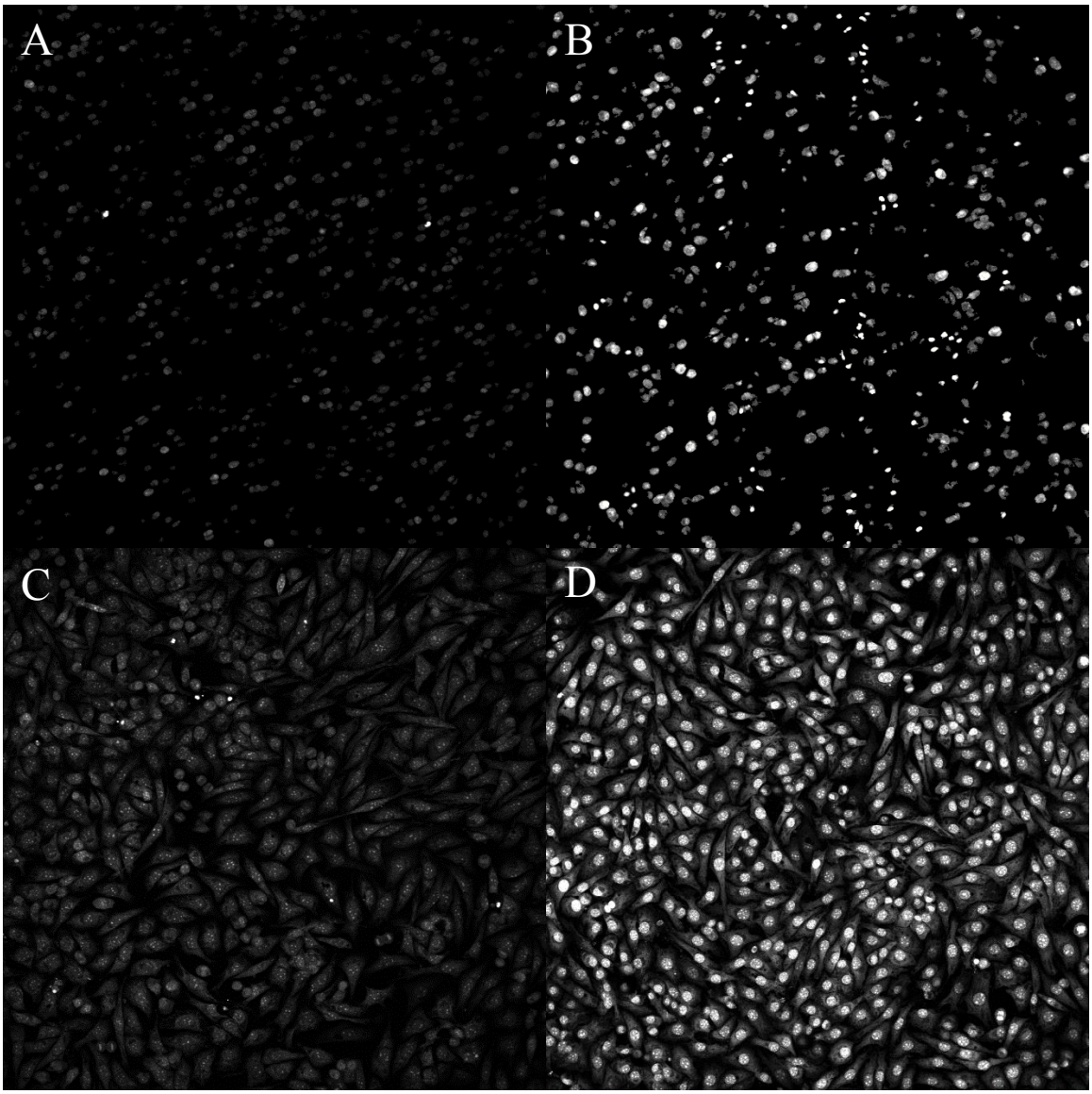

Figure 21. DHE staining for (A) untreated explant or (B) 3 hour 50 µM antimycin A treated explant. Also DHE staining for (C) isolated untreated chondrocyte cells, and (D) 30 minute 2.5 µM antimycin A treated cells

Knowing that we can induce superoxide in mitochondria via treatment with antimycin A, we used the same 3-hour treatments on unloaded cartilage explants, but varied the concentration of antimycin A in attempts to modify the ATP response. We also used the superoxide dismutase mimetic, Galera, in conjunction with antimycin A to investigate peroxide as the primary ROS responsible for the increase in ATP content. Since Galera converts superoxide into hydrogen peroxide at a very high rate constant, treatments with this chemical, in conjunction with antimycin A, should effectively increase peroxide, while maintaining lower levels of superoxide when compared to the same concentration of antimycin A alone. The combinatorial treatment of antimycin A and Galera had consistently higher ATP levels than antimycin A alone (Figure 22). The highest concentration of antimycin A (10 µM), when combined with Galera, was significantly different than the untreated control, and the 10 µM antimycin A alone treatment was close to significance. The number of explants was 7 for controls, 4 for ethanol vehicle controls, 7 for 5 µM antimycin A, 6 for 5 µM antimycin A with 4 µM galera, 3 for 10 µM antimycin A, and 3 for 10 µM antimycin A with 4 µM galera.

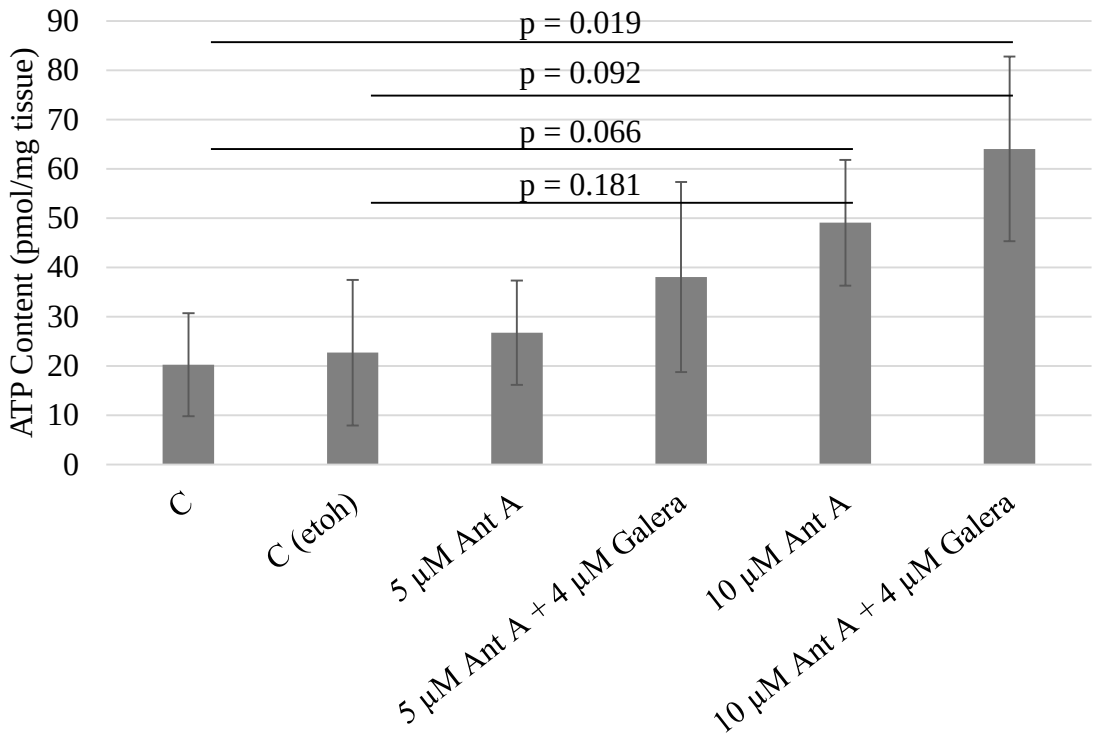

Figure 22. Treatments with increasing doses of antimycin A and galera lead to increased ATP content. Significance values are listed by bars between groups with associated p value

Galera + antimycin A treatments indicated peroxide as the primary ROS in ATP production, as Galera treatments alone on unloaded cartilage had no effect on ATP production (Figure 23). Based on previous data, our interpretation of this result is that since these samples are unloaded, and not chemically stimulated, superoxide levels are low, and thus any conversion of superoxide to peroxide is still below a threshold that would be stimulatory.

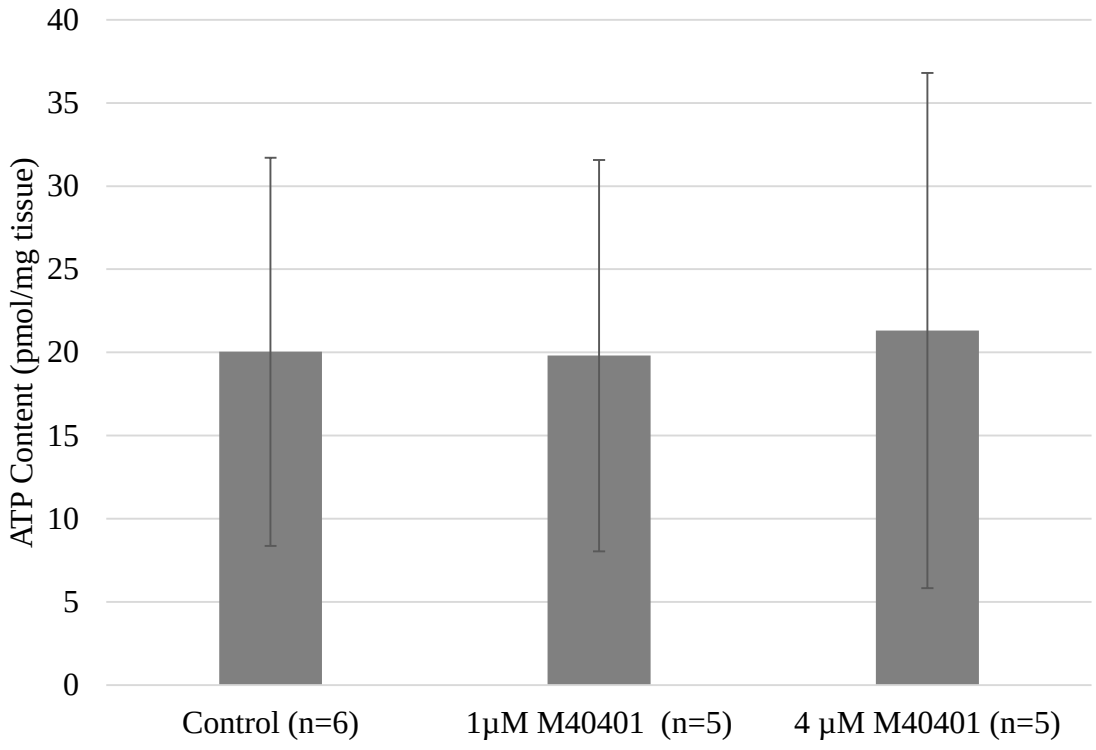

Figure 23. SOD mimetic Galera shows no effect on ATP content alone

The results show that cartilage metabolism is unique, given that blocking either ATP synthase or complex I has no discernable effect on media acidification (glycolysis, Figure 24). However, blocking complex III at any site seems to promote higher glycolytic activity. A representative run showing the OCR data is in Figure 25, with the light gray box encasing the two rate measurements before injection, the red line indicating the injection time, and the darker gray box encasing the two rates after inhibitor injection. An increase in sample size would greatly aid in the interpretation of these results, however, as we could not attain sufficient statistical power to perform a proper analysis.

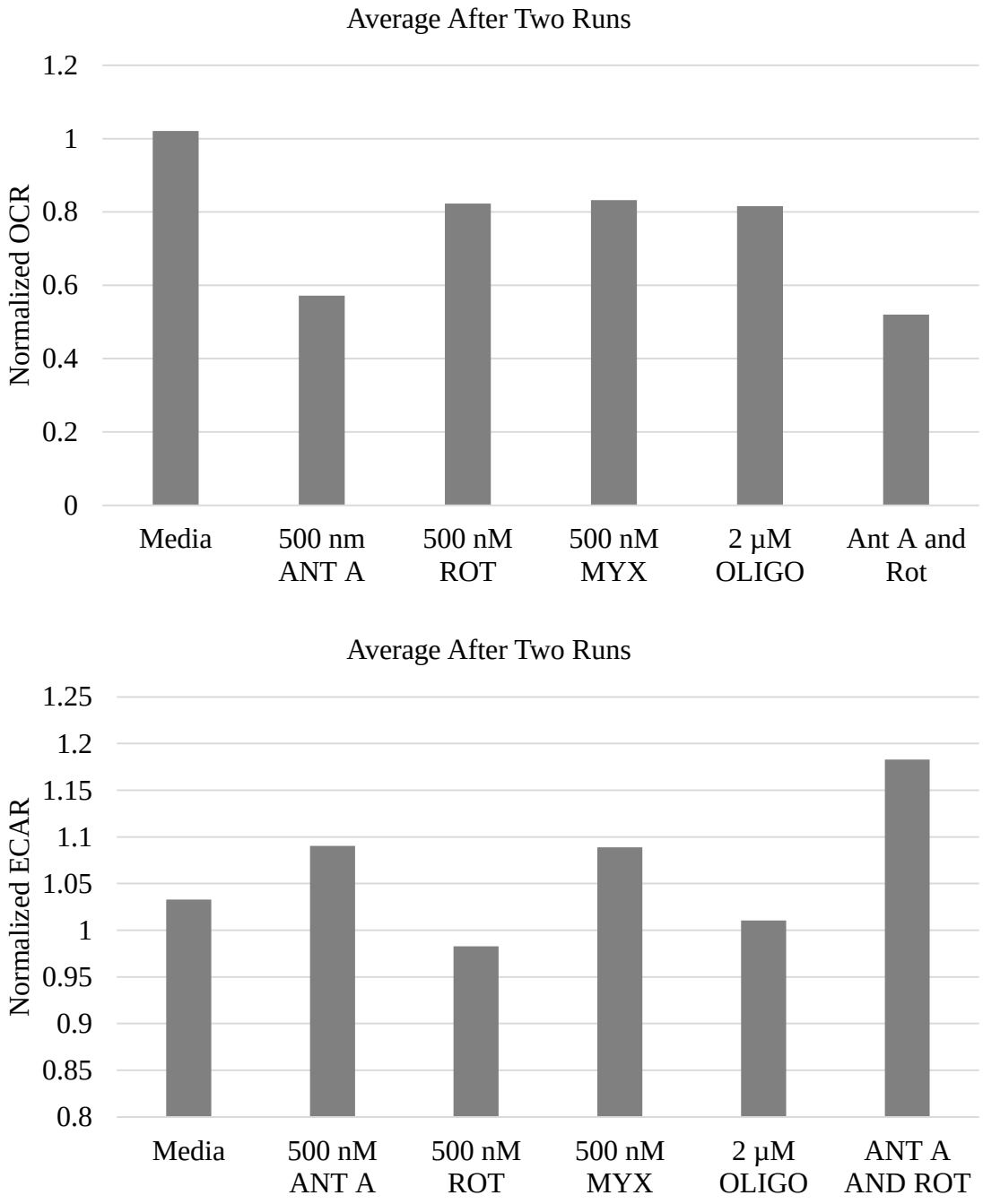

Figure 24. Single injection modified Seahorse run shows that mitochondrial inhibitors reduce oxygen consumption rate, yet have complex dependent effects on ECAR. Blocking Complex I or ATP synthase has little to no effect on ECAR, yet blocking complex III increases ECAR

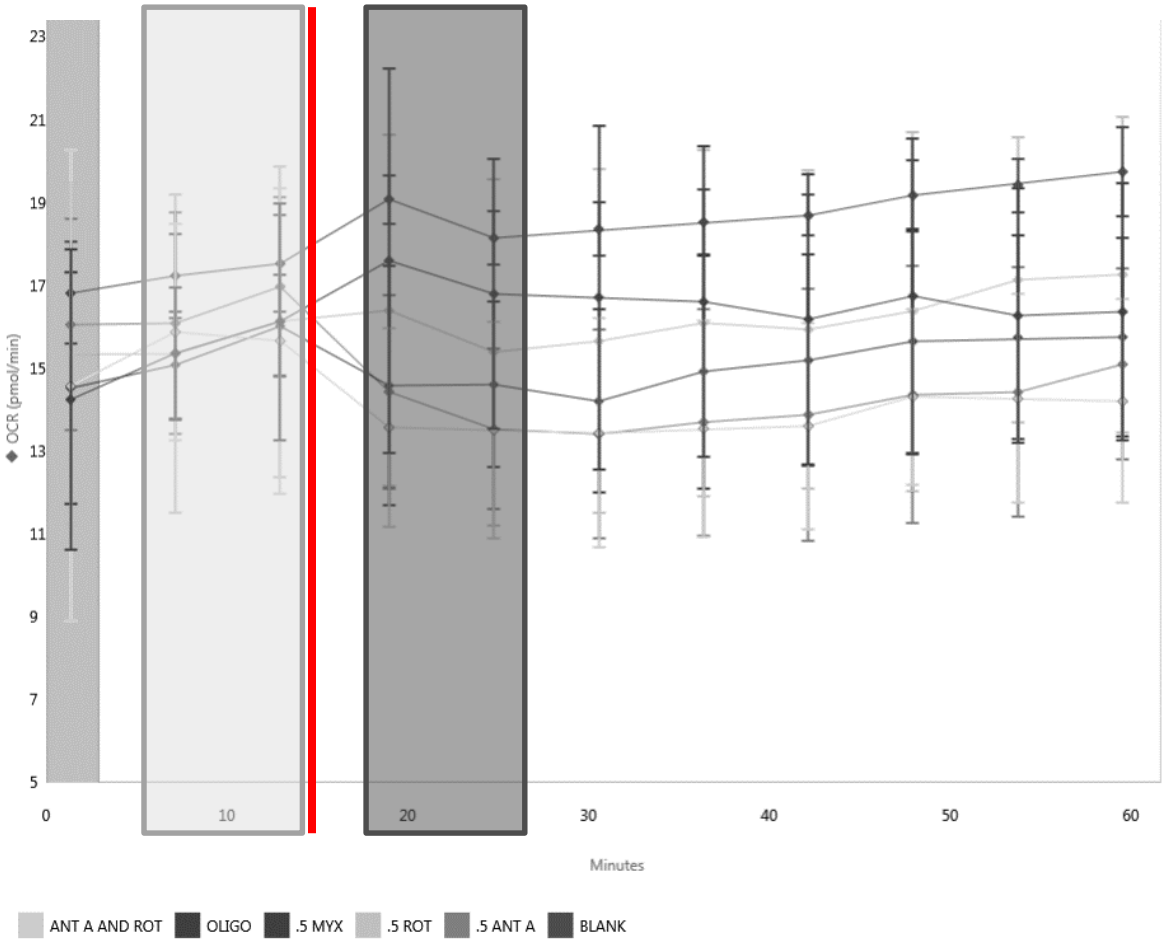

Figure 25. Example modified seahorse run. The rates after injection for each mitochondrial inhibitor will be normalized against the rates before injection. Here the injection is noted by the red line, and the two rates on either side will be used for the comparison.

The results from this chapter are encouraging. The antimycin A treatments show that modulating ROS via a chemical inhibitor known to cause superoxide at complex III, also cause the increase in ATP seen during loading. This increase in ATP content is irrespective of the capacity of the electron transport chain to create ATP for energy purposes, as blocking ATP synthase has had no effect on ATP content in previous experiments [4], and also does not seem to increase the seahorse ECAR values here. Therefore, it is not simply a case of glycolysis being stimulated to increase ATP due to the lack of ATP coming from the electron transport chain.

The modulation of ATP appears to increase with higher concentrations of antimycin A, and assumedly higher concentrations of superoxide. Ensuring that the majority of superoxide produced was converted to peroxide further strengthened the increase in ATP content. Therefore, the specificity of the site of mitochondrial superoxide is not what is most important, and instead, simply oxidizing the QH_2 pool, using oxygen as an electron acceptor, seems to be key to generating the parental ROS species from which peroxide is generated for the signaling or stimulation of glycolytic activity.

CHAPTER 6:

DYNAMIC MECHANICAL OVERLOADING INDUCES ROS PRODUCTION THAT CAUSES MITOCHONDRIAL DYSFUNCTION IN CHONDROCYTES

Introduction

In previous chapters, we demonstrated that mitochondrial superoxide can be produced by either mechanical loading or antimycin A treatment, and that the ROS released by these treatments triggered a metabolic response involving an increase in ATP content. The magnitude of ROS release correlated with intensity of the load in statically stressed explants, but whether this correlation extends to ATP content was not yet assessed. We address this, as well as whether dynamically loaded explants experience the same correlations as statically loaded explants in the following experiments.

In all previous experiments, ROS have been quantified with a binary counting system, meaning that cells are either positive or negative for DHE staining based on a set threshold. The obvious disadvantage of such a system is that differences in signal intensity beyond the threshold limit are not considered in the analysis, meaning two cells that are both 'positive' could differ dramatically in ROS levels. Therefore, to be able to link any increases in ROS to ATP content from loading, we developed a new technique to focus on the ROS signal within live cells, which is quantified as the 8- or 10-bit intensity value depending on image input, and not merely positive or negative.

Beyond incorporating multiple stress levels in our cartilage mechanical loading experiments, both the duration per loading session and number of loading sessions were also increased. Previously, all experiments were single, one-hour loading sessions,

followed immediately by confocal microscopy and 24 hours later for ATP content assessment. Here, we focused on creating an injurious, repetitive loading scenario in which we could assess various intervention strategies to prevent the damage associated with overloading. Our overall goal was to mimic the damage observed in the progression of osteoarthritis and to intervene with targeted treatments. These translational experiments were designed to further our knowledge about the pathways involved in OA disease progression and to assess whether we could use this knowledge to inhibit or reverse the effects of damage that lead to disease. N-acetylcysteine (NAC) acts to bolster intracellular antioxidant defenses against peroxide, primarily by increasing glutathione levels, and was used in the following experiments.

Methods

Explants were harvested and cultured for 48 hours as previously described. The multistage loading system was now available, and therefore two separate loading sessions could be performed simultaneously. Explants were secured within the new specimen holders and placed inside the incubator on the loading platform. The stresses used for mechanical stimulation were expanded to 0.25, 0.5, and 1.0 MPa. The duration and frequency was kept at one hour and 0.5 Hz, respectively. A separate unloaded explant was also kept from each bovine joint to allow for normalization. After the stress application, the loaded and unloaded specimens were again stained with calcein AM (live cells) and DHE (ROS), however, here, the DHE concentration was increased to 10 μM to allow for finer parsing of the ROS data. The samples were then assessed 24 hours after load application for ATP content. The unloaded explant from the same joint was used to normalize changes in ATP content.

As mentioned, a binary counting system was used to assess DHE staining in previous experiments. QCIP, the automated Matlab program applied intensity thresholding on both calcein AM and DHE images, and further discriminated any objects above the threshold based on circularity and size constraints. The total calcein AM and DHE cell counts from these automated processes were reported as a percentage of DHE stained cells. Since a more accurate assessment of ROS levels was required for the following experiments, we modified the QCIP analysis to create a mask from the live cells within the calcein AM images. This mask was then overlaid on the corresponding DHE image to isolate individual cells and their respective DHE intensity. The average intensity of all the live cells is calculated from this analysis and is referred to as the live cell DHE intensity. An example image from this type of analysis can be seen in Figure 27. The DHE intensity from the loaded specimen was normalized to the DHE intensity of the unloaded explant.

Also addressed here were the effects of increasing the duration and number of loading sessions that a cartilage explant endures at two different stresses. The load application was extended to three hours, and the number of loading sessions was also increased from one to seven. Here, a single three-hour loading session was performed once a day for seven days at 0.5 Hz and either 0.25 MPa or 1.0 MPa. After each loading session, the explant was placed in fresh media until the next day. A treatment of 10 mM N-acetylcystein (NAC) was applied to a separate 1.0 MPa loading group. This treatment consisted of pre-treatment with NAC for three hours before load application, with continued exposure during the loading session. However, explants were transferred to media without NAC immediately after loading until the next day where NAC pre-

treatment was again administered before loading. The cartilage was excised 24 hours after the final loading session.

An 8 mm full thickness cartilage plug was excised away from the subchondral bone from the loaded region and divided into 3 unequal sections. The largest section was used to digest and obtain cells for running on the Seahorse XF96 Extracellular Flux Analyzer, as previously described in Chapter 5. The cells were plated at 25,000-30,000 cells/well in the proprietary 96-well plate. After the five day culture period in the plate the standardized mitochondrial stress test protocol for the XF96 was followed to ascertain values that reflect metabolic health for the cells that experience varying loads. The mitochondrial stress test involves many of the same inhibitors previously used in the customized seahorse runs shown in the previous chapter. However, the mitochondrial stress test leverages the order in which these inhibitors are injected to ascertain the mitochondrial health. Here, the key measurement was the basal metabolic rate with regards to OCR (oxygen consumption), ECAR (media acidification), and a calculated proton leakage. Proton leakage is a derived value that represents the oxygen consumption that occurs independently from ATP production. This value is represented as a percentage of the basal oxygen consumption rate.

The two smaller sections from the remaining 8 mm cartilage tissue plug were used to determine the ATP and double stranded DNA content of the tissue. The ATP content was assessed as previously described and the DNA content was assessed with the Quant-iT™ DNA Assay Kit (Invitrogen). Here, ATP content was normalized to DNA content and reported as ATP (fmol)/DNA (ng).

Results

All stresses caused a statistically significant increase in ATP content when compared to the unloaded specimen; however, between the varying stresses, no differences were observed (Figure 26). This could be due to the single time point chosen for harvest, and expanding the range of times to measure the ATP response could show differences that are not represented from a single time point 24 hours after stimulation. Loaded explants usually had higher DHE staining (Figure 27). Despite the lack of correlation between increasing stress and ATP content, a correlation between the changes in the intracellular ROS (live cell DHE intensity) did correlate with changes in ATP content when the two explants from the same knee were compared (Figure 28). These data exhibit a general pattern: mechanical loading → increased intracellular ROS → increased ATP content.

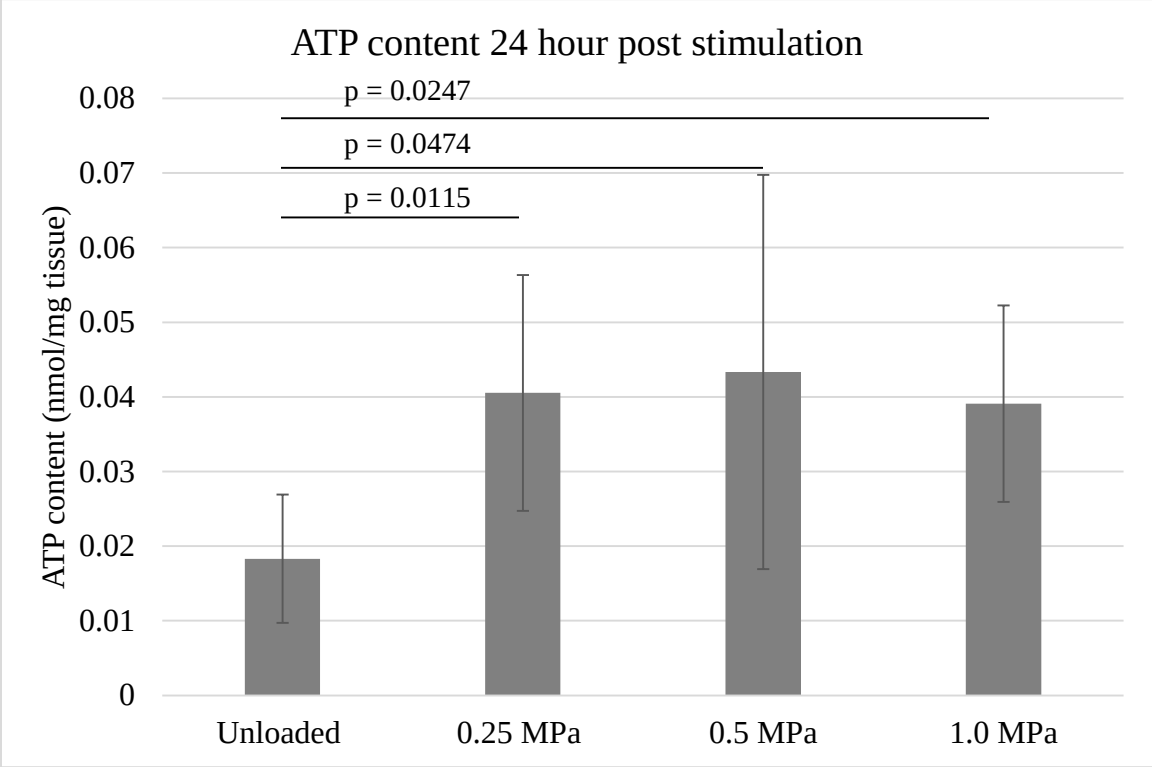

Figure 26. Increasing the stress for the one hour dynamic stimulation did not also increase the ATP content, though the general increase over unloaded specimens remained

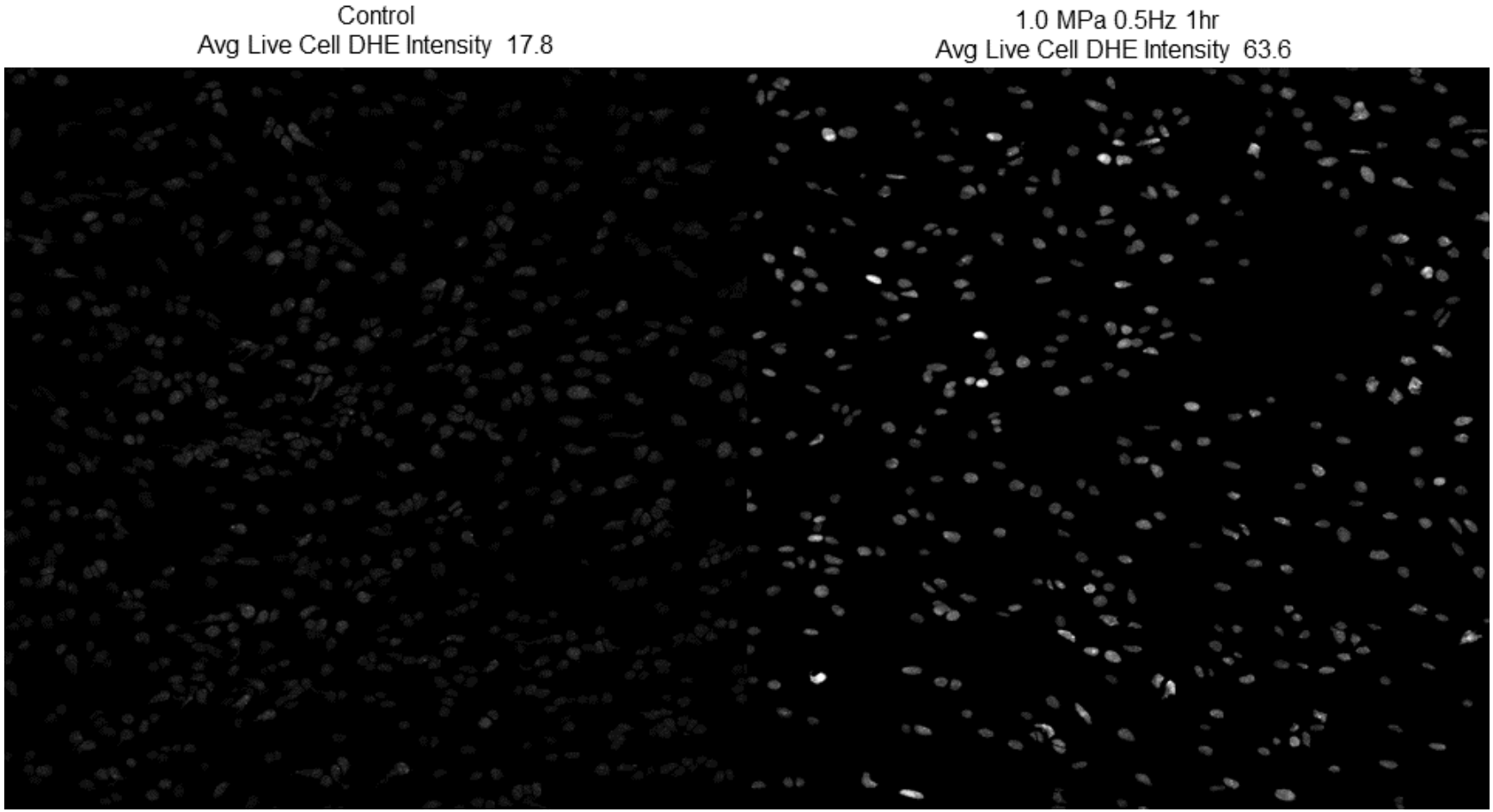

Figure 27. Example live cell DHE intensity measurements for an explant with no mechanical stimulation (left) and 1.0 MPa stimulation (right)

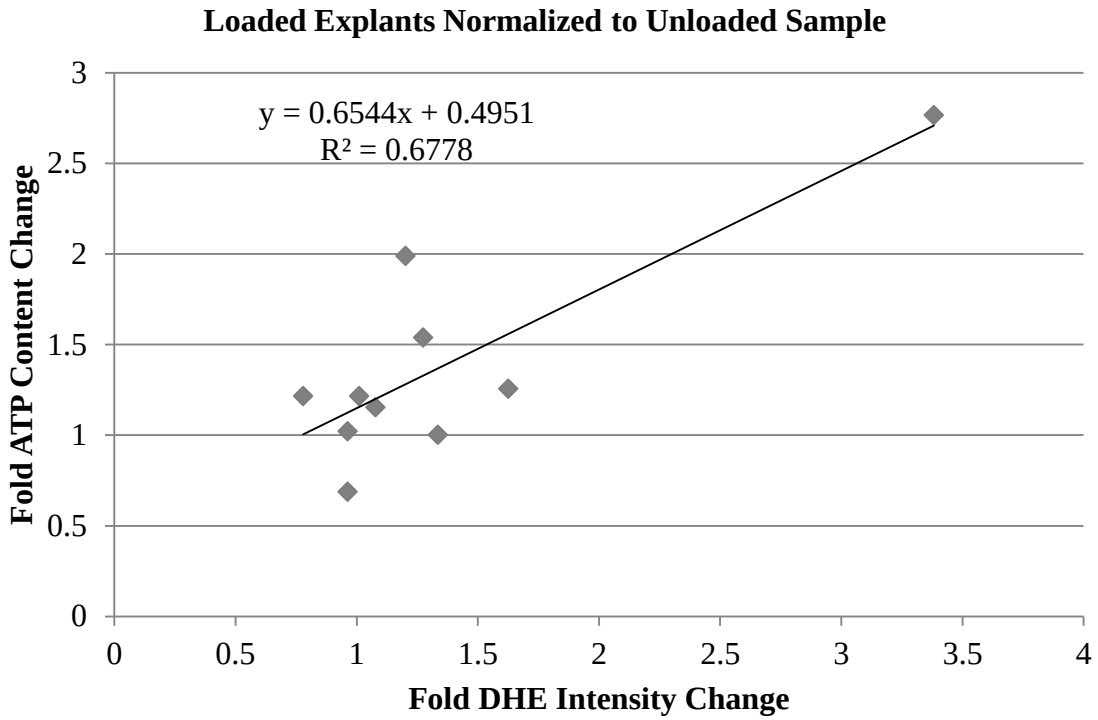

Figure 28. Correlation of fold change in DHE intensity and ATP content from paired unloaded/loaded explants from the same knee.

The expansion of the loading scheme to longer sessions over multiple days yielded changes indicative of mitochondrial dysfunction with increased load. The 1.0 MPa dynamic stress showed signs that the cartilage mitochondria were damaged; the basal respiration, media acidification, and ATP content were decreased (Figure 29). This was accompanied with an increase in proton leak. The 0.25 MPa, seven-day loading was not different from unloaded controls with regard to the above seahorse measurements (data not shown). The deleterious effects of overloading can be completely sequestered by administering 10 mM NAC before and during the dynamic loading session, indicating that this dysfunction is ROS-based.

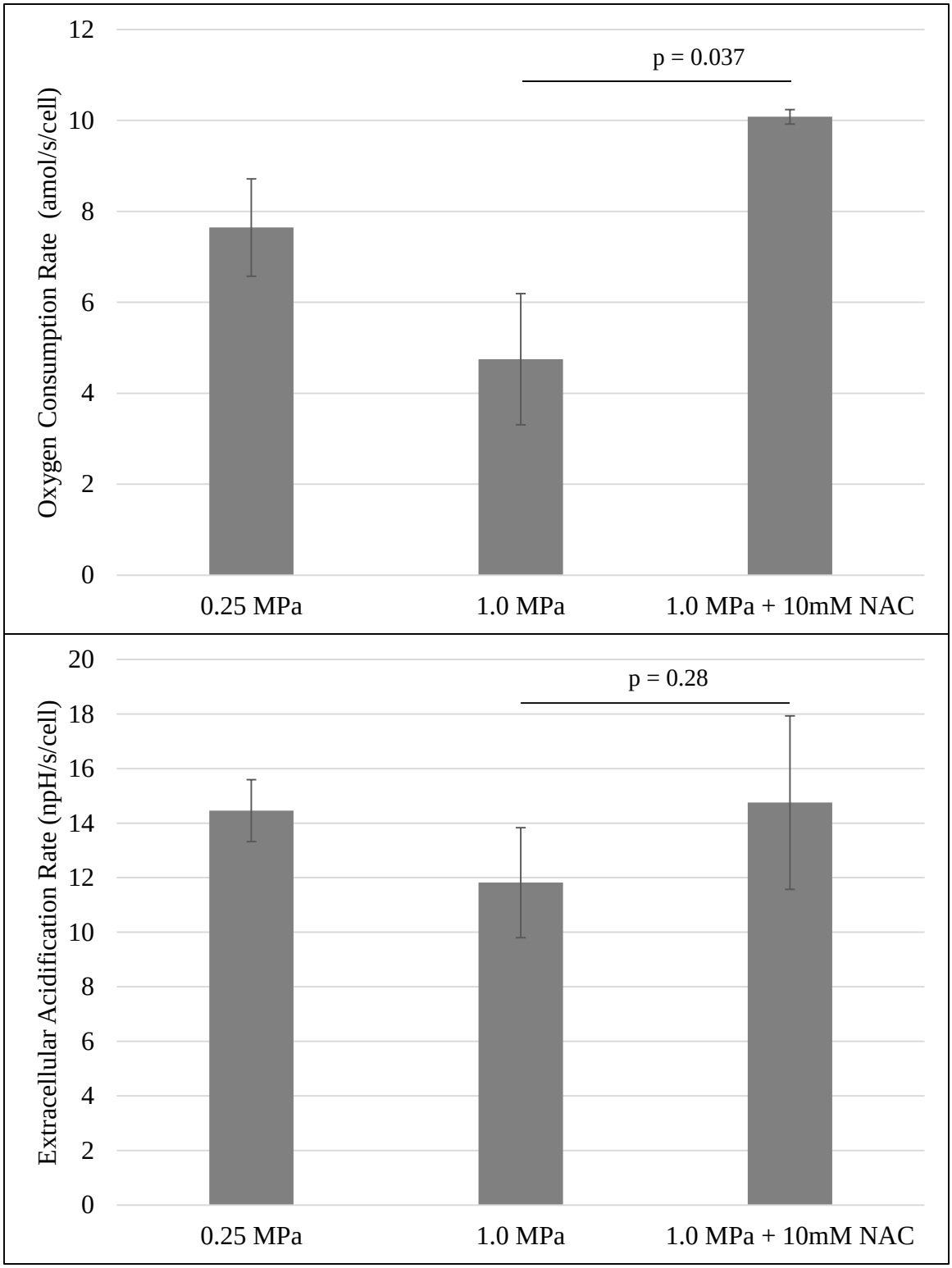

Figure 29. Derived data from mitochondrial stress test performed on explants loaded for 3 hours per day for 7 days. NAC provided overloading protection, maintaining OCR and ECAR, and ATP values close to low stress loading, while preventing proton leak increases.

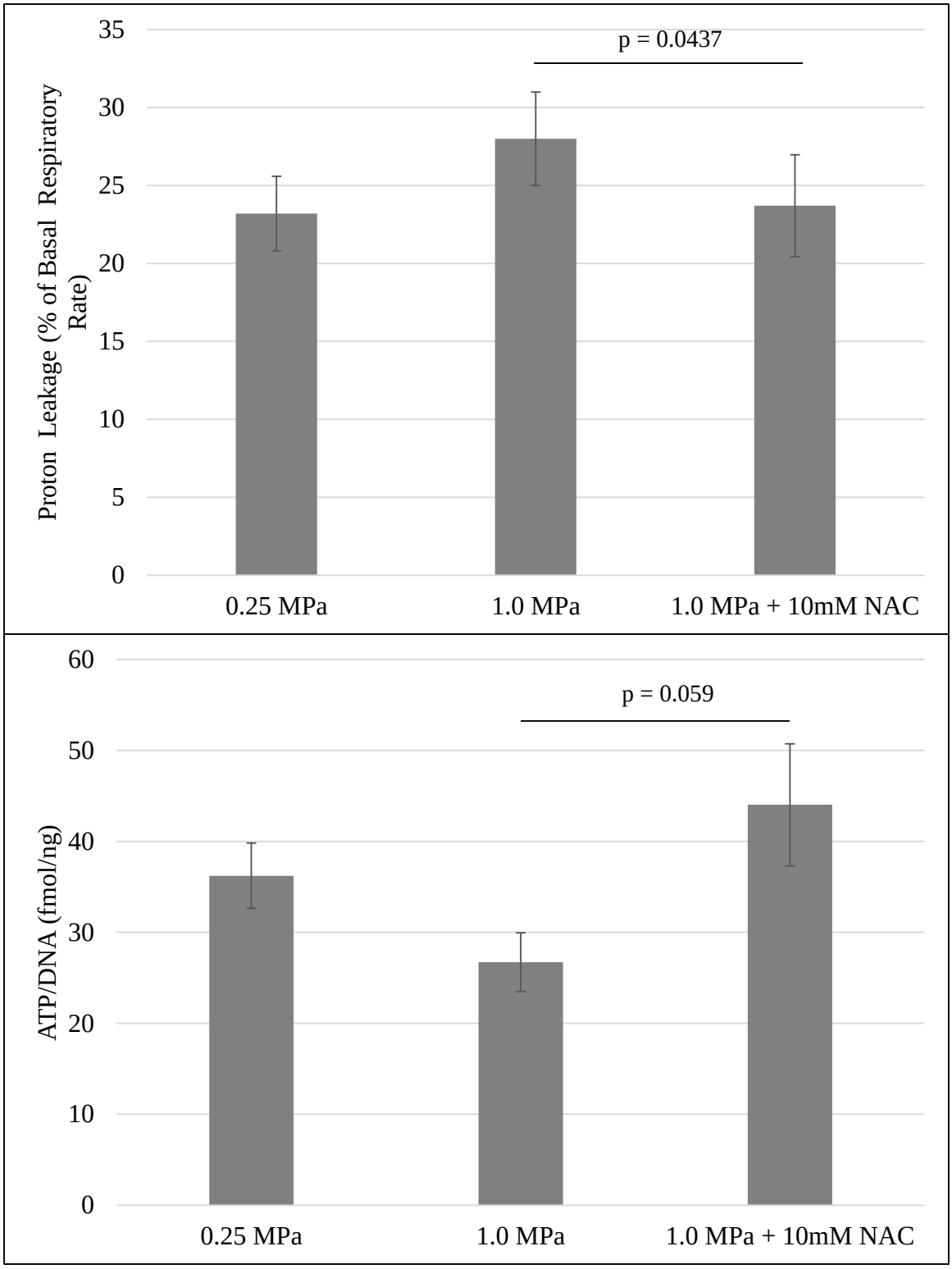

Figure 30. Derived data from mitochondrial stress test and ATP assay performed on explants loaded for 3 hours per day for 7 days. NAC provided overloading protection, preventing proton leak increases and maintaining ATP levels.

The expansion of the loading schemes used to stimulate cartilage showed that one-hour applications of varying stress levels were always associated with increased ATP content. Explants that responded to the stresses by increasing intracellular ROS were shown to also increase ATP content. However, the ROS response to higher or lower stresses varied by explant and did not consistently correlate with dynamic stress application as it did with static stress application. This variation could be due to the new analysis of DHE. The static stress experiments did not verify that the cells counted were actually alive, whereas, here, only live cells were counted. This factor alone could account for this difference, as cells that have necrosed or endured enough ROS to undergo apoptosis would stain brightly with DHE and not be counted under the current method. However, when the change in DHE intensity was compared to the change in ATP content a trend begins to appear. The validity of this correlation would be greatly enhanced with the addition of more samples.

The experiments in which explants were dynamically loaded for seven days were designed to simulate a scenario where cartilage would endure overloading, as compared to normal loading. As such, the two stresses were meant to mimic a moderate and severe load, and were chosen based on previous results. Here overloading resulted in a decrease in nearly every metabolic output and showed signs of mitochondrial damage. However, it is known that these same endpoints obtained from the Seahorse Extracellular Flux Analyzer are much higher in late stage OA chondrocytes [149]. The increased proton leak is seen in OA cartilage as well as in the 1.0 MPa loading group. These results suggest that our seven-day, 1.0 MPa loading group displays early signs of OA, which can be mediated with antioxidant treatment.

CHAPTER 7:

CRITIQUES AND DISCUSSION:

Critiques

The explant loading system has worked well, but in critically evaluating the components, several changes could be made. One potential disadvantage was that stainless steel was used for the impermeable indenter, and nickel ion release from standard 316L stainless steel has been shown to have harmful effects on biological tissues. In particular, nickel ions alone have depressed chondrocyte matrix production and proliferation [173]. An improvement to this indenter would be to use a nickel-free stainless steel, which has been shown to have better biocompatibility [174, 175]. The indenter should also be made porous to allow for unabated fluid flow and nutrient delivery. The flat end of the indenter also causes extensive shear stress at the border and has a tendency to cause cell death in this area. Rounding the edges would lessen this effect without reducing the contact area.

There were also limitations to the confocal imaging parameters. DHE is not entirely superoxide-specific [167], therefore higher levels of peroxide would also show a DHE signal. Also, DHE oxidizes in light and air, so there was risk for artificial increases in intensity. When DHE reacts with superoxide, however, a specific product is formed that has a much higher fluorescence signal than other species that can be formed from the reactions between DHE and other ROS [165, 176]. Brief work to determine if the superoxide-specific product was formed in loading scenarios was done by isolating DHE from stained cartilage. However, the low cell density within cartilage due to extensive

extracellular matrices made isolation of the DHE products difficult, and proved to dilute the sample to near undetectable levels (See Appendix). Therefore, DHE is reported as a general oxidation marker, and not an ROS-specific identifier. To assert the role of specific ROS, specific chemicals that target superoxide, or its site of generation, were used.

Despite the link between ATP content and both glycolytic activity and proteoglycan synthesis [46, 63, 171], it is not a rate measurement. It is a bulk measurement that can be affected by other intracellular process that could, themselves, be affected by the treatments used in these studies. Chondrocytes have also been shown to release ATP upon mechanical stimulation; however, ATP release was still correlated with matrix synthesis [177]. As intracellular and extracellular sources of ATP were not discriminated in the ATP measurements presented, the contribution of ATP release in our ATP measurements cannot be excluded. To minimize all controllable variations, one explant from each bovine knee was always left as an unstimulated/treated control. Energy production in chondrocytes is a very complex balance, and the inhibitors and chemicals used in these studies might have other effects that would not be captured in the limited tests performed here.

These limitations in no way invalidate the data from these studies, but they certainly should be considered in any interpretation of the results presented. With the addition of more samples to low-number treatments groups, these data sets will further disclose the complex role that mitochondrial ROS play in ATP production in cartilage.

Discussion

This dissertation project has thoroughly examined the mechano-response of chondrocytes in articular cartilage. Firstly, it has shown that superoxide is produced in response to mechanical stimulation. This superoxide production comes from the mitochondria and is necessary to stimulate an increase in ATP content from glycolysis. This same glycolytic increase can be artificially created by chemically inducing mitochondrial superoxide production at complex III, which is further enhanced by supplementation with an SOD mimetic to readily convert the superoxide into peroxide. These findings point toward a unique regulation of metabolism in articular chondrocytes. These mitochondrial ROS have also been shown to regulate intracellular pH. Antimycin A and peroxide supplementation on isolated chondrocytes significantly increased acid efflux, while hypoxia and complex I inhibitor, rotenone, decreases it [129]. This result fits well with what is reported here, as glycolytic stimulation would result in increased intracellular pH that would necessitate higher efflux values. Also, hypoxia inducible factor 1 (Hif1), is known to be stabilized and accumulate during peroxide treatment [178, 179]. This powerful transcription factor plays a large role in adapting cells' metabolic state to oxygen concentrations [180], which could play a potential role in the response of articular cartilage to load.

These same mitochondrial ROS that seem to regulate normal metabolic function also seem to have important effects in OA disease progression. The mitochondrial inhibitors that stimulate superoxide production seem to sensitize chondrocytes to inflammatory cytokines [181]. There is also a consensus that ROS accumulation plays a major role in OA development, as indicated by accumulation of lipid peroxidation,

reduction in SOD, and impaired mitochondrial function [149]. In our explant loading system, some of these initial mitochondrial impairments occurred as a result of excess mechanical load. These changes could be completely inhibited by supplementation of the antioxidant, NAC. Together, these findings have important implications for the mechanisms of OA progression as well as potential options for treatment, especially after traumatic injuries which have been shown to dramatically increase risk for developing OA [182].

Further investigation into what is signaled by peroxide to upregulate ATP production is necessary to close the mechanistic chain. I hope to continue this investigation until this loop is closed, but know that there will always be more questions than answers. A final summary of the results outlined above is that mechanical stimulation of cartilage produces mitochondrial superoxide, which converts into peroxide, whose role in articular cartilage is complex. In short term mechanical stimulations, this peroxide acts to stimulate metabolism. At higher stresses, and over longer durations, ROS cause damage which results in mitochondrial dysfunction which can prevented by bolstering intracellular defenses against peroxide.

APPENDIX

Validation of Ultrasound Based Thickness Measurements

Articular cartilage thickness was measured using a calibrated ultrasound device (Olympus 35-DL, Figure 31) for all stress experiments. The ultrasound device tip was brought to rest on top of the articular cartilage normal to the explant surface, which was immersed in media. The delay in sound pulses from the interface to the backwall (subchondral bone) was used to calculate the tissue thickness.

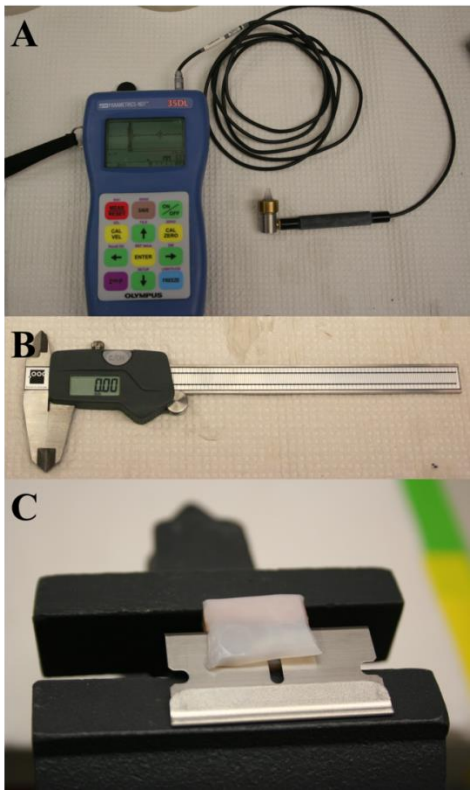

Figure 31 The cartilage measurement devices used to calculate strain measurements from stress application experiments are shown here (A and B). The extraction method for validation of the ultrasound device is also shown (C).

The correlation was very strong between caliper measurements and the ultrasound measurements (Figure 32). The average measurement difference of the ultrasound device was 4.6%.

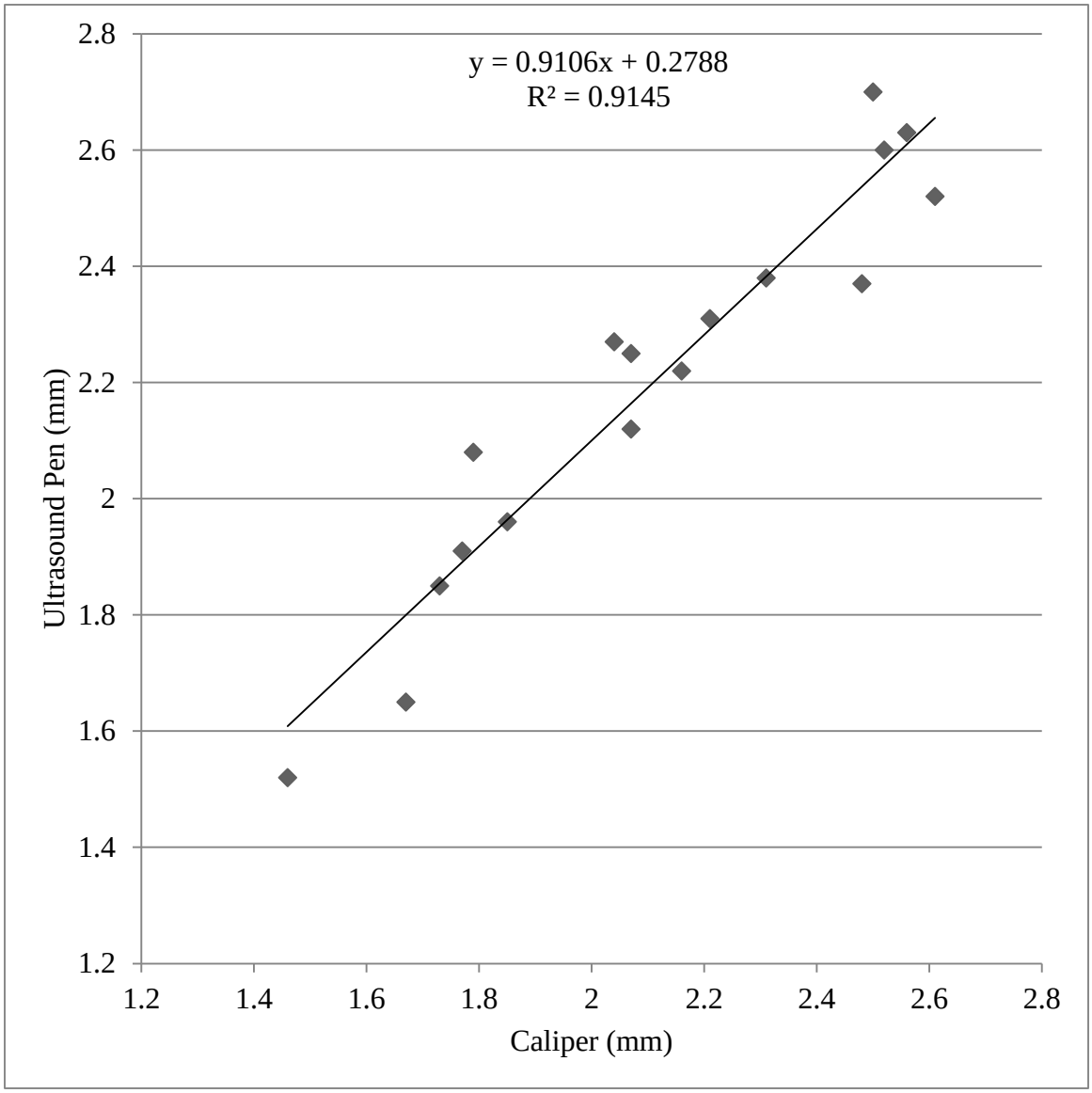

Figure 32. Correlation between the ultrasound pen measurement and caliper measurements after cartilage removal. Excellent agreement was seen with the ultrasound measurement.

These measurements allowed for rapid measurement of the cartilage thickness at points of impact or mechanical loading. This thickness was used to calculate any strain measurements from mechanical loading experiments. The lowest cartilage thickness displayed was the value recorded for each explant, under the assumption that the shortest ultrasound reflection time would be when the ultrasound pen was perpendicular with the subchondral bone surface, and thus provide the most accurate tissue thickness measurement.

DHE HPLC Results

A subgoal not fully pursued in this dissertation was to confirm that the DHE staining we observed was in fact due to superoxide. At the time of data collection, it was known that DHE was not superoxide-specific, and could react with many ROS [176]. It was also shown that when DHE does react with superoxide, it forms a specific product that can be identified through HPLC. In the chapters above, we addressed the issue of nonspecificity by targeting individual ROS with chemicals that sequester specific ROS, and then blocked specific mitochondrial proteins that produce superoxide.

Cartilage plugs (6 mm) were harvested directly after the 5 μM DHE staining step from the static stress experiments. This plug was digested with papain in the presence of 250 μM DTPA. Following this digestion, the cell debris was pelleted, and the supernatants were processed according to Zielonka et al. [183]. Brett Wagner was crucial to these experiments, as he had already separated DHE-specific products using this method. So, under his guidance, I looked for the superoxide specific product in statically loaded explants.

The initial results were promising, as the 1.0 MPa statically stressed explant did have a higher amount of the superoxide specific product (2-OH-E^+, Figure 33). This is seen by the higher response peak designated at the earlier retention time. However, this signal was deemed too weak for the concentrations of DHE used, and therefore other methods were chosen to show that superoxide was being produced in our explant system.

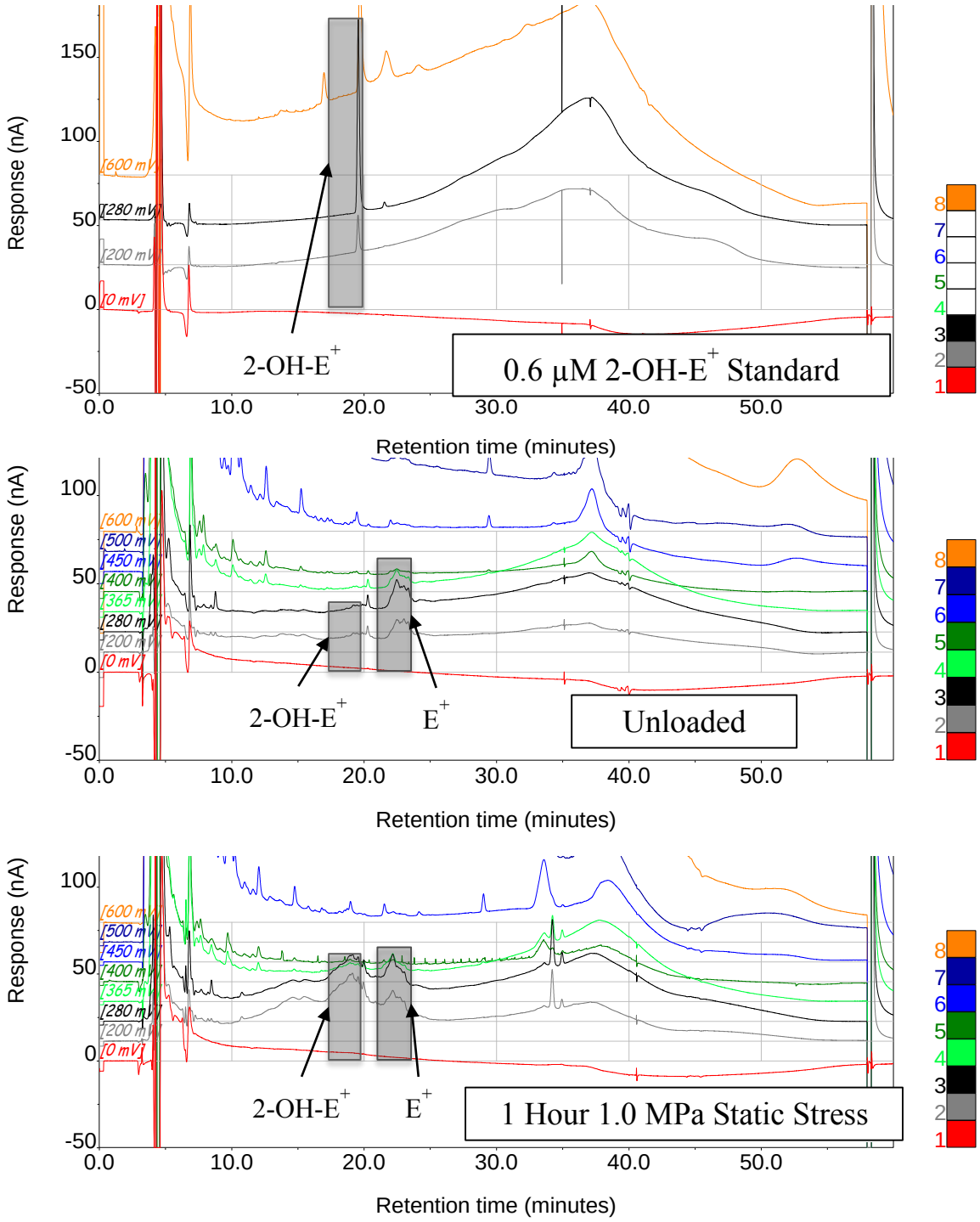

Figure 33. Initial HPLC run to separate the superoxide specific product from cartilage exposed to 1.0 MPa static stress. The stressed explant did seem to show a slight increase over the unloaded explant, however compared to the standard

ATP Assay Description

Below is the standard protocol developed to measure ATP content from bovine cartilage. It is an adaptation of the method described by Long and Guthrie [184].

Materials:

1. 1 Wallac 96-well plate and adapter – Reaction vessel
2. 1 sterile 96-well plate – Sample preparation vessel
3. 2x15 mL falcon tubes (1 full of DI water, 1 empty but covered with foil on the outside)
4. Sigma Phosphatase Inhibitor Cocktail 2 (Sigma P5726)
5. Sigma ATP Bioluminescence Assay – Dilution Buffer, Luciferase, and ATP Standard (200 µM) prepared according to Sigma directions
6. 1.5mL eppendorf tubes (2 for each cartilage specimen +1 for ATP standard)
7. Boiling water in 1000-mL beaker with eppendorf tube flotation device or heat block at 100°C

The protocol will use two vessels to prepare the ATP assay. The "sample preparation vessel" is a clear generic 96-well plate, while the "reaction vessel" is a white 96-well plate designed for luminescence reactions. Example well designations are listed below. A row will be skipped after the standard, as to avoid "bleed through" from the standards on the sample luminescence readings. Samples are prepared in triplicate.

Note: These concentrations for the standard are for the final plate read

	1	2	3	4	5	6						
A	ATP 2µM	ATP 200nM	ATP 20nM	ATP 2nM	ATP 200pM	ATP 20pM						
C	Sample 1	Sample 1	Sample 1	Sample 2	Sample 2	Sample 2						
E												
G												

The following needs to be completed before sample harvest:

1. Obtain all of the listed materials and allow them to thaw, making sure to always keep anything containing luciferase covered in foil. Also start boiling the 1000-mL beaker half full of water if you have not already.
2. Prepare phosphatase inhibitor solution for standard and samples.
    a. Standard
        i. Add 1188 µL sterile water to 1.5mL tube
        ii. Add 12 µL phosphatase inhibitor cocktail to tube for a 1:100 dilution
    b. For each cartilage sample you will be running
        i. Label the two 1.5 mL eppendorf tubes with the sample number
        ii. Add 990 µL sterile water and 10 µL phosphatase inhibitor to the first tube for a 1:100 dilution of the phosphatase inhibitor (used for ATP quantification)
        iii. Leave the other tube empty (used for DNA quantification if needed)
        iv. Tare both tubes, record mass.

c. Create the ATP standards in the clear sample preparation vessel

i. For the ATP standard (200µM), add the following amounts of phosphatase inhibitor solution prepared in step 2 above to the following wells of the sample preparation vessel:

A1	A2	A3	A4	A5	A6
190 µL	180 µL	180 µL	180 µL	180 µL	180 µL

ii. Add 10 µL standard stock to well A1, mix well, and then 20 µL from that well to well A2, and continue down the line until well A6. Discard 20 µL from the A6 vessel, which should result in the dilutions shown in the well plate diagram above.

d. Be sure the water is boiling or the heat block is at temperature for ATP extraction before you begin to harvest samples. Add a stirrer to the beaker to avoid boiling over.

Sample harvest and ATP extraction

1. Obtain a full thickness cartilage sample from each cartilage specimen. Wet weights above 10 mg provide the most consistent readings.
2. Place the sample in the tared eppendorf tube containing water and phosphatase inhibitor (ATP quantification) Measure and record the mass.
3. After all samples have been obtained, place the tubes for ATP quantification into the boiling water for 10 minutes.

4. During this 10 minute boiling session, prepare the luciferase reaction solution
    a. To the 15mL falcon tube wrapped in foil: add 90µL × (#wells + 2) of the dilution buffer and 10µL × (#wells + 2) of the luciferase. The additional number is to ensure a proper volume for each well and can be adjusted based on need/experience. Mix thoroughly.
    b. Ex: For one sample being read in wells C1-C3 and the standards the total number of wells being read would be 9. The total volume added to the 15mL falcon tube is listed below.
        i. Dilution buffer volume=(90µL)×(9wells +2)=990µL
        ii. Luciferase volume= (10µL)×(9wells +"2)=110µL
5. After mixing, distribute 100µL of the luciferase reaction solution to each well being used in the white reaction vessel
6. After the 10 minutes of boiling have elapsed, place the samples into the centrifuge for 1 min.
7. Add 100 µL of supernatant to the wells designated for each sample in the clear sample preparation vessel
8. Once all samples are ready in the clear sample preparation vessel, use the multipipettor to add 25 µL from each used well in the clear sample preparation vessel to the corresponding well in the white reaction vessel. Mix by pipetting up and down several times.
9. Immediately, take the white reaction vessel to the Luminescence counter, place the 96-well plate in its appropriate adapter, and run the plate in a luminescence counter.

Other Mechanical Stimulation Machines

Below are the devices that have been program offshoots from the dynamic loading platform originally created in chapter 2 (Figure 34). The machine built to measure the dynamic frictional force of cartilage were designed/built by Dr. Prem Ramakrishnan and Dr. James Rudert. Dr. Rudert also designed and built the drawer tester, which is used to measure the stiffness of rabbit knee joints. Tom Baer built the initial loading platform used in chapters 3 and 4, the specimen holders, and the pushout tester. The 48-well plate loader was designed with the help of Timothy Weaver at the University of Iowa Medical Machine Shop. Mr. Weaver was also responsible for building the additional two platforms for the dynamic loading devices used in chapter 6. This list displays how the modular nature of the initial motion control program designed allowed for quick turnaround in adapting it to other uses.

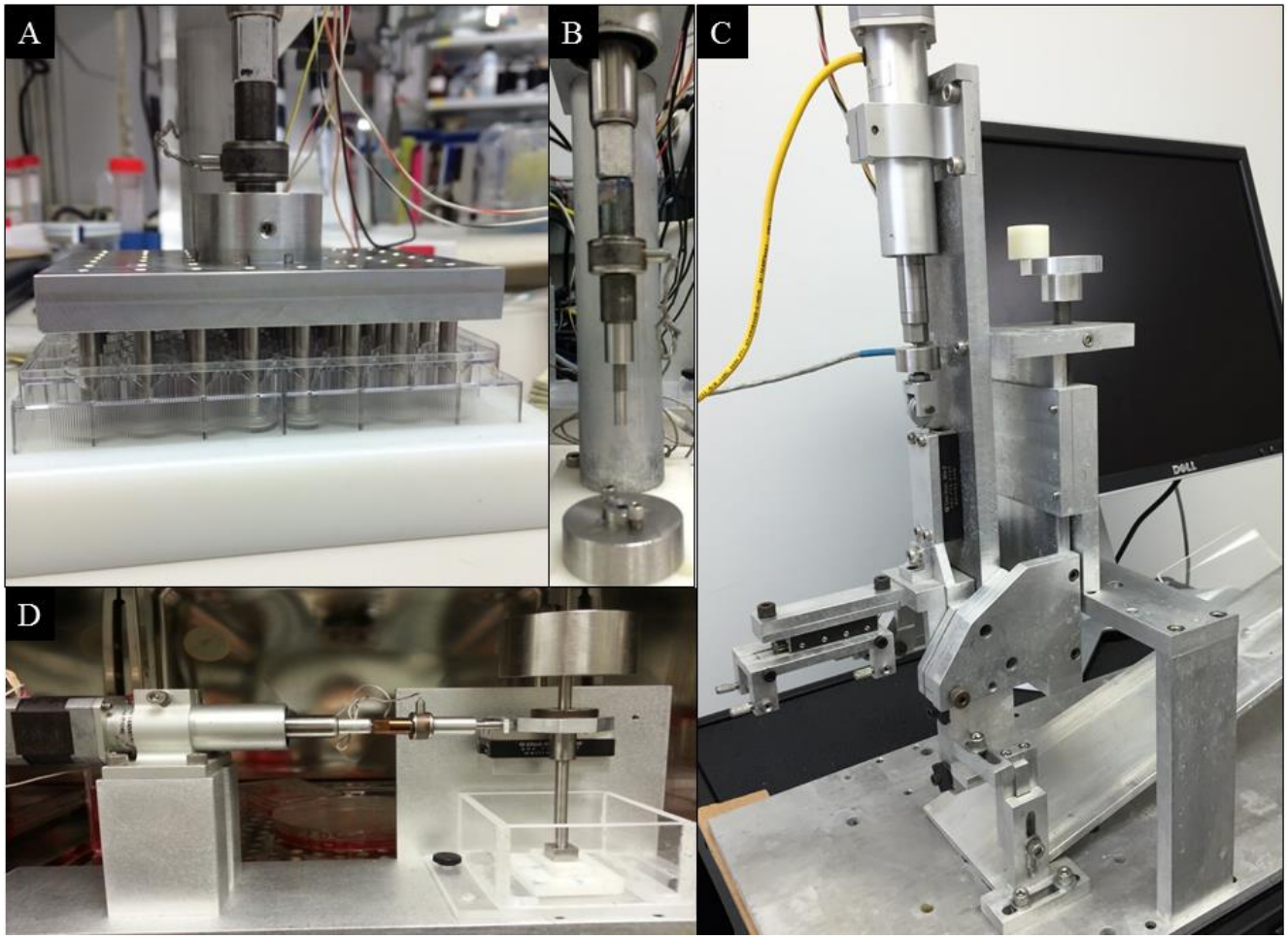

Figure 34. The various other devices made possible by adapting the initial dynamic loading program. A) 48 Well Tissue Culture Plate Stimulator, B) Pushout-tester, C) Drawer Tester, D) Frictional Loader/Measurement Device

REFERENCES

1. Beecher, B.R., et al., *Antioxidants block cyclic loading induced chondrocyte death.* Iowa Orthop J, 2007. **27**: p. 1-8.
2. Martin, J.A., et al., *N-acetylcysteine inhibits post-impact chondrocyte death in osteochondral explants.* J Bone Joint Surg Am, 2009. **91**(8): p. 1890-7.
3. Sauter, E., et al., *Cytoskeletal dissolution blocks oxidant release and cell death in injured cartilage.* J Orthop Res, 2011.
4. Martin, J.A., et al., *Mitochondrial electron transport and glycolysis are coupled in articular cartilage.* Osteoarthritis Cartilage, 2012. **20**(4): p. 323-9.
5. Quinn, T.M., et al., *Mechanical compression alters proteoglycan deposition and matrix deformation around individual cells in cartilage explants.* J Cell Sci, 1998. **111 (Pt 5)**: p. 573-83.
6. Quinn, T.M., V. Morel, and J.J. Meister, *Static compression of articular cartilage can reduce solute diffusivity and partitioning: implications for the chondrocyte biological response.* J Biomech, 2001. **34**(11): p. 1463-9.
7. Stevens, A.L., et al., *Mechanical injury and cytokines cause loss of cartilage integrity and upregulate proteins associated with catabolism, immunity, inflammation, and repair.* Mol Cell Proteomics, 2009. **8**(7): p. 1475-89.
8. Torzilli, P.A., X.H. Deng, and M. Ramcharan, *Effect of compressive strain on cell viability in statically loaded articular cartilage.* Biomech Model Mechanobiol, 2006. **5**(2-3): p. 123-32.
9. Segal, N.A., et al., *Baseline articular contact stress levels predict incident symptomatic knee osteoarthritis development in the MOST cohort.* J Orthop Res, 2009. **27**(12): p. 1562-8.
10. Kotlarz, H., et al., *Insurer and out-of-pocket costs of osteoarthritis in the US: Evidence from national survey data.* Arthritis & Rheumatism, 2009. **60**(12): p. 3546-3553.
11. Hootman, J.M. and C.G. Helmick, *Projections of US prevalence of arthritis and associated activity limitations.* Arthritis Rheum, 2006. **54**(1): p. 226-9.
12. Bhosale, A.M. and J.B. Richardson, *Articular cartilage: structure, injuries and review of management.* Br Med Bull, 2008. **87**: p. 77-95.
13. Poole, A.R., et al., *Composition and structure of articular cartilage: a template for tissue repair.* Clin Orthop Relat Res, 2001(391 Suppl): p. S26-33.
14. Roughley, P.J., *The structure and function of cartilage proteoglycans.* Eur Cell Mater, 2006. **12**: p. 92-101.
15. Stockwell, R.A., *The cell density of human articular and costal cartilage.* J Anat, 1967. **101**(Pt 4): p. 753-63.
16. Poole, C.A., S. Ayad, and J.R. Schofield, *Chondrons from articular cartilage: I. Immunolocalization of type VI collagen in the pericellular capsule of isolated canine tibial chondrons.* J Cell Sci, 1988. **90 (Pt 4)**: p. 635-43.
17. Poole, C.A., et al., *Chondrons from articular cartilage (II): Analysis of the glycosaminoglycans in the cellular microenvironment of isolated canine chondrons.* Connect Tissue Res, 1990. **24**(3-4): p. 319-30.

18. Poole, C.A., T.T. Glant, and J.R. Schofield, *Chondrons from articular cartilage. (IV). Immunolocalization of proteoglycan epitopes in isolated canine tibial chondrons.* J Histochem Cytochem, 1991. **39**(9): p. 1175-87.
19. Poole, C.A., et al., *Immunolocalization of type IX collagen in normal and spontaneously osteoarthritic canine tibial cartilage and isolated chondrons.* Osteoarthritis Cartilage, 1997. **5**(3): p. 191-204.
20. Poole, C.A., M.H. Flint, and B.W. Beaumont, *Chondrons in cartilage: ultrastructural analysis of the pericellular microenvironment in adult human articular cartilages.* J Orthop Res, 1987. **5**(4): p. 509-22.
21. Lee, G.M., et al., *Isolated chondrons: a viable alternative for studies of chondrocyte metabolism in vitro.* Osteoarthritis Cartilage, 1997. **5**(4): p. 261-74.
22. Schinagl, R.M., et al., *Depth-dependent confined compression modulus of full-thickness bovine articular cartilage.* J Orthop Res, 1997. **15**(4): p. 499-506.
23. Wilusz, R.E., L.E. DeFrate, and F. Guilak, *Immunofluorescence-guided atomic force microscopy to measure the micromechanical properties of the pericellular matrix of porcine articular cartilage.* J R Soc Interface, 2012. **9**(76): p. 2997-3007.
24. Choi, J.B., et al., *Zonal changes in the three-dimensional morphology of the chondron under compression: the relationship among cellular, pericellular, and extracellular deformation in articular cartilage.* J Biomech, 2007. **40**(12): p. 2596-603.
25. Wilusz, R.E., S. Zauscher, and F. Guilak, *Micromechanical mapping of early osteoarthritic changes in the pericellular matrix of human articular cartilage.* Osteoarthritis Cartilage, 2013. **21**(12): p. 1895-903.
26. Tian, J., F.J. Zhang, and G.H. Lei, *Role of integrins and their ligands in osteoarthritic cartilage.* Rheumatol Int, 2015. **35**(5): p. 787-98.
27. Loeser, R.F., *Integrins and chondrocyte-matrix interactions in articular cartilage.* Matrix Biol, 2014. **39**: p. 11-6.
28. Baker, E.L. and M.H. Zaman, *The biomechanical integrin.* J Biomech, 2010. **43**(1): p. 38-44.
29. Wright, M.O., et al., *Hyperpolarisation of cultured human chondrocytes following cyclical pressure-induced strain: evidence of a role for alpha 5 beta 1 integrin as a chondrocyte mechanoreceptor.* J Orthop Res, 1997. **15**(5): p. 742-7.
30. Zemmyo, M., et al., *Accelerated, aging-dependent development of osteoarthritis in alpha1 integrin-deficient mice.* Arthritis Rheum, 2003. **48**(10): p. 2873-80.
31. Lapadula, G., et al., *Integrin expression on chondrocytes: correlations with the degree of cartilage damage in human osteoarthritis.* Clin Exp Rheumatol, 1997. **15**(3): p. 247-54.
32. Trickey, W.R., T.P. Vail, and F. Guilak, *The role of the cytoskeleton in the viscoelastic properties of human articular chondrocytes.* J Orthop Res, 2004. **22**(1): p. 131-9.
33. Brouillette, M.J., *Static compressive stress induces mitochondrial oxidant production in articular cartilage*. 2012, The University of Iowa: Ann Arbor. p. 52.
34. Wilusz, R.E., J. Sanchez-Adams, and F. Guilak, *The structure and function of the pericellular matrix of articular cartilage.* Matrix Biol, 2014. **39**: p. 25-32.

35. Heinegard, D. and T. Saxne, *The role of the cartilage matrix in osteoarthritis.* Nat Rev Rheumatol, 2011. **7**(1): p. 50-6.
36. Schnabel, M., et al., *Dedifferentiation-associated changes in morphology and gene expression in primary human articular chondrocytes in cell culture.* Osteoarthritis Cartilage, 2002. **10**(1): p. 62-70.
37. Stokes, D.G., et al., *Assessment of the gene expression profile of differentiated and dedifferentiated human fetal chondrocytes by microarray analysis.* Arthritis Rheum, 2002. **46**(2): p. 404-19.
38. Zhou, S., Z. Cui, and J.P. Urban, *Factors influencing the oxygen concentration gradient from the synovial surface of articular cartilage to the cartilage-bone interface: a modeling study.* Arthritis Rheum, 2004. **50**(12): p. 3915-24.
39. Falchuk, K.H., E.J. Goetzl, and J.P. Kulka, *Respiratory gases of synovial fluids. An approach to synovial tissue circulatory-metabolic imbalance in rheumatoid arthritis.* Am J Med, 1970. **49**(2): p. 223-31.
40. Ferrell, W.R. and H. Najafipour, *Changes in synovial PO2 and blood flow in the rabbit knee joint due to stimulation of the posterior articular nerve.* J Physiol, 1992. **449**: p. 607-17.
41. Lund-Olesen, K., *Oxygen tension in synovial fluids.* Arthritis Rheum, 1970. **13**(6): p. 769-76.
42. Najafipour, H. and W.R. Ferrell, *Comparison of synovial PO2 and sympathetic vasoconstrictor responses in normal and acutely inflamed rabbit knee joints.* Exp Physiol, 1995. **80**(2): p. 209-20.
43. Urban, J.P., *The chondrocyte: a cell under pressure.* Br J Rheumatol, 1994. **33**(10): p. 901-8.
44. Clark, C.C., B.S. Tolin, and C.T. Brighton, *The effect of oxygen tension on proteoglycan synthesis and aggregation in mammalian growth plate chondrocytes.* J Orthop Res, 1991. **9**(4): p. 477-84.
45. Henderson, G.E. and R.M. Mason, *Effect of oxygen tension on 35S-glycosaminoglycan synthesis and UDP-sugar pool size in articular cartilage.* Biochem Soc Trans, 1991. **19**(4): p. 364S.
46. Lee, R.B. and J.P. Urban, *Evidence for a negative Pasteur effect in articular cartilage.* Biochem J, 1997. **321 (Pt 1)**: p. 95-102.
47. Heywood, H.K., D.L. Bader, and D.A. Lee, *Rate of oxygen consumption by isolated articular chondrocytes is sensitive to medium glucose concentration.* J Cell Physiol, 2006. **206**(2): p. 402-10.
48. Haapala, J., et al., *Incomplete restoration of immobilization induced softening of young beagle knee articular cartilage after 50-week remobilization.* Int J Sports Med, 2000. **21**(1): p. 76-81.
49. Ng, N.T., K.C. Heesch, and W.J. Brown, *Strategies for Managing Osteoarthritis.* Int J Behav Med, 2011.
50. Hagiwara, Y., et al., *Changes of articular cartilage after immobilization in a rat knee contracture model.* J Orthop Res, 2009. **27**(2): p. 236-42.
51. Haapala, J., et al., *Remobilization does not fully restore immobilization induced articular cartilage atrophy.* Clin Orthop Relat Res, 1999(362): p. 218-29.
52. Hinterwimmer, S., et al., *Cartilage atrophy in the knees of patients after seven weeks of partial load bearing.* Arthritis Rheum, 2004. **50**(8): p. 2516-20.

53. Kurz, B., et al., *Biosynthetic response and mechanical properties of articular cartilage after injurious compression.* J Orthop Res, 2001. **19**(6): p. 1140-6.
54. Arendt, E. and R. Dick, *Knee injury patterns among men and women in collegiate basketball and soccer. NCAA data and review of literature.* Am J Sports Med, 1995. **23**(6): p. 694-701.
55. Fransen, M., S. McConnell, and M. Bell, *Therapeutic exercise for people with osteoarthritis of the hip or knee. A systematic review.* J Rheumatol, 2002. **29**(8): p. 1737-45.
56. Dowthwaite, G.P., et al., *The surface of articular cartilage contains a progenitor cell population.* J Cell Sci, 2004. **117**(Pt 6): p. 889-97.
57. Koelling, S., et al., *Migratory chondrogenic progenitor cells from repair tissue during the later stages of human osteoarthritis.* Cell Stem Cell, 2009. **4**(4): p. 324-35.
58. Seol, D., et al., *Chondrogenic progenitor cells respond to cartilage injury.* Arthritis Rheum, 2012. **64**(11): p. 3626-37.
59. Williams, R., et al., *Identification and clonal characterisation of a progenitor cell sub-population in normal human articular cartilage.* PLoS One, 2010. **5**(10): p. e13246.
60. Yu, Y., et al., *Single cell sorting identifies progenitor cell population from full thickness bovine articular cartilage.* Osteoarthritis Cartilage, 2014. **22**(9): p. 1318-26.
61. Zhou, C., et al., *Gene expression profiles reveal that chondrogenic progenitor cells and synovial cells are closely related.* J Orthop Res, 2014. **32**(8): p. 981-8.
62. Brighton, C.T., T. Kitajima, and R.M. Hunt, *Zonal analysis of cytoplasmic components of articular cartilage chondrocytes.* Arthritis Rheum, 1984. **27**(11): p. 1290-9.
63. Lee, R.B. and J.P. Urban, *Functional replacement of oxygen by other oxidants in articular cartilage.* Arthritis Rheum, 2002. **46**(12): p. 3190-200.
64. Schneider, N., et al., *Oxygen consumption of equine articular chondrocytes: Influence of applied oxygen tension and glucose concentration during culture.* Cell Biol Int, 2007. **31**(9): p. 878-86.
65. Berg, J.M., J.L. Tymoczko, and L. Stryer, *Biochemistry*. 2007: W. H. Freeman.
66. Hirst, J., *Energy transduction by respiratory complex I--an evaluation of current knowledge.* Biochem Soc Trans, 2005. **33**(Pt 3): p. 525-9.
67. Iverson, T.M., *Catalytic mechanisms of complex II enzymes: a structural perspective.* Biochim Biophys Acta, 2013. **1827**(5): p. 648-57.
68. Kim, H.J. and D.R. Winge, *Emerging concepts in the flavinylation of succinate dehydrogenase.* Biochim Biophys Acta, 2013. **1827**(5): p. 627-36.
69. Mulkidjanian, A.Y., *Activated Q-cycle as a common mechanism for cytochrome bc1 and cytochrome b6f complexes.* Biochimica et Biophysica Acta (BBA) - Bioenergetics, 2010. **1797**(12): p. 1858-1868.
70. Zhang, Z., et al., *Electron transfer by domain movement in cytochrome bc1.* Nature, 1998. **392**(6677): p. 677-84.
71. Bleier, L. and S. Drose, *Superoxide generation by complex III: from mechanistic rationales to functional consequences.* Biochim Biophys Acta, 2013. **1827**(11-12): p. 1320-31.

72. Mulkidjanian, A.Y., *Ubiquinol oxidation in the cytochrome bc1 complex: reaction mechanism and prevention of short-circuiting.* Biochim Biophys Acta, 2005. **1709**(1): p. 5-34.
73. Berry, E.A. and L.S. Huang, *Conformationally linked interaction in the cytochrome bc(1) complex between inhibitors of the Q(o) site and the Rieske iron-sulfur protein.* Biochim Biophys Acta, 2011. **1807**(10): p. 1349-63.
74. Cen, X., L. Yu, and C.A. Yu, *Domain movement of iron sulfur protein in cytochrome bc1 complex is facilitated by the electron transfer from cytochrome b(L) to b(H).* FEBS Lett, 2008. **582**(4): p. 523-6.
75. Ding, H., et al., *Cytochrome bc1 complex [2Fe-2S] cluster and its interaction with ubiquinone and ubihydroquinone at the Qo site: a double-occupancy Qo site model.* Biochemistry, 1992. **31**(12): p. 3144-58.
76. Bartoschek, S., et al., *Three molecules of ubiquinone bind specifically to mitochondrial cytochrome bc1 complex.* J Biol Chem, 2001. **276**(38): p. 35231-4.
77. Zhu, J., et al., *Simultaneous reduction of iron-sulfur protein and cytochrome b(L) during ubiquinol oxidation in cytochrome bc(1) complex.* Proc Natl Acad Sci U S A, 2007. **104**(12): p. 4864-9.
78. Murphy, M.P., *How mitochondria produce reactive oxygen species.* Biochem J, 2009. **417**(1): p. 1-13.
79. Jensen, P.K., *Antimycin-insensitive oxidation of succinate and reduced nicotinamide-adenine dinucleotide in electron-transport particles. I. pH dependency and hydrogen peroxide formation.* Biochim Biophys Acta, 1966. **122**(2): p. 157-66.
80. Loschen, G., L. Flohe, and B. Chance, *Respiratory chain linked H(2)O(2) production in pigeon heart mitochondria.* FEBS Lett, 1971. **18**(2): p. 261-264.
81. Boveris, A. and B. Chance, *The mitochondrial generation of hydrogen peroxide. General properties and effect of hyperbaric oxygen.* Biochem J, 1973. **134**(3): p. 707-16.
82. Weisiger, R.A. and I. Fridovich, *Superoxide dismutase. Organelle specificity.* J Biol Chem, 1973. **248**(10): p. 3582-92.
83. Weisiger, R.A. and I. Fridovich, *Mitochondrial superoxide dimutase. Site of synthesis and intramitochondrial localization.* J Biol Chem, 1973. **248**(13): p. 4793-6.
84. Forman, H.J. and J.A. Kennedy, *Role of superoxide radical in mitochondrial dehydrogenase reactions.* Biochem Biophys Res Commun, 1974. **60**(3): p. 1044-50.
85. Loschen, G., et al., *Superoxide radicals as precursors of mitochondrial hydrogen peroxide.* FEBS Lett, 1974. **42**(1): p. 68-72.
86. Kussmaul, L. and J. Hirst, *The mechanism of superoxide production by NADH:ubiquinone oxidoreductase (complex I) from bovine heart mitochondria.* Proc Natl Acad Sci U S A, 2006. **103**(20): p. 7607-12.
87. Votyakova, T.V. and I.J. Reynolds, *DeltaPsi(m)-Dependent and -independent production of reactive oxygen species by rat brain mitochondria.* J Neurochem, 2001. **79**(2): p. 266-77.

88. Lambert, A.J. and M.D. Brand, *Inhibitors of the quinone-binding site allow rapid superoxide production from mitochondrial NADH:ubiquinone oxidoreductase (complex I).* J Biol Chem, 2004. **279**(38): p. 39414-20.
89. Lambert, A.J. and M.D. Brand, *Superoxide production by NADH:ubiquinone oxidoreductase (complex I) depends on the pH gradient across the mitochondrial inner membrane.* Biochem J, 2004. **382**(Pt 2): p. 511-7.
90. Andreyev, A.Y., Y.E. Kushnareva, and A.A. Starkov, *Mitochondrial metabolism of reactive oxygen species.* Biochemistry (Mosc), 2005. **70**(2): p. 200-14.
91. Demin, O.V., B.N. Kholodenko, and V.P. Skulachev, *A model of O2.-generation in the complex III of the electron transport chain.* Mol Cell Biochem, 1998. **184**(1-2): p. 21-33.
92. Gille, L. and H. Nohl, *The ubiquinol/bc1 redox couple regulates mitochondrial oxygen radical formation.* Arch Biochem Biophys, 2001. **388**(1): p. 34-8.
93. Han, D., et al., *Voltage-dependent anion channels control the release of the superoxide anion from mitochondria to cytosol.* J Biol Chem, 2003. **278**(8): p. 5557-63.
94. Han, D., E. Williams, and E. Cadenas, *Mitochondrial respiratory chain-dependent generation of superoxide anion and its release into the intermembrane space.* Biochem J, 2001. **353**(Pt 2): p. 411-6.
95. Turrens, J.F., *Mitochondrial formation of reactive oxygen species.* J Physiol, 2003. **552**(Pt 2): p. 335-44.
96. Starkov, A.A. and G. Fiskum, *Myxothiazol induces H(2)O(2) production from mitochondrial respiratory chain.* Biochem Biophys Res Commun, 2001. **281**(3): p. 645-50.
97. Zhao, Y., et al., *p53 translocation to mitochondria precedes its nuclear translocation and targets mitochondrial oxidative defense protein-manganese superoxide dismutase.* Cancer Res, 2005. **65**(9): p. 3745-50.
98. Case, A.J., et al., *Elevated mitochondrial superoxide disrupts normal T cell development, impairing adaptive immune responses to an influenza challenge.* Free Radic Biol Med, 2011. **50**(3): p. 448-58.
99. Fridovich, I., *Superoxide radical and superoxide dismutases.* Annu Rev Biochem, 1995. **64**: p. 97-112.
100. Peshavariya, H.M., G.J. Dusting, and S. Selemidis, *Analysis of dihydroethidium fluorescence for the detection of intracellular and extracellular superoxide produced by NADPH oxidase.* Free Radic Res, 2007. **41**(6): p. 699-712.
101. Araujo-Chaves, J.C., et al., *Towards the mechanisms involved in the antioxidant action of MnIII [meso-tetrakis(4-N-methyl pyridinium) porphyrin] in mitochondria.* J Bioenerg Biomembr, 2011. **43**(6): p. 663-71.
102. Gardner, P.R., D.D. Nguyen, and C.W. White, *Superoxide scavenging by Mn(II/III) tetrakis (1-methyl-4-pyridyl) porphyrin in mammalian cells.* Arch Biochem Biophys, 1996. **325**(1): p. 20-8.
103. Smith, R.A., R.C. Hartley, and M.P. Murphy, *Mitochondria-targeted small molecule therapeutics and probes.* Antioxid Redox Signal, 2011. **15**(12): p. 3021-38.
104. Miriyala, S., et al., *Manganese superoxide dismutase, MnSOD and its mimics.* Biochim Biophys Acta, 2012. **1822**(5): p. 794-814.

105. Cuzzocrea, S., et al., *Protective effects of a new stable, highly active SOD mimetic, M40401 in splanchnic artery occlusion and reperfusion.* Br J Pharmacol, 2001. **132**(1): p. 19-29.
106. Gibson, J.S., et al., *Oxygen and reactive oxygen species in articular cartilage: modulators of ionic homeostasis.* Pflugers Arch, 2008. **455**(4): p. 563-73.
107. Grodzinsky, A.J., et al., *Cartilage tissue remodeling in response to mechanical forces.* Annu Rev Biomed Eng, 2000. **2**: p. 691-713.
108. Kuster, M.S., et al., *Joint load considerations in total knee replacement.* J Bone Joint Surg Br, 1997. **79**(1): p. 109-13.
109. Thambyah, A., B.P. Pereira, and U. Wyss, *Estimation of bone-on-bone contact forces in the tibiofemoral joint during walking.* Knee, 2005. **12**(5): p. 383-8.
110. Thambyah, A., J.C. Goh, and S.D. De, *Contact stresses in the knee joint in deep flexion.* Med Eng Phys, 2005. **27**(4): p. 329-35.
111. Bedi, A., et al., *Dynamic contact mechanics of the medial meniscus as a function of radial tear, repair, and partial meniscectomy.* J Bone Joint Surg Am, 2010. **92**(6): p. 1398-408.
112. Brown, T.D. and D.T. Shaw, *In vitro contact stress distribution on the femoral condyles.* J Orthop Res, 1984. **2**(2): p. 190-9.
113. Gilbert, S., et al., *Dynamic contact mechanics on the tibial plateau of the human knee during activities of daily living.* J Biomech, 2014. **47**(9): p. 2006-12.
114. Wang, H., et al., *Dynamic contact stress patterns on the tibial plateaus during simulated gait: a novel application of normalized cross correlation.* J Biomech, 2014. **47**(2): p. 568-74.
115. Hodge, W.A., et al., *Contact pressures in the human hip joint measured in vivo.* Proc Natl Acad Sci U S A, 1986. **83**(9): p. 2879-83.
116. Hosseini, A., et al., *In-vivo time-dependent articular cartilage contact behavior of the tibiofemoral joint.* Osteoarthritis Cartilage, 2010. **18**(7): p. 909-16.
117. Bingham, J.T., et al., *In vivo cartilage contact deformation in the healthy human tibiofemoral joint.* Rheumatology (Oxford), 2008. **47**(11): p. 1622-7.
118. Erne, O.K., et al., *Depth-dependent strain of patellofemoral articular cartilage in unconfined compression.* J Biomech, 2005. **38**(4): p. 667-72.
119. Gao, L.L., et al., *Depth and rate dependent mechanical behaviors for articular cartilage: experiments and theoretical predictions.* Mater Sci Eng C Mater Biol Appl, 2014. **38**: p. 244-51.
120. Guilak, F., A. Ratcliffe, and V.C. Mow, *Chondrocyte deformation and local tissue strain in articular cartilage: a confocal microscopy study.* J Orthop Res, 1995. **13**(3): p. 410-21.
121. Buckwalter, J.A., *Osteoarthritis and articular cartilage use, disuse, and abuse: experimental studies.* J Rheumatol Suppl, 1995. **43**: p. 13-5.
122. Oliveria, S.A., et al., *Body weight, body mass index, and incident symptomatic osteoarthritis of the hand, hip, and knee.* Epidemiology, 1999. **10**(2): p. 161-6.
123. Muller, F.J., et al., *Centrifugal and biochemical comparison of proteoglycan aggregates from articular cartilage in experimental joint disuse and joint instability.* J Orthop Res, 1994. **12**(4): p. 498-508.

124. Palmoski, M., E. Perricone, and K.D. Brandt, *Development and reversal of a proteoglycan aggregation defect in normal canine knee cartilage after immobilization.* Arthritis Rheum, 1979. **22**(5): p. 508-17.
125. Sah, R.L., et al., *Biosynthetic response of cartilage explants to dynamic compression.* J Orthop Res, 1989. **7**(5): p. 619-36.
126. Szafranski, J.D., et al., *Chondrocyte mechanotransduction: effects of compression on deformation of intracellular organelles and relevance to cellular biosynthesis.* Osteoarthritis Cartilage, 2004. **12**(12): p. 937-46.
127. Guilak, F., *Compression-induced changes in the shape and volume of the chondrocyte nucleus.* J Biomech, 1995. **28**(12): p. 1529-41.
128. Ohashi, T., et al., *Intracellular mechanics and mechanotransduction associated with chondrocyte deformation during pipette aspiration.* Biorheology, 2006. **43**(3-4): p. 201-14.
129. Milner, P.I., R.J. Wilkins, and J.S. Gibson, *The role of mitochondrial reactive oxygen species in pH regulation in articular chondrocytes.* Osteoarthritis Cartilage, 2007. **15**(7): p. 735-42.
130. Tomiyama, T., et al., *Cyclic compression loaded on cartilage explants enhances the production of reactive oxygen species.* J Rheumatol, 2007. **34**(3): p. 556-62.
131. Goodwin, W., et al., *Rotenone prevents impact-induced chondrocyte death.* J Orthop Res, 2010. **28**(8): p. 1057-63.
132. Ramakrishnan, P., et al., *Oxidant conditioning protects cartilage from mechanically induced damage.* J Orthop Res, 2010. **28**(7): p. 914-20.
133. Blanco, F.J., I. Rego, and C. Ruiz-Romero, *The role of mitochondria in osteoarthritis.* Nat Rev Rheumatol, 2011. **7**(3): p. 161-9.
134. Zhang, Q., et al., *Circulating mitochondrial DAMPs cause inflammatory responses to injury.* Nature, 2010. **464**(7285): p. 104-7.
135. Coskun, P., et al., *A mitochondrial etiology of Alzheimer and Parkinson disease.* Biochim Biophys Acta, 2011.
136. Gilmer, L.K., et al., *Early mitochondrial dysfunction after cortical contusion injury.* J Neurotrauma, 2009. **26**(8): p. 1271-80.
137. Hartings, J.A., et al., *Spreading depolarizations and late secondary insults after traumatic brain injury.* J Neurotrauma, 2009. **26**(11): p. 1857-66.
138. Sullivan, P.G., M.B. Thompson, and S.W. Scheff, *Cyclosporin A attenuates acute mitochondrial dysfunction following traumatic brain injury.* Exp Neurol, 1999. **160**(1): p. 226-34.
139. Anderson, D.D., et al., *Post-traumatic osteoarthritis: improved understanding and opportunities for early intervention.* J Orthop Res, 2011. **29**(6): p. 802-9.
140. Situnayake, R.D., et al., *Chain breaking antioxidant status in rheumatoid arthritis: clinical and laboratory correlates.* Ann Rheum Dis, 1991. **50**(2): p. 81-6.
141. Grabowski, P.S., et al., *Immunolocalization of inducible nitric oxide synthase in synovium and cartilage in rheumatoid arthritis and osteoarthritis.* Br J Rheumatol, 1997. **36**(6): p. 651-5.
142. Loeser, R.F., et al., *Detection of nitrotyrosine in aging and osteoarthritic cartilage: Correlation of oxidative damage with the presence of interleukin-1beta*

and with chondrocyte resistance to insulin-like growth factor 1. Arthritis Rheum, 2002. **46**(9): p. 2349-57.
143. Uesugi, M., K. Yoshida, and H.E. Jasin, *Inflammatory properties of IgG modified by oxygen radicals and peroxynitrite.* J Immunol, 2000. **165**(11): p. 6532-7.
144. Chen, A.F., et al., *Oxidative DNA damage in osteoarthritic porcine articular cartilage.* J Cell Physiol, 2008. **217**(3): p. 828-33.
145. Grishko, V.I., et al., *Diminished mitochondrial DNA integrity and repair capacity in OA chondrocytes.* Osteoarthritis Cartilage, 2009. **17**(1): p. 107-13.
146. Reed, K.N., et al., *The role of mitochondrial reactive oxygen species in cartilage matrix destruction.* Mol Cell Biochem, 2014. **397**(1-2): p. 195-201.
147. Ruiz-Romero, C., et al., *Mitochondrial dysregulation of osteoarthritic human articular chondrocytes analyzed by proteomics: a decrease in mitochondrial superoxide dismutase points to a redox imbalance.* Mol Cell Proteomics, 2009. **8**(1): p. 172-89.
148. Aigner, T., et al., *Large-scale gene expression profiling reveals major pathogenetic pathways of cartilage degeneration in osteoarthritis.* Arthritis Rheum, 2006. **54**(11): p. 3533-44.
149. Gavriilidis, C., et al., *Mitochondrial dysfunction in osteoarthritis is associated with down-regulation of superoxide dismutase 2.* Arthritis Rheum, 2013. **65**(2): p. 378-87.
150. Touyz, R.M., *Mitochondrial redox control of matrix metalloproteinase signaling in resistance arteries.* Arterioscler Thromb Vasc Biol, 2006. **26**(4): p. 685-8.
151. Del Carlo, M., et al., *Endogenous production of reactive oxygen species is required for stimulation of human articular chondrocyte matrix metalloproteinase production by fibronectin fragments.* Free Radic Biol Med, 2007. **42**(9): p. 1350-8.
152. Lyyra, T., et al., *In vivo characterization of indentation stiffness of articular cartilage in the normal human knee.* J Biomed Mater Res, 1999. **48**(4): p. 482-7.
153. Franz, T., et al., *In situ compressive stiffness, biochemical composition, and structural integrity of articular cartilage of the human knee joint.* Osteoarthritis Cartilage, 2001. **9**(6): p. 582-92.
154. Bae, W.C., et al., *Indentation testing of human cartilage: sensitivity to articular surface degeneration.* Arthritis Rheum, 2003. **48**(12): p. 3382-94.
155. Taskiran, D., et al., *Nitric oxide mediates suppression of cartilage proteoglycan synthesis by interleukin-1*. Biochem Biophys Res Commun, 1994. **200**(1): p. 142-8.
156. Maneiro, E., et al., *Mitochondrial respiratory activity is altered in osteoarthritic human articular chondrocytes.* Arthritis Rheum, 2003. **48**(3): p. 700-8.
157. Lee, R.C., et al., *A comparison of in vitro cellular responses to mechanical and electrical stimulation.* Am Surg, 1982. **48**(11): p. 567-74.
158. Gray, M.L., et al., *Mechanical and physiochemical determinants of the chondrocyte biosynthetic response.* J Orthop Res, 1988. **6**(6): p. 777-92.
159. Parkkinen, J.J., et al., *A mechanical apparatus with microprocessor controlled stress profile for cyclic compression of cultured articular cartilage explants.* J Biomech, 1989. **22**(11-12): p. 1285-91.

160. Torzilli, P.A., et al., *Characterization of cartilage metabolic response to static and dynamic stress using a mechanical explant test system.* J Biomech, 1997. **30**(1): p. 1-9.
161. Heiner, A.D. and J.A. Martin, *Cartilage responses to a novel triaxial mechanostimulatory culture system.* J Biomech, 2004. **37**(5): p. 689-95.
162. Ramakrishnan, P.S., et al., *Biomechanical disc culture system: feasibility study using rat intervertebral discs.* Proc Inst Mech Eng H, 2011. **225**(6): p. 611-20.
163. Imai, Y., et al., *Evaluation of polysulfone as a potential biomedical material.* J Bioeng, 1978. **2**(1-2): p. 103-7.
164. Wenz, L.M., et al., *In vitro biocompatibility of polyetheretherketone and polysulfone composites.* J Biomed Mater Res, 1990. **24**(2): p. 207-15.
165. Zielonka, J., J. Vasquez-Vivar, and B. Kalyanaraman, *Detection of 2-hydroxyethidium in cellular systems: a unique marker product of superoxide and hydroethidine.* Nat Protoc, 2008. **3**(1): p. 8-21.
166. Michalski, R., et al., *On the use of fluorescence lifetime imaging and dihydroethidium to detect superoxide in intact animals and ex vivo tissues: a reassessment.* Free Radic Biol Med, 2014. **67**: p. 278-84.
167. Zielonka, J. and B. Kalyanaraman, *Hydroethidine- and MitoSOX-derived red fluorescence is not a reliable indicator of intracellular superoxide formation: another inconvenient truth.* Free Radic Biol Med, 2010. **48**(8): p. 983-1001.
168. Journot, B.J., *The effects of cyclic hydrostatic pressure on chondrocytes in an alginate substrate*. 2012, The University of Iowa: Ann Arbor. p. 62.
169. Brouillette, M.J., et al., *Strain-dependent oxidant release in articular cartilage originates from mitochondria.* Biomech Model Mechanobiol, 2014. **13**(3): p. 565-72.
170. Fermor, B., et al., *The effects of static and intermittent compression on nitric oxide production in articular cartilage explants.* J Orthop Res, 2001. **19**(4): p. 729-37.
171. Lee, R.B., et al., *The effect of mechanical stress on cartilage energy metabolism.* Biorheology, 2002. **39**(1-2): p. 133-43.
172. Wolff, K.J., et al., *Mechanical stress and ATP synthesis are coupled by mitochondrial oxidants in articular cartilage.* J Orthop Res, 2013. **31**(2): p. 191-6.
173. Kirkpatrick, C.J., W. Mohr, and O. Haferkamp, *The effects of nickel ions on articular chondrocyte growth in monolayer culture.* Res Exp Med (Berl), 1982. **181**(3): p. 259-64.
174. Talha, M., C.K. Behera, and O.P. Sinha, *A review on nickel-free nitrogen containing austenitic stainless steels for biomedical applications.* Mater Sci Eng C Mater Biol Appl, 2013. **33**(7): p. 3563-75.
175. Li, M., et al., *Study of biocompatibility of medical grade high nitrogen nickel-free austenitic stainless steel in vitro.* Mater Sci Eng C Mater Biol Appl, 2014. **43**: p. 641-8.
176. Zhao, H., et al., *Superoxide reacts with hydroethidine but forms a fluorescent product that is distinctly different from ethidium: potential implications in intracellular fluorescence detection of superoxide.* Free Radic Biol Med, 2003. **34**(11): p. 1359-68.

177. Wann, A.K., et al., *Primary cilia mediate mechanotransduction through control of ATP-induced Ca2+ signaling in compressed chondrocytes.* FASEB J, 2012. **26**(4): p. 1663-71.
178. Masson, N., et al., *The FIH hydroxylase is a cellular peroxide sensor that modulates HIF transcriptional activity.* EMBO Rep, 2012. **13**(3): p. 251-7.
179. Niecknig, H., et al., *Role of reactive oxygen species in the regulation of HIF-1 by prolyl hydroxylase 2 under mild hypoxia.* Free Radic Res, 2012. **46**(6): p. 705-17.
180. Palazon, A., et al., *HIF transcription factors, inflammation, and immunity.* Immunity, 2014. **41**(4): p. 518-28.
181. Vaamonde-Garcia, C., et al., *Mitochondrial dysfunction increases inflammatory responsiveness to cytokines in normal human chondrocytes.* Arthritis Rheum, 2012. **64**(9): p. 2927-36.
182. Buckwalter, J.A., et al., *The Roles of Mechanical Stresses in the Pathogenesis of Osteoarthritis: Implications for Treatment of Joint Injuries.* Cartilage, 2013. **4**(4): p. 286-294.
183. Zielonka, J., M. Hardy, and B. Kalyanaraman, *HPLC study of oxidation products of hydroethidine in chemical and biological systems: ramifications in superoxide measurements.* Free Radic Biol Med, 2009. **46**(3): p. 329-38.
184. Long, J.A. and H.D. Guthrie, *Validation of a rapid, large-scale assay to quantify ATP concentration in spermatozoa.* Theriogenology, 2006. **65**(8): p. 1620-30.